Search for squarks and gluinos in final states with jets and missing transverse momentum using 36 fb^{-1} of $\sqrt{s}=13$ TeV pp collision data with the ATLAS detector

M. Aaboud *et al.*[*]
(ATLAS Collaboration)

(Received 7 December 2017; published 6 June 2018)

A search for the supersymmetric partners of quarks and gluons (squarks and gluinos) in final states containing hadronic jets and missing transverse momentum, but no electrons or muons, is presented. The data used in this search were recorded in 2015 and 2016 by the ATLAS experiment in $\sqrt{s}=13$ TeV proton-proton collisions at the Large Hadron Collider, corresponding to an integrated luminosity of 36.1 fb^{-1}. The results are interpreted in the context of various models where squarks and gluinos are pair produced and the neutralino is the lightest supersymmetric particle. An exclusion limit at the 95% confidence level on the mass of the gluino is set at 2.03 TeV for a simplified model incorporating only a gluino and the lightest neutralino, assuming the lightest neutralino is massless. For a simplified model involving the strong production of mass-degenerate first- and second-generation squarks, squark masses below 1.55 TeV are excluded if the lightest neutralino is massless. These limits substantially extend the region of supersymmetric parameter space previously excluded by searches with the ATLAS detector.

DOI: 10.1103/PhysRevD.97.112001

I. INTRODUCTION

Supersymmetry (SUSY) [1–6] is a generalization of space-time symmetries that predicts new bosonic partners for the fermions and new fermionic partners for the bosons of the Standard Model (SM). If R-parity is conserved [7], SUSY particles, called sparticles, are produced in pairs and the lightest supersymmetric particle (LSP) is stable and represents a possible dark-matter candidate. The scalar partners of the left- and right-handed quarks, the squarks $\tilde{q}_{\mathrm{L}}$ and $\tilde{q}_{\mathrm{R}}$, mix to form two mass eigenstates $\tilde{q}_1$ and $\tilde{q}_2$ ordered by increasing mass. Superpartners of the charged and neutral electroweak and Higgs bosons also mix, producing charginos ($\tilde{\chi}^{\pm}$) and neutralinos ($\tilde{\chi}^0$). Squarks and the fermionic partners of the gluons, the gluinos ($\tilde{g}$), could be produced in strong-interaction processes at the Large Hadron Collider (LHC) [8] and decay via cascades ending with the stable LSP, which escapes the detector unseen, producing substantial missing transverse momentum ($\vec{E}_{\mathrm{T}}^{\mathrm{miss}}$).

The large cross sections predicted for the strong production of supersymmetric particles make the production of gluinos and squarks a primary target in searches for SUSY in proton-proton (pp) collisions at a center-of-mass energy of 13 TeV at the LHC. Interest in these searches is motivated by the large available choice of parameters for R-parity-conserving models in the minimal supersymmetric Standard Model (MSSM) [9,10] where squarks (including antisquarks) and gluinos can be produced in pairs ($\tilde{g}\tilde{g}$, $\tilde{q}\tilde{q}$, $\tilde{q}\tilde{g}$) and can decay through $\tilde{q}\to q\tilde{\chi}_1^0$ and $\tilde{g}\to q\bar{q}\tilde{\chi}_1^0$ to the lightest neutralino, $\tilde{\chi}_1^0$, assumed to be the LSP. Additional decay modes can include the production of charginos via $\tilde{q}\to q\tilde{\chi}^{\pm}$ (where $\tilde{q}$ and q are of different flavor) and $\tilde{g}\to qq\tilde{\chi}^{\pm}$, or neutralinos via $\tilde{g}\to qq\tilde{\chi}_2^0$. Subsequent chargino decay to $W^{\pm}\tilde{\chi}_1^0$ or neutralino decay to $Z\tilde{\chi}_1^0$ or $h\tilde{\chi}_1^0$, depending on the decay modes of W, Z, and h bosons, can increase the jet multiplicity and missing transverse momentum.

This paper presents two approaches to search for these sparticles in final states containing only hadronic jets and large missing transverse momentum. The first is an update of the analysis [11] (referred to as "Meff-based search" in the following). The second is a complementary search using the recursive jigsaw reconstruction (RJR) technique [12–14] in the construction of a discriminating variable set ("RJR-based search"). By using a dedicated set of selection criteria, the RJR-based search improves the sensitivity to supersymmetric models with small mass splittings between the sparticles (models with compressed spectra). Both searches presented here adopt the same general approach as the analysis of the 7, 8, and 13 TeV data collected during Run 1 and Run 2 of the LHC, described in Ref. [11].

[*]Full author list given at the end of the article.

The CMS Collaboration has set limits on similar models in Refs. [15–18].

In the searches presented here, events with reconstructed electrons or muons are rejected to avoid any overlap with a complementary ATLAS search in final states with one lepton, jets, and missing transverse momentum [19], and to reduce the background from events with neutrinos ($W \to e\nu, \mu\nu$). The selection criteria are optimized in the $m_{\tilde{g}}, m_{\tilde{\chi}_1^0}$ and $m_{\tilde{q}}, m_{\tilde{\chi}_1^0}$ planes, (where $m_{\tilde{g}}$, $m_{\tilde{q}}$, and $m_{\tilde{\chi}_1^0}$ are the gluino, squark, and LSP masses, respectively) for simplified models [20–22], and in the $m_{\tilde{g}}, m_{\tilde{q}}$ plane for the simplified phenomenological MSSM (pMSSM) models [23,24] in which the number of MSSM parameters is reduced using existing experimental and theoretical constraints. Although interpreted in terms of SUSY models, the results of this analysis could also constrain any model of new physics that predicts the production of jets in association with missing transverse momentum.

The paper is organized as follows. Section II describes the ATLAS experiment and data samples used, and Sec. III Monte Carlo (MC) simulation samples used for background and signal modeling. Event reconstruction and identification are presented in Sec. IV. The analysis strategy used by both searches is given in Sec. V. Since the RJR technique is a new approach for this search, Sec. VI is dedicated to the description of the technique and associated variables. Searches are performed in signal regions that are defined in Sec. VII. Summaries of the background estimation methodology and corresponding systematic uncertainties are presented in Secs. VIII and IX, respectively. Results obtained using the signal regions optimized for both searches are reported in Sec. X. Section XI is devoted to conclusions.

II. THE ATLAS DETECTOR AND DATA SAMPLES

The ATLAS detector [25] is a multipurpose detector with a forward-backward symmetric cylindrical geometry and nearly 4π coverage in solid angle.[1] The inner detector (ID) tracking system consists of pixel and silicon microstrip detectors covering the pseudorapidity region $|\eta| < 2.5$, surrounded by a transition radiation tracker, which improves electron identification over the region $|\eta| < 2.0$. The innermost pixel layer, the insertable B-layer [26], was added between Run 1 and Run 2 of the LHC, at a radius of 33 mm around a new, narrower, and thinner beam pipe. The ID is surrounded by a thin superconducting solenoid providing an axial 2 T magnetic field and by a fine-granularity lead/liquid-argon (LAr) electromagnetic calorimeter covering $|\eta| < 3.2$. A steel/scintillator-tile calorimeter provides hadronic coverage in the central pseudorapidity range ($|\eta| < 1.7$). The endcap and forward regions ($1.5 < |\eta| < 4.9$) are made of LAr active layers with either copper or tungsten as the absorber material for electromagnetic and hadronic measurements. The muon spectrometer with an air-core toroid magnet system surrounds the calorimeters. Three layers of high-precision tracking chambers provide coverage in the range $|\eta| < 2.7$, while dedicated chambers allow triggering in the region $|\eta| < 2.4$.

The ATLAS trigger system [27] consists of two levels; the first level is a hardware-based system, while the second is a software-based system called the high-level trigger. The events used by the searches described in this paper were selected using a trigger logic that accepts events with a missing transverse momentum above 70 GeV (for data collected during 2015) or above 90–110 GeV (depending on data-taking period for data collected in 2016) calculated using a vectorial sum of the jet transverse momenta. The trigger is 100% efficient for the event selections considered in these analyses. Auxiliary data samples used to estimate the yields of background events were selected using triggers requiring at least one isolated electron ($p_{\mathrm{T}} > 24$ GeV), muon ($p_{\mathrm{T}} > 20$ GeV), or photon ($p_{\mathrm{T}} > 120$ GeV) for data collected in 2015. For the 2016 data, the events used for the background estimation were selected using triggers requiring at least one isolated electron or muon ($p_{\mathrm{T}} > 26$ GeV) or photon ($p_{\mathrm{T}} > 140$ GeV).

The data were collected by the ATLAS detector during 2015 with a peak delivered instantaneous luminosity of $L = 5.2 \times 10^{33}$ cm^{-2} s^{-1}, and during 2016 with a maximum of $L = 1.37 \times 10^{34}$ cm^{-2} s^{-1}. The mean number of pp interactions per bunch crossing in the data set was 14 in 2015 and 24 in 2016. Application of beam, detector, and data-quality criteria resulted in a total integrated luminosity of 36.1 fb^{-1}. The uncertainty in the integrated luminosity averaged over both years is 3.2%. It is derived, following a methodology similar to that detailed in Ref. [28], from a preliminary calibration of the luminosity scale using a pair of x-y beam-separation scans performed in August 2015 and May 2016.

III. MONTE CARLO SAMPLES

A set of simulated MC event samples was used to optimize the selections, estimate backgrounds, and assess the sensitivity to specific SUSY signal models.

Simplified models and pMSSM models are both used as SUSY signals in this paper. Simplified models are defined

[1]ATLAS uses a right-handed coordinate system with its origin at the nominal interaction point in the center of the detector. The positive x axis is defined by the direction from the interaction point to the center of the LHC ring, with the positive y axis pointing upwards, while the beam direction defines the z axis. Cylindrical coordinates (r, ϕ) are used in the transverse plane, ϕ being the azimuthal angle around the z axis. The pseudorapidity η is defined in terms of the polar angle θ by $\eta = -\ln\tan(\theta/2)$ and the rapidity is defined as $y = (1/2)\ln[(E + p_z)/(E - p_z)]$ where E is the energy and p_z the longitudinal momentum of the object of interest. The transverse momentum p_{T}, the transverse energy E_{T}, and the missing transverse momentum $E_{\mathrm{T}}^{\mathrm{miss}}$ are defined in the x-y plane unless stated otherwise.

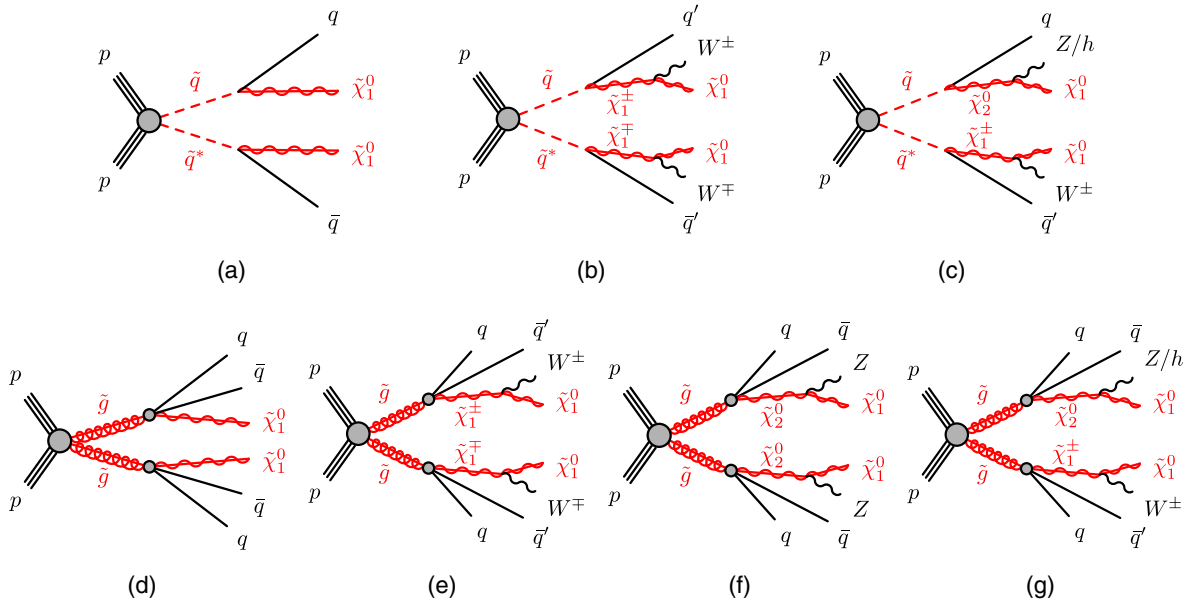

FIG. 1. Decay topologies of (a)–(c) squark pair production and (d)–(g) gluino pair production in the simplified models with (a) direct or (b),(c) one-step decays of squarks and (d) direct or (e)–(g) one-step decays of gluinos.

by an effective Lagrangian describing the interactions of a small number of new particles, assuming one production process and one decay channel with a 100% branching fraction. Signal samples are used to describe squark and gluino pair production, followed by the direct ($\tilde{q} \to q\tilde{\chi}_1^0$) or one-step ($\tilde{q} \to qW\tilde{\chi}_1^0$) decays of squarks and direct ($\tilde{g} \to qq\tilde{\chi}_1^0$) or one-step ($\tilde{g} \to qqW/Z/h\tilde{\chi}_1^0$) decays of gluinos as shown in Fig. 1. Direct decays are those where the considered SUSY particles decay directly into SM particles and the LSP, while the one-step decays refer to the cases where the decays occur via one intermediate on-shell SUSY particle, as indicated in parentheses. In pMSSM models, gluino and first- and second-generation squark production are considered inclusively, followed by direct decays of squarks and gluinos, or decays of squarks via gluinos ($\tilde{q} \to q\tilde{g}$) and decays of gluinos via squarks ($\tilde{g} \to q\tilde{q}$) if kinematically possible. All other supersymmetric particles, including the squarks of the third generation, have their masses set such that the particles are effectively decoupled. These samples were generated with up to two (simplified models) or one (pMSSM models) extra partons in the matrix element using the MG5_aMC@NLO 2.2.2 or 2.3.3 event generator [29] interfaced to PYTHIA 8.186 [30]. The CKKW-L merging scheme [31] was applied with a scale parameter that was set to a quarter of the mass of the gluino for $\tilde{g}\,\tilde{g}$ production or of the squark for $\tilde{q}\,\tilde{q}$ production in simplified models. In pMSSM models, a quarter of the smaller of the gluino and squark masses was used for the CKKW-L merging scale. The A14 [32] set of tuned parameters (tune) was used for initial/final-state radiation (ISR/FSR) and underlying-event parameters together with the NNPDF2.3LO [33] parton distribution function (PDF) set. The signal cross sections were calculated at next-to-leading order (NLO) in the strong coupling constant, adding the resummation of soft gluon emission at next-to-leading-logarithmic accuracy (NLO + NLL) [34–38]. The nominal squark and gluino cross sections were taken from an envelope of predictions using different PDF sets and factorization and renormalization scales, as described in Ref. [39], considering only first- and second-generation squarks ($\tilde{u}$, $\tilde{d}$, $\tilde{s}$, $\tilde{c}$). Eightfold degeneracy of first- and second-generation squarks is assumed for the simplified models with direct decays of squarks and pMSSM models while fourfold degeneracy is assumed for the simplified models with one-step decays of squarks. In the case of gluino pair (squark pair) production in simplified models, cross sections were evaluated assuming arbitrarily high masses of 450 TeV for the first- and second-generation squarks (gluinos) in order to decouple them. The free parameters are $m_{\tilde{\chi}_1^0}$ and $m_{\tilde{q}}$ ($m_{\tilde{g}}$) for squark pair (gluino pair) production in simplified models, while both $m_{\tilde{q}}$ and $m_{\tilde{g}}$ are varied in pMSSM models with $m_{\tilde{\chi}_1^0}$ fixed.

In the simulation of the production of W or Z/γ^* bosons in association with jets [40] using the SHERPA 2.2.1 event generator [41], the matrix elements were calculated for up to two partons at NLO and up to two additional partons at leading order (LO) using the COMIX [42] and OPEN LOOPS [43] matrix-element generators, and merged with the SHERPA parton shower [44] using the ME+PS@NLO prescription [45]. Simulated events containing a photon in association with jets were generated requiring a photon transverse momentum above 35 GeV. For these events, matrix elements were calculated at LO with up to three or four partons depending on the p_{T} of the photon, and

merged with the SHERPA parton shower using the ME+PS@LO prescription [46]. The $W/Z+$jets events were normalized using their NNLO cross sections [47] while for the $\gamma+$jets process the LO cross section, taken directly from the SHERPA MC event generator, was multiplied by a correction factor as described in Sec. VIII.

For the generation of $t\bar{t}$ and single-top processes in the Wt and s-channel [48], the POWHEG-BOX v2 [49] generator was used, while electroweak (EW) t-channel single-top events were modeled using POWHEG-BOX v1. This latter generator uses the four-flavor scheme for the NLO matrix-element calculations together with the fixed four-flavor PDF set CT10f4 [50]. For each of these processes, the decay of the top quark was simulated using MADSPIN [51] preserving all spin correlations, while for all processes the parton shower, fragmentation, and the underlying event were generated using PYTHIA 6.428 [52] with the CTEQ6L1 [53] PDF set and the corresponding PERUGIA 2012 tune (P2012) [54]. The top quark mass was set to 172.5 GeV. The h_{damp} parameter, which controls the p_{T} of the first additional emission beyond the Born configuration, was set to the mass of the top quark in the $t\bar{t}$ process. The main effect of this parameter is to regulate the high-p_{T} emission against which the $t\bar{t}$ system recoils [48]. The $t\bar{t}$ events were normalized using cross sections calculated at NNLO + NNLL [55,56] accuracy, while s- and t-channel single-top events were normalized using the NLO cross sections [57,58], and the Wt-channel single-top events were normalized using the NNLO + NNLL cross sections [59,60]. Production of a top quark in association with a Z boson is generated with the MG5_AMC@NLO 2.2.1 generator at LO with CTEQ6L1 PDF set.

For the generation of $t\bar{t}+$EW processes ($t\bar{t}+W/Z/WW$) [61], the MG5_AMC@NLO 2.2.3 generator at LO interfaced to the PYTHIA 8.186 parton-shower model was used, with up to two [$t\bar{t}+W$, $t\bar{t}+Z(\to\nu\nu/qq)$], one [$t\bar{t}+Z(\to\ell\ell)$], or no ($t\bar{t}+WW$) extra partons included in the matrix element. The events were normalized using their respective NLO cross sections [62,63] and the top quark mass was set to 172.5 GeV.

Diboson processes (WW, WZ, ZZ) [64] were simulated using the SHERPA 2.1.1 generator. For processes with four charged leptons (4ℓ), three charged leptons and a neutrino ($3\ell+1\nu$), or two charged leptons and two neutrinos ($2\ell+2\nu$), the matrix elements contain all diagrams with four electroweak couplings, and were calculated for up to one (4ℓ, $2\ell+2\nu$) or no partons ($3\ell+1\nu$) at NLO. For processes in which one of the bosons decays hadronically and the other leptonically, matrix elements were calculated for up to one (ZZ) or no (WW, WZ) additional partons at NLO. All diboson samples also simulated up to three additional partons at LO using the COMIX and OPENLOOPS matrix-element generators, and were merged with the SHERPA parton shower using the ME+PS@NLO prescription.

A summary of the SUSY signals and the SM background processes together with the MC event generators, cross section calculation orders in α_{s}, PDFs, parton shower, and tunes used is given in Table I.

For all SM background samples the response of the detector to particles was modeled with a full ATLAS detector simulation [65] based on GEANT4 [66]. Signal samples were prepared using a fast simulation based on a parametrization of the performance of the ATLAS electromagnetic and hadronic calorimeters [67] and on GEANT4 elsewhere. The EVTGEN v1.2.0 program [68] was used to describe the properties of the b- and c-hadron decays in the signal samples, and the background samples except those produced with SHERPA [41].

All simulated events were overlaid with multiple pp collisions simulated with PYTHIA 8.186 using the A2 tune [32] and the MSTW2008LO parton distribution functions [69]. The MC samples were generated with a variable number of additional pp interactions (pileup) and were

TABLE I. SUSY signals and the SM background MC simulation samples used in this paper. Generators, order in α_{s} of cross section calculations used for yield normalization, PDF sets, parton showers, and tunes used for the underlying event are shown.

Physics process	Generator	Cross-section normalization	PDF set	Parton shower	Tune
SUSY processes	MG5_AMC@NLO 2.2.2–2.3.3	NLO + NLL	NNPDF2.3LO	PYTHIA 8.186	A14
$W(\to\ell\nu)+$jets	SHERPA 2.2.1	NNLO	NNPDF3.0NNLO	SHERPA	SHERPA default
$Z/\gamma^*(\to\ell\bar{\ell})+$jets	SHERPA 2.2.1	NNLO	NNPDF3.0NNLO	SHERPA	SHERPA default
$\gamma+$jets	SHERPA 2.1.1	LO	CT10	SHERPA	SHERPA default
$t\bar{t}$	POWHEG-BOX v2	NNLO + NNLL	CT10	PYTHIA 6.428	PERUGIA2012
Single top (Wt-channel)	POWHEG-BOX v2	NNLO + NNLL	CT10	PYTHIA 6.428	PERUGIA2012
Single top (s-channel)	POWHEG-BOX v2	NLO	CT10	PYTHIA 6.428	PERUGIA2012
Single top (t-channel)	POWHEG-BOX v1	NLO	CT10f4	PYTHIA 6.428	PERUGIA2012
Single top (Zt-channel)	MG5_AMC@NLO 2.2.1	LO	CTEQ6L1	PYTHIA 6.428	PERUGIA2012
$t\bar{t}+W/Z/WW$	MG5_AMC@NLO 2.2.3	NLO	NNPDF2.3LO	PYTHIA 8.186	A14
WW, WZ, ZZ	SHERPA 2.1.1	NLO	CT10	SHERPA	SHERPA default

reweighted to match the distribution of the mean number of interactions observed in data.

IV. EVENT RECONSTRUCTION AND IDENTIFICATION

The reconstructed primary vertex of the event is required to be consistent with the luminous region and to have at least two associated tracks with $p_{\mathrm{T}} > 400$ MeV. When more than one such vertex is found, the vertex with the largest $\sum p_{\mathrm{T}}^2$ of the associated tracks is chosen.

Jet candidates are reconstructed using the anti-k_t jet clustering algorithm [70,71] with a jet radius parameter of 0.4 starting from clusters of calorimeter cells [72]. The jets are corrected for energy from pileup using the method described in Ref. [73]: a contribution equal to the product of the jet area and the median energy density of the event is subtracted from the jet energy [74]. Further corrections, referred to as the jet energy scale corrections, are derived from MC simulation and data, and are used to calibrate the average energies of jets to the scale of their constituent particles [75]. Only corrected jet candidates with $p_{\mathrm{T}} > 20$ GeV and $|\eta| < 2.8$ are retained. An algorithm based on boosted decision trees, 'MV2c10' [76,77], is used to identify jets containing a b-hadron (b-jets), with an operating point corresponding to an efficiency of 77%, and rejection factors of 134 for light-quark jets and 6 for charm jets [77] for reconstructed jets with $p_{\mathrm{T}} > 20$ GeV and $|\eta| < 2.5$ in simulated $t\bar{t}$ events. Candidate b-jets are required to have $p_{\mathrm{T}} > 50$ GeV and $|\eta| < 2.5$. Events with jets originating from detector noise and noncollision background are rejected if the jets fail to satisfy the "LooseBad" quality criteria, or if at least one of the two leading jets with $p_{\mathrm{T}} > 100$ GeV fails to satisfy the "TightBad" quality criteria, both described in Ref. [78]. The application of these requirements reduces the data sample by less than 1%. In order to reduce the number of jets coming from pileup, a significant fraction of the tracks associated with each jet must have an origin compatible with the primary vertex. This is enforced by using the jet vertex tagger (JVT) output using the momentum fraction of tracks [79]. The requirement JVT > 0.59 is only applied to jets with $p_{\mathrm{T}} < 60$ GeV and $|\eta| < 2.4$.

Two different classes of reconstructed lepton candidates (electrons or muons) are used in the analyses presented here. When selecting samples for the search, events containing a "baseline" electron or muon are rejected. The selections applied to identify baseline leptons are designed to maximize the efficiency with which $W+$ jets and top quark background events are rejected. When selecting "control region" samples for the purpose of estimating residual $W+$ jets and top quark backgrounds, additional requirements are applied to leptons to ensure greater purity of these backgrounds. These leptons are referred to as "high-purity" leptons below and form a subset of the baseline leptons.

Baseline muon candidates are formed by combining information from the muon spectrometer and inner detector as described in Ref. [80] and are required to have $p_{\mathrm{T}} > 7$ GeV and $|\eta| < 2.7$. High-purity muon candidates must additionally have $p_{\mathrm{T}} > 27$ GeV and $|\eta| < 2.4$, the significance of the transverse impact parameter with respect to the primary vertex $|d_0^{\mathrm{PV}}|/\sigma(d_0^{\mathrm{PV}}) < 3$, and the longitudinal impact parameter with respect to the primary vertex $|z_0^{\mathrm{PV}} \sin(\theta)| < 0.5$ mm. Furthermore, high-purity candidates must satisfy the "GradientLoose" isolation requirements described in Ref. [80], which rely on tracking-based and calorimeter-based variables and implement a set of η- and p_{T}-dependent criteria.

Baseline electron candidates are reconstructed from an isolated electromagnetic calorimeter energy deposit matched to an ID track and are required to have $p_{\mathrm{T}} > 7$ GeV, $|\eta| < 2.47$, and to satisfy "Loose" likelihood-based identification criteria described in Ref. [81]. High-purity electron candidates additionally must satisfy "Tight" selection criteria described in Ref. [81], and the leading electron must have $p_{\mathrm{T}} > 27$ GeV. They are also required to have $|d_0^{\mathrm{PV}}|/\sigma(d_0^{\mathrm{PV}}) < 5$, $|z_0^{\mathrm{PV}} \sin(\theta)| < 0.5$ mm, and to satisfy isolation requirements similar to those applied to high-purity muons [81].

After the selections described above, ambiguities between candidate jets with $|\eta| < 2.8$ and leptons are resolved as follows: first, any such jet candidate that is not tagged as b-jet, lying within a distance $\Delta R \equiv \sqrt{(\Delta\eta)^2 + (\Delta\phi)^2} = 0.2$ of a baseline electron is discarded. If a jet candidate is b-tagged it is interpreted as a jet and the overlapping electron is ignored. Additionally, if a baseline electron (muon) and a jet passing the JVT selection described above are found within $0.2 \leq \Delta R < 0.4$ [$< \min(0.4, 0.04 + 10\ \mathrm{GeV}/p_{\mathrm{T}}^{\mu})$], it is interpreted as a jet and the nearby electron (muon) candidate is discarded. Finally, if a baseline muon and jet are found within $\Delta R < 0.2$, it is treated as a muon and the overlapping jet is ignored, unless the jet satisfies $N_{\mathrm{trk}} < 3$, where N_{trk} refers to the number of tracks with $p_{\mathrm{T}} > 500$ MeV that are associated with the jet, in which case the muon is ignored. This criterion rejects jets consistent with final-state radiation or hard bremsstrahlung.

Additional ambiguities between electrons and muons in a jet, originating from the decays of hadrons, are resolved to avoid double counting and/or remove nonisolated leptons: the electron is discarded if a baseline electron and a baseline muon share the same ID track.

Reconstructed photons are used in the missing transverse momentum reconstruction as well as in the control region used to constrain the $Z+$ jets background, as explained in Sec. VIII. These latter photon candidates are required to satisfy $p_{\mathrm{T}} > 150$ GeV and $|\eta| < 2.37$, photon shower shape, and electron rejection criteria, and to be isolated [82]. The reduced η range for photons is chosen to avoid a region of coarse granularity at high η where photon and π^0

separation worsens. Ambiguities between candidate jets and photons (when used in the event selection) are resolved by discarding any jet candidates lying within $\Delta R = 0.4$ of a photon candidate. Additional selections to remove ambiguities between electrons or muons and photons are applied such that a photon is discarded if it is within $\Delta R = 0.4$ of a baseline electron or muon.

The measurement of the missing transverse momentum vector $\vec{E}_{\mathrm{T}}^{\mathrm{miss}}$ (and its magnitude $E_{\mathrm{T}}^{\mathrm{miss}}$) is based on the calibrated transverse momenta of all electron, muon, jet candidates, photons and all tracks originating from the primary vertex and not associated with such objects [83].

Initial jet-finding is extended using an approach called jet reclustering [84]. This allows the use of larger-radius-jet algorithms while maintaining the calibrations and systematic uncertainties associated with the input jets. Jets with a radius parameter 0.4 described above surviving the resolution of ambiguities and having $p_{\mathrm{T}} > 25$ GeV are used as input to an anti-k_t algorithm with a jet radius parameter 1.0. A grooming scheme called "reclustered jet trimming" is applied to remove any small-radius jet constituent j of a large-radius reclustered jet J if $p_{\mathrm{T}}^{j} < f_{\mathrm{cut}} \times p_{\mathrm{T}}^{J}$ where the parameter f_{cut} is set to be 0.05.

Corrections derived from data control samples are applied to account for differences between data and simulation for the lepton and photon trigger and reconstruction efficiencies, the lepton momentum/energy scale and resolution, and for the efficiency and mistag rate of the b-tagging algorithm.

V. ANALYSIS STRATEGY AND BACKGROUND PREDICTION

This section summarizes the common analysis strategy and statistical techniques that are employed in the searches presented in this paper.

To search for a possible signal, selection criteria are defined to enhance the expected signal yield relative to the SM backgrounds. Signal regions (SRs) are defined using the MC simulation of SUSY signals and the SM background processes. They are optimized to maximize the expected discovery sensitivity for each model considered. To estimate the SM backgrounds in an accurate and robust fashion, control regions (CRs) are defined for each of the signal regions. They are chosen to be orthogonal to the SR selections in order to provide independent data samples enriched in particular backgrounds, and are used to normalize the background MC simulation. The CR selections are optimized to have negligible SUSY signal contamination for the models near the previously excluded boundary [11], while minimizing the systematic uncertainties arising from the extrapolation of the CR event yields to estimate backgrounds in the SR. Cross-checks of the background estimates are performed with data in several validation regions (VRs) selected with requirements such that these regions do not overlap with the CR and SR selections, and also have a low expected signal contamination.

In order to ensure sensitivity to the variety of squark and gluino production signals targeted in this search, a collection of inclusive SRs is considered. Each of the SR selection requirements is optimized to exploit expected differences in masses, kinematics, and jet multiplicities, and each represents its own counting experiment. Two different approaches are used in defining these SRs, with Meff-based and RJR-based selection criteria described in Secs. VII A and VII B, respectively. These two approaches are complementary because of differences in selected event populations and the strategy for balancing the signal-to-background ratio against systematic uncertainties. A discussion of differences in these approaches is provided in Sec. VII C.

To extract the final results, three different classes of likelihood fits are employed: background-only, model-independent, and model-dependent fits [85]. A background-only fit is used to estimate the background yields in each SR. The fit is performed using the observed event yields in the CRs associated with the SR as the only constraints, but not the yields in the SR itself. It is assumed that signal events from physics beyond the Standard Model (BSM) do not contribute to these CR yields. The scale factors represent the normalization of background components relative to MC predictions ($\mu(W + \mathrm{jets})$, $\mu(Z + \mathrm{jets})$, $\mu(\mathrm{Top})$), and are simultaneously determined in the fit to all the CRs associated with a SR. The expected background in the SR is based on the yields predicted by simulation for $W/Z + \mathrm{jets}$ and background processes containing top quarks, corrected by the scale factors derived from the fit. In the case of multijet background, the estimate is based on the data-driven method described in Sec. VIII. The systematic and MC statistical uncertainties in the expected values are included in the fit as nuisance parameters that are constrained by Gaussian distributions with widths corresponding to the sizes of the uncertainties considered and by Poisson distributions, respectively. The background-only fit is also used to estimate the background event yields in the VRs.

A model-independent fit is used to quantify the level of agreement between background predictions and observed yields and to set upper limits on the number of BSM signal events in each SR. This fit proceeds in the same way as the background-only fit, where yields in the CRs are used to constrain the predictions of backgrounds in each SR, while the SR yield is also used in the likelihood with an additional nuisance parameter describing potential signal contributions. The observed and expected upper limits at 95% confidence level (C.L.) on the number of events from BSM phenomena for each signal region (S_{obs}^{95} and S_{exp}^{95}) are derived using the $\mathrm{CL_s}$ prescription [86], neglecting any possible signal contamination in the CRs. These limits, when normalized by the integrated luminosity of the data sample, may be interpreted as upper limits on the visible

cross section of BSM physics ($\langle\epsilon\sigma\rangle_{\mathrm{obs}}^{95}$), where the visible cross section is defined as the product of production cross section, acceptance, and efficiency. The model-independent fit is also used to compute the one-sided p-value (p_0) of the background-only hypothesis, which quantifies the statistical significance of an excess.

Finally, a model-dependent fit is used to set exclusion limits on the signal cross sections for specific SUSY models. Such a fit proceeds in the same way as the model-independent fit, except that both the signal yield in the signal region and the signal contamination in the CRs are taken into account. Correlations between signal and background systematic uncertainties are taken into account where appropriate. Signal-yield systematic uncertainties due to detector effects and the theoretical uncertainties in the signal acceptance are included in the fit.

VI. THE RECURSIVE JIGSAW RECONSTRUCTION TECHNIQUE

The RJR technique [12–14] is a method for defining kinematic variables event by event. While it is straightforward to fully describe an event's underlying kinematic features when all objects are fully reconstructed, events involving invisible weakly interacting particles present a challenge, as the loss of information from escaping particles constrains the kinematic variable construction to take place in the lab frame instead of the more physically natural frames of the hypothesized decays. The RJR method partially mitigates this loss of information by determining approximations of the rest frames of intermediate particle states in each event. This reconstructed view of the event gives rise to a natural basis of kinematic observables, calculated by evaluating the momenta and energy of different objects in these reference frames.

All jets with $p_T > 50$ GeV and $|\eta| < 2.8$ and the missing transverse momentum are used as input to the RJR algorithm. Motivated by searches for strong production of sparticles in R-parity-conserving models, a decay tree, shown in Fig. 2(a), is used in the analysis of events. Each event is evaluated as if two sparticles (the intermediate states P_{a} and P_{b}) were produced and then decayed to the particles observed in the detector (the collections V_{a} and V_{b}). The benchmark signal models probed in this search give rise to signal events with at least two weakly interacting particles associated with two systems of invisible particles (I_{a} and I_{b}), the respective children of the initially produced sparticles.

This decay tree includes several kinematic and combinatoric unknowns. In the final state with no leptons, the objects observed in the detector are exclusively jets and it is necessary to decide how to partition these jets into the two groups V_a and V_b in order to calculate the observables associated with the decay tree. In this analysis, the grouping that minimizes the masses of the four-momentum sum of group constituents is chosen.

More explicitly, the collection of reconstructed jet four-momenta, $V \equiv \{p_i\}$ and their four-momentum sum p_V are considered. Each of the four-momenta is evaluated in the rest frame of p_V (V frame) and different partitions of these jets $V_i = \{p_1, \ldots, p_{N_i}\}$ are considered such that $V_a \cap V_b = 0$ and $V_a \cup V_b = V$. For each partition, the sum of four-momenta $p_{V_i} = \sum_{j=1}^{N_i} p_j$ is calculated and the combination that maximizes the sum of momentum of the two groups, $|\vec{p}_{V_a}| + |\vec{p}_{V_b}|$, is chosen. The axis that this partition implicitly defines in the V rest frame is equivalent to the thrust axis of the jets, and the masses $M_{V_i} = \sqrt{p_{V_i}^2}$ are simultaneously minimized.

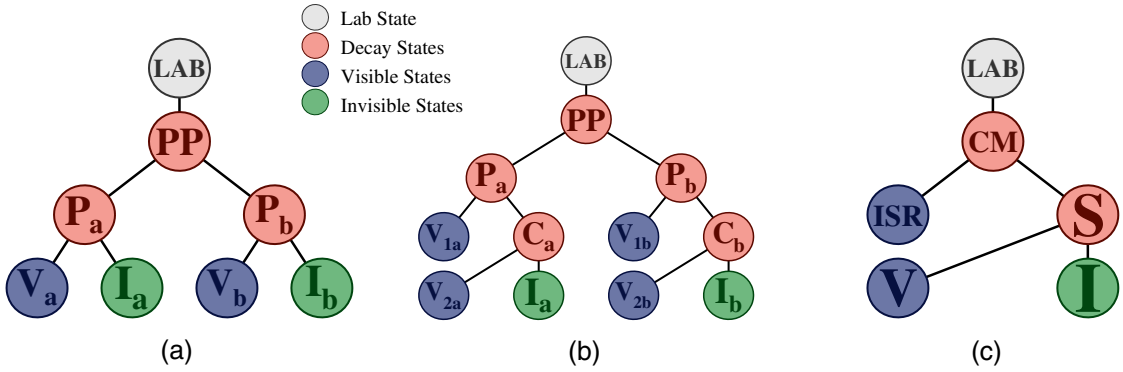

FIG. 2. (a) Inclusive strong sparticle production decay tree. Two sparticles (P_{a} and P_{b}) are nonresonantly pair produced with each decaying to one or more visible particles (V_{a} and V_{b}) that are reconstructed in the detector, and two systems of invisible particles (I_{a} and I_{b}) whose four-momenta are only partially constrained. (b) An additional level of decays can be added when requiring more than two visible objects. This tree is particularly useful for the search for gluino pair production described in the text. The di-sparticle production frame is denoted PP. Intermediate decay states are labeled C. (c) Strong sparticle production with ISR decay tree for use with small mass splitting spectra. CM refers to the center-of-mass of the whole reaction. A signal sparticle system S decays into visible particles (V) and a system of invisible particles (I) that recoil from a jet radiation system ISR.

When the decay tree shown in Fig. 2(b) is used to analyze events, each of the groups V_a and V_b are further subdivided, with each group undergoing exactly the same partitioning algorithm (based on selecting the combination maximizing the scalar sum of the momentum of the two partitions), resulting in a finer partition with subgroups $V_{1a/2a}$ and $V_{1b/2b}$. Similarly, the same algorithm is used to decide which jets are assigned to the groups V and ISR when analyzing events according to the decay tree shown in Fig. 2(c), where the $E_{\mathrm{T}}^{\mathrm{miss}}$, represented as I, is treated as an additional, massless jet in the partitioning algorithm. The reconstruction code for the algorithm can be found in Ref. [87].

The remaining unknowns in the event are associated with the two collections of weakly interacting particles: their masses, longitudinal momenta, and information about how the two groups contribute to the $\vec{E}_T^{\mathrm{miss}}$. The RJR algorithm determines these unknowns through subsequent minimizations of the intermediate particle masses appearing in the decay tree. In each of these newly constructed rest frames, all relevant momenta are defined and can be used to construct any variable—multiobject invariant masses, angles between objects, etc. The primary energy-scale-sensitive observables used in the search presented here are a suite of variables denoted by H. These H variables denote *hemispheres*, with the H suggesting similarities with H_{T}, the scalar sum of visible transverse momenta. However, in contrast to H_{T}, these H variables are constructed using different combinations of objects' momenta, including contributions from the invisible four-momenta, and are not necessarily evaluated in the lab frame, nor only in the transverse plane.

The H variables are labeled with a superscript F and two subscripts n and m, $H_{n,m}^{F}$. The F represents the rest frame in which the momenta are evaluated. In this analysis, this may be the lab frame, the proxy frame for the sparticle-sparticle frame PP, or the proxy frame for an individual sparticle's rest frame P. The subscripts n and m represent the number of visible and invisible momentum vectors considered, respectively. This means, given the number of visible momentum vectors in the frame, these are summed until only n distinct vectors remain. The choice for which vectors are summed is made by finding jets with smallest mutual four vector dot products, using the minimization procedure described above. The same is done for the invisible system so that only m distinct vectors remain. For events with fewer than n visible objects, the sum only runs over the available vectors. The additional subscript "T" can denote a transverse version of the variable, where the transverse plane is defined in a frame F as follows: The Lorentz transformation relating F to the lab frame is decomposed into a boost along the beam axis, followed by a subsequent transverse boost. The transverse plane is defined to be normal to the longitudinal boost. In practice, this is similar to the plane transverse to the beam line.

The variables that are used to define the signal and control regions are listed below. As few requirements are placed on dimensionful variables as possible, in order to increase the generality of the signal regions' sensitivity. Additional discrimination is achieved through a minimal set of dimensionless variable requirements with selections imposed on unitless quantities exploiting common mass-independent features of the signals considered.

To select signal events in models with squark pair production, the following variables are used:

(i) $H_{1,1}^{PP}$: scale variable as described above. Measures the momentum of missing particles in the PP frame and behaves similarly to $E_{\mathrm{T}}^{\mathrm{miss}}$.

(ii) $H_{\mathrm{T2},1}^{PP}$: scale variable as described above. Behaves similarly to effective mass, m_{eff} (defined as the scalar sum of the transverse momenta of the two leading jets and $E_{\mathrm{T}}^{\mathrm{miss}}$) for squark pair production signals with two-jet final states.

(iii) $H_{1,1}^{PP}/H_{2,1}^{PP}$: provides additional information in testing the balance of the two scale variables, where in the denominator the $H_{2,1}^{PP}$ is no longer solely transverse. This provides excellent discrimination against unbalanced events where the large scale is dominated by a particular object p_{T} or by high $E_{\mathrm{T}}^{\mathrm{miss}}$.

(iv) $p_{PP,z}^{\mathrm{lab}}/(p_{PP,z}^{\mathrm{lab}} + H_{\mathrm{T2},1}^{PP})$: compares the z-momentum of all the objects associated with the PP system in the lab frame ($p_{PP,z}^{\mathrm{lab}}$) to the overall transverse scale variable considered. This variable tests for significant boost in the z direction.

(v) $p_{\mathrm{Tj2}}^{PP}/H_{\mathrm{T2},1}^{PP}$: the ratio of the p_{T} of the second leading jet, evaluated in the PP frame (p_{Tj2}^{PP}) to the transverse scale variable, with small values generally more backgroundlike.

For signal topologies with higher jet multiplicities, there is the option to exploit the internal structure of the hemispheres by using a decay tree with an additional decay. For gluino pair production, the tree shown in Fig. 2(b) can be used and the variables used by this search are as follows:

(i) $H_{1,1}^{PP}$: described above.

(ii) $H_{\mathrm{T4},1}^{PP}$: analogous to the transverse scale variable described above but more appropriate for four-jet final states expected from gluino pair production.

(iii) $H_{1,1}^{PP}/H_{4,1}^{PP}$: analogous to $H_{1,1}^{PP}/H_{2,1}^{PP}$ for the squark search.

(iv) $H_{\mathrm{T4},1}^{PP}/H_{4,1}^{PP}$: a measure of the fraction of the momentum that lies in the transverse plane.

(v) $p_{PP,z}^{\mathrm{lab}}/(p_{PP,z}^{\mathrm{lab}} + H_{\mathrm{T4},1}^{PP})$: analogous to $p_{PP,z}^{\mathrm{lab}}/(p_{PP,z}^{\mathrm{lab}} + H_{\mathrm{T2},1}^{PP})$ above.

(vi) $\min_i (p_{\mathrm{Tj2}i}^{PP}/H_{\mathrm{T2},1i}^{PP})$: represents the fraction of a hemisphere's overall scale due to the second-highest-p_{T} jet (in the PP frame) compared to the overall scale, independently for each hemisphere. The smaller of the values in the two hemispheres is used, corresponding to the index i.

(vii) $\max_i (H_{1,0}^{P_i}/H_{2,0}^{P_i})$: testing balance of solely the jets momentum in a given hemisphere's approximate sparticle rest frame (P_i, index i indicating each hemisphere) provides additional discrimination against a small but otherwise signal-like subset of background events with a vector boson and associated jets.

In order to reject events where the $E_{\mathrm{T}}^{\mathrm{miss}}$ results from mismeasurements of jets, the $E_{\mathrm{T}}^{\mathrm{miss}}$ is attributed to one or more jets using a transverse clustering scheme. The transverse components of reconstructed jet four vectors and the $E_{\mathrm{T}}^{\mathrm{miss}}$, treated as massless, are organized into a binary decay tree by choosing associations through the recursive minimization of subgroup masses at each decay step using the previously described algorithm. The jet(s) appearing in the decay step where the $E_{\mathrm{T}}^{\mathrm{miss}}$ appears alone are those that have the smallest inner product with the system of invisible particles in the event, and their mutual transverse momentum is compared with the $E_{\mathrm{T}}^{\mathrm{miss}}$ using the ratio R_{QCD}:

$$R_{\mathrm{QCD}} = \frac{\max(\vec{p}_{\mathrm{T}}^{\,\mathrm{jets}} \cdot \vec{E}_{\mathrm{T}}^{\mathrm{miss}}, 0)}{(E_{\mathrm{T}}^{\mathrm{miss}})^2 + \max(\vec{p}_{\mathrm{T}}^{\,\mathrm{jets}} \cdot \vec{E}_{\mathrm{T}}^{\mathrm{miss}}, 0)}, \tag{1}$$

where $\vec{p}_{\mathrm{T}}^{\,\mathrm{jets}}$ is the transverse momentum of the $E_{\mathrm{T}}^{\mathrm{miss}}$-associated jet(s) or system of jets in the lab frame. Alternatively, the magnitude and direction of these jets can be compared with the $E_{\mathrm{T}}^{\mathrm{miss}}$ by considering the "decay angle" of the jet(s)/$E_{\mathrm{T}}^{\mathrm{miss}}$ system, $\cos(\phi_{\mathrm{j},E_{\mathrm{T}}^{\mathrm{miss}}})$, defined using the transverse jet(s) and $E_{\mathrm{T}}^{\mathrm{miss}}$ four vectors of the binary decay tree. These quantities are combined into a discriminant Δ_{QCD}, defined as

$$\Delta_{\mathrm{QCD}} = \frac{1 + \cos(\phi_{\mathrm{j},E_{\mathrm{T}}^{\mathrm{miss}}}) - 2R_{\mathrm{QCD}}}{1 + \cos(\phi_{\mathrm{j},E_{\mathrm{T}}^{\mathrm{miss}}}) + 2R_{\mathrm{QCD}}}. \tag{2}$$

This observable is used to quantify the likelihood that mismeasurements of these jets were responsible for the $E_{\mathrm{T}}^{\mathrm{miss}}$. Multijet events with severe jet mismeasurements tend to have Δ_{QCD} values in the interval $[-1, 0]$ while events with $E_{\mathrm{T}}^{\mathrm{miss}}$ from weakly interacting particles are more likely to have values in the interval [0, 1].

In addition to trying to resolve the entirety of the signal event, it can be useful for sparticle spectra with smaller mass splittings and lower intrinsic $E_{\mathrm{T}}^{\mathrm{miss}}$ to instead select events with a partially resolved sparticle system recoiling from a high-p_{T} jet from initial-state radiation. To target such topologies, a separate tree for compressed spectra is shown in Fig. 2(c). This tree is somewhat simpler and attempts to identify visible (V) and invisible (I) systems that are the result of an intermediate state corresponding to the system of sparticles and their decay products (S). As the $E_{\mathrm{T}}^{\mathrm{miss}}$ is used to choose which jets are identified as ISR, a transverse view of the reconstructed event is used which ignores the longitudinal momentum of the jets. The reference frames appearing in the decay tree shown in Fig. 2(c), such as the estimate of the center-of-mass frame (CM), are then approximations in this transverse projection. This tree yields a slightly different set of variables:

(i) p_{TS}^{CM}: the magnitude of the vector-summed transverse momenta of all S-associated jets ($|\vec{p}_{TS}^{\,\mathrm{CM}}|$) and $E_{\mathrm{T}}^{\mathrm{miss}}$ evaluated in the CM frame.

(ii) $R_{\mathrm{ISR}} \equiv \vec{p}_I^{\,\mathrm{CM}} \cdot \hat{p}_{TS}^{\,\mathrm{CM}}/p_{TS}^{\mathrm{CM}}$: serves as an estimate of $m_{\tilde{\chi}}/m_{\tilde{g}/\tilde{q}}$. This is the fraction of the momentum of the S system that is carried by its invisible system I, with momentum $\vec{p}_I^{\,\mathrm{CM}}$ in the CM frame. As p_{TS}^{CM} grows it becomes increasingly hard for backgrounds to possess a large value in this ratio—a feature exhibited by compressed signals.

(iii) M_{TS}: the transverse mass of the S system.

(iv) N_{jet}^{V}: number of jets assigned to the visible system (V) and not associated with the ISR system.

(v) $\Delta\phi_{\mathrm{ISR},I}$: the azimuthal opening angle between the ISR system and the invisible system in the CM frame.

VII. EVENT SELECTION AND SIGNAL REGIONS DEFINITIONS

Following the event reconstruction described in Sec. IV, in both searches documented here, events are discarded if a baseline electron or muon with $p_{\mathrm{T}} > 7$ GeV remains, or if they contain a jet failing to satisfy quality selection criteria designed to suppress detector noise and noncollision backgrounds (described in Sec. IV). Events are rejected if no jets with $p_{\mathrm{T}} > 50$ GeV are found. The remaining events are then analyzed in two complementary searches, both of which require the presence of jets and significant missing transverse momentum. The selections in the two searches are designed to be generic enough to ensure sensitivity in a broad set of models with jets and $E_{\mathrm{T}}^{\mathrm{miss}}$ in the final state.

In order to maximize the sensitivity in the $m_{\tilde{g}}, m_{\tilde{q}}$ plane, a variety of signal regions are defined. Squarks typically generate at least one jet in their decays, for instance through $\tilde{q} \to q\tilde{\chi}_1^0$, while gluinos typically generate at least two jets, for instance through $\tilde{g} \to q\bar{q}\tilde{\chi}_1^0$. Processes contributing to $\tilde{q}\,\tilde{q}$ and $\tilde{g}\,\tilde{g}$ final states therefore lead to events containing at least two or four jets, respectively. Decays of heavy SUSY and SM particles produced in longer $\tilde{q}$ and $\tilde{g}$ decay cascades (such as those involving chargino production with subsequent decays e.g., $\tilde{\chi}_1^{\pm} \to qq'\tilde{\chi}_1^0$) tend to further increase the jet multiplicity in the final state. To target different scenarios, signal regions with different jet multiplicity requirements (in the case of Meff-based search) or different decay trees (in the case of RJR-based search) are assumed. The optimized signal regions used in both searches are summarized in the following.

A. The jets + $E_{\mathrm{T}}^{\mathrm{miss}}$ Meff-based search

Due to the high mass scale expected for the SUSY models considered in this study, the 'effective mass', m_{eff} [88], is a powerful discriminant between the signal and SM backgrounds. When selecting events with at least N_{j} jets, $m_{\mathrm{eff}}(N_{\mathrm{j}})$ is defined to be the scalar sum of the transverse momenta of the leading N_{j} jets and $E_{\mathrm{T}}^{\mathrm{miss}}$. Requirements placed on $m_{\mathrm{eff}}(N_{\mathrm{j}})$ and $E_{\mathrm{T}}^{\mathrm{miss}}$ form the basis of the Meff-based search by strongly suppressing the multijet background where jet energy mismeasurement generates missing transverse momentum. The final signal selection uses a requirement on $m_{\mathrm{eff}}(\mathrm{incl})$, which sums over all jets with $p_{\mathrm{T}} > 50$ GeV and $E_{\mathrm{T}}^{\mathrm{miss}}$ to suppress SM backgrounds, which tend to have low jet multiplicity.

Twenty-four inclusive SRs characterized by increasing the minimum jet multiplicity, from two to six, are defined in Table II: eight regions target models characterized by the squark pair production with the direct decay of squarks, seven regions target models with gluino pair production followed by the direct decay of gluinos, and nine regions target squark pair or gluino pair production followed by the one-step decay of squarks/gluinos via an intermediate chargino or neutralino. Signal regions requiring the same jet multiplicity are distinguished by increasing the threshold of the $m_{\mathrm{eff}}(\mathrm{incl})$ and $E_{\mathrm{T}}^{\mathrm{miss}}/m_{\mathrm{eff}}(N_{\mathrm{j}})$ or $E_{\mathrm{T}}^{\mathrm{miss}}/\sqrt{H_{\mathrm{T}}}$ requirements. This ensures the sensitivity to a range of sparticle masses for each decay mode. All signal regions corresponding to the Meff-based approach are labeled with the prefix "Meff." For SRs with a low number of hard jets, $E_{\mathrm{T}}^{\mathrm{miss}}/\sqrt{H_{\mathrm{T}}}$ is found to be more discriminant than $E_{\mathrm{T}}^{\mathrm{miss}}/m_{\mathrm{eff}}(N_{\mathrm{j}})$.

In each region, different requirements are applied for jet momenta and pseudorapidities. These thresholds are defined to reduce the SM background while keeping high efficiency for targeted signal events. Signal regions with high $m_{\mathrm{eff}}(\mathrm{incl})$ thresholds are optimized for large mass differences, leading to hard jets in the central region of the detector. For the SRs Meff-2j-2100, Meff-3j-1300 (and Meff-5j-1700) that are optimized for small mass differences between $\tilde{q}$ ($\tilde{g}$) and $\tilde{\chi}_1^0$, a very high p_{T} threshold is applied to the leading jet in order to explicitly tag a jet originating from initial-state radiation, which results in asymmetric p_{T} requirements on the leading jet and the other jets.

Two signal regions, Meff-2jB-1600/2400, optimized for one-step decay models are designed to improve the sensitivity to models with the cascade squark decay via $\tilde{\chi}^{\pm}$ to $qW\tilde{\chi}_1^0$ [Fig. 1(b)] or gluino decay via $\tilde{\chi}^{\pm}$ ($\tilde{\chi}_2^0$) to $qqW\tilde{\chi}_1^0$ (or $qqZ\tilde{\chi}_1^0$) [Figs. 1(e) and 1(f)], in cases where the $\tilde{\chi}^{\pm}$ ($\tilde{\chi}_2^0$) is nearly degenerate in mass with the squarks or the gluino. These signal regions place additional requirements on the mass of the large-radius jets to select the candidate hadronically decaying W or Z bosons that, due to the small mass difference between the parent SUSY particles and intermediate chargino or neutralino, can have significant transverse momentum and appear as a single high-mass jet. The signal regions Meff-5j-2000/2600 target similar models and have similar $E_{\mathrm{T}}^{\mathrm{miss}}/\sqrt{H_{\mathrm{T}}}$ and $m_{\mathrm{eff}}(\mathrm{incl})$ selections to the 2jB signal regions, filling the coverage gaps between the 2jB SRs and the other nonboosted SRs. In the other regions with at least four jets in the final state, jets from signal processes are distributed isotropically. Additional suppression of background processes is based on the aplanarity variable, which is defined as $A = 3/2\lambda_3$, where

TABLE II. Selection criteria and targeted signal models from Fig. 1 used to define signal regions in the Meff-based search, indicated by the prefix Meff. The first block of SRs targets Fig. 1(a); the second block of SRs targets Fig. 1(d). The third and fourth blocks of SRs target Figs. 1(b) and 1(e). Each SR is labeled with the inclusive jet multiplicity considered (2j, 3j etc.) together with the m_{eff} requirement. The $E_{\mathrm{T}}^{\mathrm{miss}}/m_{\mathrm{eff}}(N_{\mathrm{j}})$ cut in any N_{j}-jet channel uses a value of m_{eff} constructed from only the leading N_{j} jets [$m_{\mathrm{eff}}(N_{\mathrm{j}})$]. However, the final $m_{\mathrm{eff}}(\mathrm{incl})$ selection, which is used to define the signal regions, includes all jets with $p_{\mathrm{T}} > 50$ GeV. Large-radius reclustered jets are denoted by large-R j.

Targeted signal	$\tilde{q}\,\tilde{q}$, $\tilde{q} \to q\tilde{\chi}_1^0$							
	Signal region [Meff-]							
Requirement	2j-1200	2j-1600	2j-2000	2j-2400	2j-2800	2j-3600	2j-2100	3j-1300
$E_{\mathrm{T}}^{\mathrm{miss}}$ [GeV] >	250							
$p_{\mathrm{T}}(j_1)$ [GeV] >	250	300		350			600	700
$p_{\mathrm{T}}(j_2)$ [GeV] >	250	300		350			50	
$p_{\mathrm{T}}(j_3)$ [GeV] >				...				50
$\lvert\eta(j_{1,2})\rvert$ <	0.8		1.2				2.8	
$\Delta\phi(\mathrm{jet}_{1,2,(3)}, \vec{E})_{\mathrm{min}}$ >			0.8				0.4	
$\Delta\phi(\mathrm{jet}_{i>3}, \vec{E})_{\mathrm{min}}$ >			0.4				0.2	
$E_{\mathrm{T}}^{\mathrm{miss}}/\sqrt{H_{\mathrm{T}}}$ [GeV$^{1/2}$] >	14			18			26	16
$m_{\mathrm{eff}}(\mathrm{incl})$ [GeV] >	1200	1600	2000	2400	2800	3600	2100	1300

(Table continued)

TABLE II. *(Continued)*

Targeted signal	$\tilde{g}\tilde{g}$, $\tilde{g} \to q\bar{q}\tilde{\chi}_1^0$						
	Signal region [Meff-]						
Requirement	4j-1000	4j-1400	4j-1800	4j-2200	4j-2600	4j-3000	5j-1700
$E_{\mathrm{T}}^{\mathrm{miss}}$ [GeV] >				250			
$p_{\mathrm{T}}(j_1)$ [GeV] >			200				700
$p_{\mathrm{T}}(j_4)$ [GeV] >		100				150	50
$p_{\mathrm{T}}(j_5)$ [GeV] >			⋯				50
$\lvert\eta(j_{1,2,3,4})\rvert$ <	1.2			2.0			2.8
$\Delta\phi(\mathrm{jet}_{1,2,(3)}, \vec{E})_{\mathrm{min}}$ >				0.4			
$\Delta\phi(\mathrm{jet}_{i>3}, \vec{E}_{\mathrm{T}}^{\mathrm{miss}})_{\mathrm{min}}$ >			0.4				0.2
$E_{\mathrm{T}}^{\mathrm{miss}}/m_{\mathrm{eff}}(N_{\mathrm{j}})$ >	0.3		0.25			0.2	0.3
Aplanarity >			0.04				⋯
m_{eff}(incl) [GeV] >	1000	1400	1800	2200	2600	3000	1700

Targeted signal	$\tilde{g}\tilde{g}$, $\tilde{g} \to q\bar{q}W\tilde{\chi}_1^0$ and $\tilde{q}\tilde{q}$, $\tilde{q} \to qW\tilde{\chi}_1^0$						
	Signal region [Meff-]						
Requirement	5j-1600	5j-2000	5j-2600	6j-1200	6j-1800	6j-2200	6j-2600
$E_{\mathrm{T}}^{\mathrm{miss}}$ [GeV] >				250			
$p_{\mathrm{T}}(j_1)$ [GeV] >				200			
$p_{\mathrm{T}}(j_5)$ [GeV] >			50			100	
$p_{\mathrm{T}}(j_6)$ [GeV] >		⋯		50		100	
$\lvert\eta(j_{1,\ldots,6})\rvert$ <		2.8			2.0		2.8
$\Delta\phi(\mathrm{jet}_{1,2,(3)}, \vec{E}_{\mathrm{T}}^{\mathrm{miss}})_{\mathrm{min}}$ >	0.4		0.8		0.4		
$\Delta\phi(\mathrm{jet}_{i>3}, \vec{E}_{\mathrm{T}}^{\mathrm{miss}})_{\mathrm{min}}$ >	0.2	0.4			0.2		
$E_{\mathrm{T}}^{\mathrm{miss}}/m_{\mathrm{eff}}(N_{\mathrm{j}})$ >	0.15	⋯		0.25	0.2		0.15
$E_{\mathrm{T}}^{\mathrm{miss}}/\sqrt{H_{\mathrm{T}}}$ [GeV$^{1/2}$] >	⋯	15	18		⋯		
Aplanarity >	0.08		⋯		0.04	0.08	
m_{eff}(incl) [GeV] >	1600	2000	2600	1200	1800	2200	2600

Targeted signal	$\tilde{g}\tilde{g}$, $\tilde{g} \to q\bar{q}W\tilde{\chi}_1^0$ and $\tilde{q}\tilde{q}$, $\tilde{q} \to qW\tilde{\chi}_1^0$	
	Signal region [Meff-]	
Requirement	2jB-1600	2jB-2400
$E_{\mathrm{T}}^{\mathrm{miss}}$ [GeV] >	250	
p_{T}(large-Rj_1) [GeV] >	200	
p_{T}(large-Rj_2)[GeV] >	200	
m(large-Rj_1) [GeV]	[60,110]	
m(large-Rj_2) [GeV]	[60,110]	
$\Delta\phi(\mathrm{jet}_{1,2,(3)}, \vec{E})_{\mathrm{min}}$ >	0.6	
$\Delta\phi(\mathrm{jet}_{i>3}, \vec{E})_{\mathrm{min}}$ >	0.4	
$E_{\mathrm{T}}^{\mathrm{miss}}/\sqrt{H_{\mathrm{T}}}$ [GeV$^{1/2}$] >	20	
m_{eff}(incl) [GeV] >	1600	2400

λ_3 is the smallest eigenvalue of the normalized momentum tensor of the jets [89].

To reduce the background from multijet processes, requirements are placed on two variables: $\Delta\phi(\mathrm{jet}, \vec{E})_{\mathrm{min}}$ and $E_{\mathrm{T}}^{\mathrm{miss}}/m_{\mathrm{eff}}(N_{\mathrm{j}})$. The former is defined to be the smallest azimuthal separation between $\vec{E}_T^{\mathrm{miss}}$ and the momentum vector of any of the reconstructed jets with $p_{\mathrm{T}} > 50$ GeV. The exact requirements, which depend on the jet multiplicity in each SR, are summarized in Table II, where the criteria for all the Meff-based signal regions can also be found.

B. The jets + $E_{\mathrm{T}}^{\mathrm{miss}}$ RJR-based search

The procedure adopted is such that, as the mass splitting between parent sparticle and the LSP increases, the criteria applied to the scale variables are tightened, while the

criteria for dimensionless variables are loosened. In searching for the squark pair production, the overall balance of the events is studied with $H_{1,1}^{PP}/H_{2,1}^{PP}$. The range selected in this ratio rejects those events where the missing transverse momentum dominates the scale (upper bound) and ensures the sufficient balance between the scales of visible and invisible particles (lower bound). The selection on the $p_{\mathrm{Tj2}}^{PP}/H_{\mathrm{T2},1}^{PP}$ ratio serves to ensure that each of the jets contributes to the overall scale significantly. This particular ratio is a powerful criterion against imbalanced events with

TABLE III. Selection criteria and targeted signal model from Fig. 1 used to define signal regions in the RJR-based search, indicated by the prefix RJR. Each SR is labeled with the targeted SUSY particle or the targeted region of parameter space, such that S, G, and C denote search regions for squark pairs, gluino pairs, or compressed spectra, respectively.

Targeted signal	$\tilde{q}\,\tilde{q}$, $\tilde{q} \to q\tilde{\chi}_1^0$			
	Signal region			
Requirement	RJR-S1	RJR-S2	RJR-S3	RJR-S4
$H_{1,1}^{PP}/H_{2,1}^{PP} \geq$	0.55	0.5	0.45	···
$H_{1,1}^{PP}/H_{2,1}^{PP} \leq$	0.9	0.95	0.98	···
$p_{\mathrm{Tj2}}^{PP}/H_{\mathrm{T2},1}^{PP} \geq$	0.16	0.14	0.13	0.13
$\lvert\eta_{\mathrm{j1,j2}}\rvert \leq$	0.8	1.1	1.4	2.8
$\Delta_{\mathrm{QCD}} \geq$	0.1	0.05	0.025	0
$p_{PP,\mathrm{T}}^{\mathrm{lab}}/(p_{PP,\mathrm{T}}^{\mathrm{lab}} + H_{\mathrm{T2},1}^{PP}) \leq$		0.08		

	RJR-S1a	RJR-S1b	RJR-S2a	RJR-S2b	RJR-S3a	RJR-S3b	RJR-S4
$H_{\mathrm{T2},1}^{PP}$ [GeV] >	1000	1200	1400	1600	1800	2100	2400
$H_{1,1}^{PP}$ [GeV] >	800	1000	1200	1400	1700	1900	2100

Targeted signal	$\tilde{g}\,\tilde{g}$, $\tilde{g} \to q\bar{q}\tilde{\chi}_1^0$			
	Signal region			
Requirement	RJR-G1	RJR-G2	RJR-G3	RJR-G4
$H_{1,1}^{PP}/H_{4,1}^{PP} \geq$	0.45	0.3	0.2	···
$H_{\mathrm{T4},1}^{PP}/H_{4,1}^{PP} \geq$	0.7	0.7	0.65	0.65
min $(p_{\mathrm{Tj2}i}^{PP}/H_{\mathrm{T2},1i}^{PP}) \geq$	0.12	0.1	0.08	0.07
max $(H_{1,0}^{P_i}/H_{2,0}^{P_i}) \leq$	0.96	0.97	0.98	0.98
$\lvert\eta_{\mathrm{j1,2},a,b}\rvert \leq$	1.4	2.0	2.4	2.8
$\Delta_{\mathrm{QCD}} \geq$	0.05	0.025	0	0
$p_{PP,z}^{\mathrm{lab}}/(p_{PP,z}^{\mathrm{lab}} + H_{\mathrm{T4},1}^{PP}) \leq$	0.5	0.55	0.6	0.65
$p_{PP,\mathrm{T}}^{\mathrm{lab}}/(p_{PP,\mathrm{T}}^{\mathrm{lab}} + H_{\mathrm{T4},1}^{PP}) \leq$		0.08		

	RJR-G1a	RJR-G1b	RJR-G2a	RJR-G2b	RJR-G3a	RJR-G3b	RJR-G4
$H_{\mathrm{T4},1}^{PP}$ [GeV] >	1200	1400	1600	2000	2400	2800	3000
$H_{1,1}^{PP}$ [GeV] >	700		800		900		1000

Targeted signal	Compressed spectra in $\tilde{q}\,\tilde{q}$ ($\tilde{q} \to q\tilde{\chi}_1^0$); $\tilde{g}\,\tilde{g}$ ($\tilde{g} \to q\bar{q}\tilde{\chi}_1^0$)				
	Signal region				
Requirement	RJR-C1	RJR-C2	RJR-C3	RJR-C4	RJR-C5
$R_{\mathrm{ISR}} \geq$	0.95	0.9	0.8	0.7	0.7
p_{TS}^{CM} [GeV] $\geq$	1000	1000	800	700	700
$\Delta\phi_{\mathrm{ISR},I}/\pi \geq$	0.95	0.97	0.98	0.95	0.95
$\Delta\phi(\mathrm{jet}_{1,2}, \vec{E}_{\mathrm{T}}^{\mathrm{miss}})_{\mathrm{min}} >$	···	···	···	0.4	0.4
M_{TS} [GeV] $\geq$	···	100	200	450	450
$N_{\mathrm{jet}}^{V} \geq$	1	1	2	2	3
$\lvert\eta_{\mathrm{j}V}\rvert \leq$	2.8	1.2	1.4	1.4	1.4

W/Z + jets, where one of the jets has a much higher momentum than the subleading jet.

For signals of gluino pair production, the same principles are followed. Tight requirements are placed on $H^{PP}_{1,1}/H^{PP}_{4,1}$ and $H^{PP}_{\mathrm{T4},1}/H^{PP}_{4,1}$ to target scenarios with more compressed spectra. A selection is applied to the ratio $p^{\mathrm{lab}}_{PP,z}/(p^{\mathrm{lab}}_{PP,z}+H^{PP}_{\mathrm{T4},1})$ to test the size of the total z-component of momentum relative to the overall scale, requiring that it should be small. A lower bound is placed on $p^{PP}_{\mathrm{Tj2}}/H^{PP}_{\mathrm{T2},1}$. This provides a very strong constraint against events where the two hemispheres are well balanced but one of the jets dominates the scale variable contribution. In order to reject events where the $E^{\mathrm{miss}}_{\mathrm{T}}$ results from mismeasurements of jets, a requirement on the variable Δ_{QCD} is applied, rejecting events where this is deemed likely.

Additionally, separate SRs are defined for models with extremely compressed spectra. Following the pattern of successive SRs targeting larger mass splitting scenarios, several regions designed to be sensitive to various mass splittings utilize the ISR-boosted compressed decay tree described in Sec. VI. These regions target mass splittings between parent squarks and gluinos and $\tilde{\chi}^0_1$ from roughly 25 to 200 GeV.

The selection criteria of the resulting 19 signal regions are summarized in Table III. The entries for $|\eta_{\mathrm{j1,j2}}|$ and $|\eta_{\mathrm{j1,2},a,b}|$ correspond to upper bounds on the pseudorapidities of the leading two jets in each event and the leading two jets in each hemisphere a, b, respectively, while $|\eta_{\mathrm{j}V}|$ corresponds to the jets associated with the system V. All signal regions included in the RJR-based search have an RJR prefix.

C. Meff-based and RJR-based signal region comparison

Even though the selection requirements that define the Meff-based and RJR-based SRs use different sets of kinematic observables, the regions are not necessarily orthogonal. The fraction of events common to different regions, for both the SM backgrounds and the SUSY signals, reflects the complementarity of using these two approaches. For models with large $\tilde{q}/\tilde{g}$ masses, the signal efficiency is prioritized due to low production cross sections. In these cases, stringent requirements on the similarly behaving m_{eff} and $H^{PP}_{\mathrm{T2},1}/H^{PP}_{\mathrm{T4},1}$ variables result in a larger overlap between the Meff-based and RJR-based signal regions. Conversely, signal regions designed for increasingly compressed mass spectra have looser m_{eff} and $H^{PP}_{\mathrm{T2},1}/H^{PP}_{\mathrm{T4},1}$, and backgrounds must be suppressed with other, complementary, kinematic requirements. As these additional kinematic observables can be quite different between Meff-based and RJR-based approaches, the orthogonality of these respective SRs increases with decreasing sparticle mass splittings.

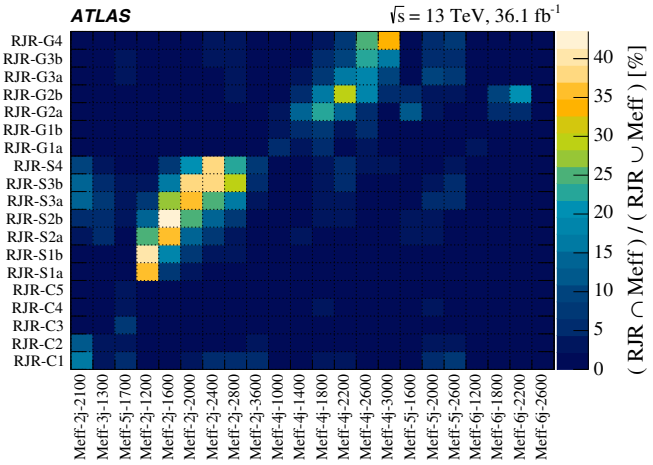

FIG. 3. Fractional overlap of data events selected in Meff-based and RJR-based SRs. Meff-based SRs are listed along the x axis with RJR-based regions on the y axis. The intersection events falling in each pair of regions, normalized by the union, is shown on the z axis. The Meff-based boosted boson SRs (Meff-2jB-1600,Meff-2jB-2400) are not included as they have negligible overlap with other regions due to their unique requirements.

This behavior can be observed in Fig. 3, which shows the fractional overlap of selected events in data between the Meff-based and RJR-based SRs. Each of the axes listing the various SRs are organized in the same order, with SRs targeting compressed mass spectra in the lower left of the figure, followed by squark regions with increasing sparticle masses, and then gluinos with increasing mass. This ordering results in a diagonal pattern of larger overlap, as SRs targeting the same signals are more similar. The SRs searching for evidence of squark production (RJR-Sx and Meff-2j-x) have fractions of overlapping events between 25% and 45%, while those targeting gluino production (RJR-Gx and Meff-4j-x) have smaller intersections, ranging from a few percent to 35%. This decrease in overlap for gluino SRs follows from increasing differences between the selections used in the Meff-based and RJR-based approaches. While observables such as $E^{\mathrm{miss}}_{\mathrm{T}}/m_{\mathrm{eff}}(N_{\mathrm{j}})$ and aplanarity are sensitive to global event properties, the RJR-based analysis for gluinos attempts to decompose the event into two hemispheres representing each gluino. Kinematic variables used in the definitions of SRs are calculated from each hemisphere independently, providing complementarity to those describing the total event. Using this additional information in the RJR-based selections leads to generally tighter SRs, adding increased sensitivity for intermediate mass splittings.

Similar trends in event overlaps between SRs are expected for signal contributions, as shown in Figs. 4(a) and 4(b) where a simulated squark signal with $m_{\tilde{q}} = 1.5$ TeV and massless $\tilde{\chi}^0_1$, and a gluino signal with $m_{\tilde{g}} = 2$ TeV and massless $\tilde{\chi}^0_1$ are used as examples. In these cases, the SRs targeting squarks and gluinos share a large

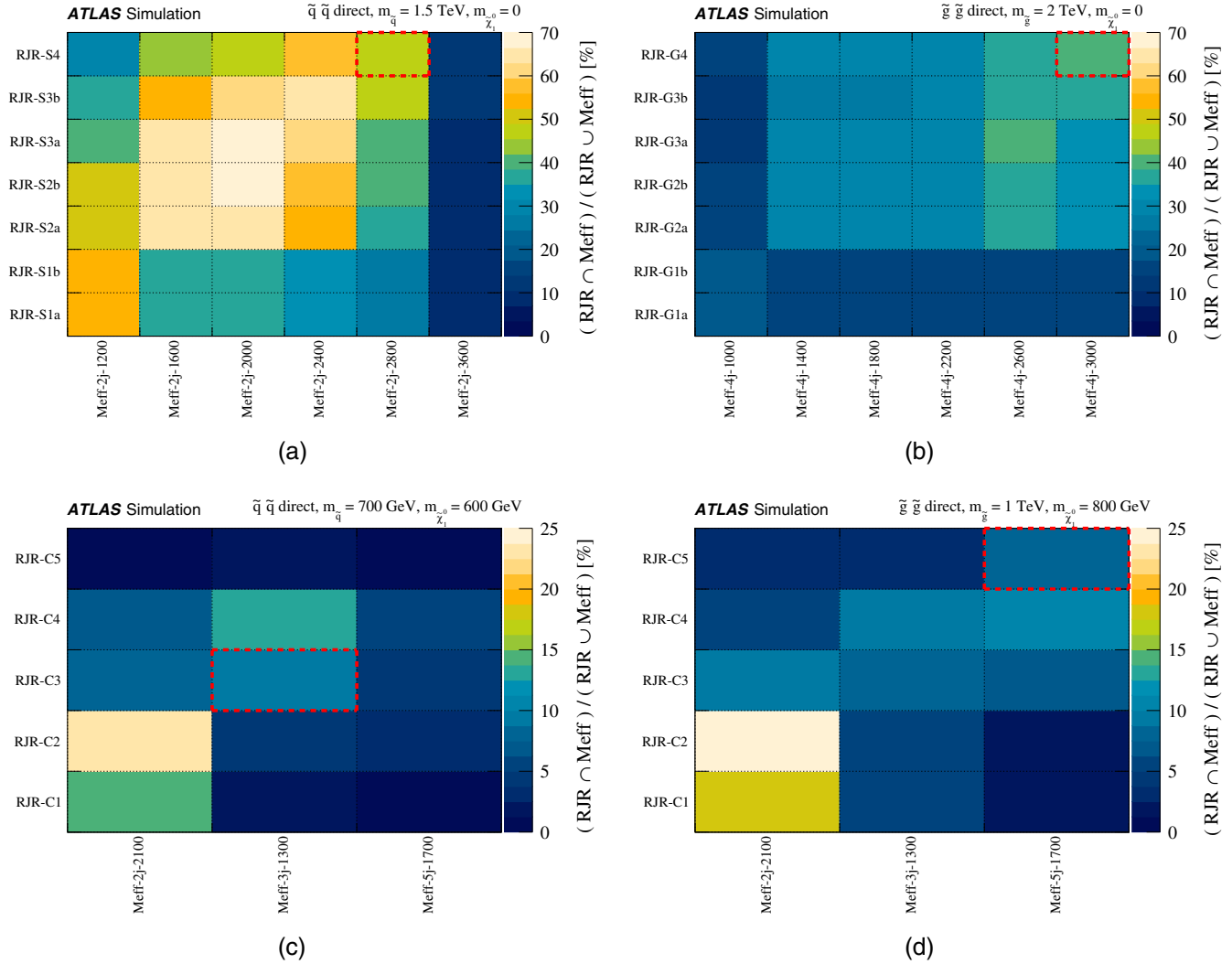

FIG. 4. Fractional overlap of simulated squark and gluino pair events selected in Meff-based and RJR-based SRs. For these signals each squark (gluino) decays to one (two) quarks and a $\tilde{\chi}_1^0$. Figures correspond to simulated signals with (a) $m_{\tilde{q}} = 1.5$ TeV, $m_{\tilde{\chi}_1^0} = 0$, (b) $m_{\tilde{g}} = 2$ TeV, $m_{\tilde{\chi}_1^0} = 0$, (c) $m_{\tilde{q}} = 700$ GeV, $m_{\tilde{\chi}_1^0} = 600$ GeV, and (d) $m_{\tilde{g}} = 1$ TeV, $m_{\tilde{\chi}_1^0} = 800$ GeV. These selected signal points are near the limit of expected sensitivity for these SRs. Meff-based SRs are listed along the x axis with RJR-based regions on the y axis. The intersection events falling in each pair of regions, normalized by the union, is shown on the z axis. The Meff- and RJR-based SRs best suited to each signal, respectively, are indicated by dashed red boxes.

fraction of their events, with the RJR-S4 and Meff-2j-2800 regions best suited to this squark signal having 45% of selected events in common and the analogous gluino SRs (RJR-G4 and Meff-4j-3000) having an overlap of 40%. In the case of a squark signal, the largest overlap of 65% is seen with the RJR-S2a and Meff-2j-1600, with smaller overlap between tighter SRs favored for this signal point.

The RJR-Cx SRs targeting signals with the most compressed mass spectra ($0 < m_{\tilde{q}/\tilde{g}} - m_{\tilde{\chi}_1^0} \lesssim 200$ GeV) are the most dissimilar from their Meff-based analogs. They attempt to explicitly identify the strong initial-state radiation system that provides the escaping $\tilde{\chi}_1^0$ pair the $E_{\mathrm{T}}^{\mathrm{miss}}$ needed to satisfy trigger and selection requirements and use kinematic requirements based on this interpretation of the event. The Meff-based SRs designed for these signals (Meff-2j-2100/3j-1300/5j-1700) exploit this compressed-mass-spectra event topology by requiring large $E_{\mathrm{T}}^{\mathrm{miss}}/\sqrt{H_{\mathrm{T}}}$ or large $E_{\mathrm{T}}^{\mathrm{miss}}/m_{\mathrm{eff}}(N_{\mathrm{j}})$ and a hard leading jet corresponding to the ISR system, and the modest m_{eff} requirements result in SRs with relatively large expected background yields and low systematic uncertainties. The RJR-Cx SRs take a more restrictive approach, using observables designed specifically for this ISR event topology, with the corresponding SRs having much lower event yields, higher signal-to-background ratios, but larger uncertainties. This results in much smaller event overlap for both signal and background, as seen in Figs. 4(c) and 4(d) for an example simulated squark signal with $m_{\tilde{q}} = 700$ GeV and

$m_{\tilde{\chi}_1^0} = 600$ GeV, and a gluino signal with $m_{\tilde{g}} = 1$ TeV and $m_{\tilde{\chi}_1^0} = 800$ GeV. For these signals, the overlap between the best-suited SRs (RJR-C3 and Meff-3j-1300 for the squark signal, RJR-C5 and Meff-5j-1700 for the gluino) is only about 10%. On the other hand, 65% (35%) of the signal events in RJR-C3 (RJR-C4) are also selected in Meff-3j-1300 (Meff-5j-1700). The more stringent selection strategy employed in the RJR-Cx regions leads to increased sensitivity for compressed mass spectra for each of the signal variants considered in this analysis.

VIII. BACKGROUND ESTIMATION

Standard Model background processes contribute to the event counts in the signal regions. The largest backgrounds in both searches presented here are $Z+$jets, $W+$jets, top quark pair, single top quark, diboson, and multijet production. Noncollision backgrounds are negligible.

Generally, the largest background results from an irreducible component of $Z+$jets events in which $Z \to \nu\bar{\nu}$ decays generate large $E_{\mathrm{T}}^{\mathrm{miss}}$. Similarly, most of the $W+$jets background is composed of $W \to \tau\nu$ events in which the τ-lepton decays to hadrons, with additional contributions from $W \to e\nu, \mu\nu$ events in which no baseline electron or muon is reconstructed, with $E_{\mathrm{T}}^{\mathrm{miss}}$ due to neutrinos. Top quark pair production, followed by semileptonic decays, in particular $t\bar{t} \to b\bar{b}\tau\nu qq'$ (with the τ-lepton decaying to hadrons), as well as single-top-quark events, can also generate large $E_{\mathrm{T}}^{\mathrm{miss}}$ and satisfy the jet and lepton-veto requirements. Each of these primary backgrounds is estimated using dedicated control regions, as described in the following section, while diboson production is estimated with MC simulated data normalized using NLO cross section predictions, as described in Sec. III.

The multijet background in the signal regions is due to missing transverse momentum from misreconstruction of jet energies in the calorimeters, jets misidentified as electrons, jets lost due to the JVT requirement, as well as neutrinos from semileptonic decays of heavy-flavor hadrons. After applying the requirements based on $\Delta\phi(\mathrm{jet}, \vec{E})_{\mathrm{min}}$ and $E_{\mathrm{T}}^{\mathrm{miss}}/m_{\mathrm{eff}}(N_j)$ in the Meff-based search, or Δ_{QCD}, $p_{\mathrm{Tj2}}^{PP}/H_{\mathrm{T2,1}}^{PP}$ and $\Delta\phi(\mathrm{jet}, \vec{E})_{\mathrm{min}}$ in the RJR-based search, as indicated in Tables II and III, the remaining multijet background is negligible.

A. Control regions

In order to estimate the expected background yields, control regions are defined for each of the signal regions in four different final states. In the Meff-based search, each SR has its own set of four CRs, while in the RJR-based search, a common set of CRs is used for all SRs in every targeted signal category (RJR-S, RJR-G or RJR-C). The CR selections are optimized to maintain adequate statistical precision while minimizing the systematic uncertainties arising from the extrapolation of the CR event yield to estimate the background in the SR. The latter is addressed through the fact that the jet p_{T} thresholds and $m_{\mathrm{eff}}(\mathrm{incl})$ selections in the CRs are the same as those used for the SR in the Meff-based search. In the RJR-based search, requirements on discriminating variables are chosen to match those used in the SRs as closely as possible. The basic CR definitions in both searches are listed in Table IV.

The $\gamma+$jets region in both searches (labeled as Meff/RJR-CRγ in Table IV) is used to estimate the contribution of $Z(\to \nu\bar{\nu})+$jets background events to each SR by selecting a sample of $\gamma+$jets events with $p_{\mathrm{T}}(\gamma) > 150$ GeV and then treating the reconstructed photon as invisible in the $E_{\mathrm{T}}^{\mathrm{miss}}$ calculation. For $p_{\mathrm{T}}(\gamma)$ significantly larger than m_Z the kinematic properties of such events strongly resemble those of $Z+$jets events [90]. In order to reduce the theoretical uncertainties associated with the Z/γ^*+jets background predictions in SRs arising from the use of LO $\gamma+$jets cross sections, a correction factor is applied to the Meff/RJR-CRγ events as a function of the requirement on the number of jets. This correction factor, κ, ranges from 1.41 to 2.26 for two to six jets, and is determined by comparing Meff-CRγ observations with those in a highly populated auxiliary control region defined by selecting events with two electrons or muons for which

TABLE IV. Summary of CRs for the Meff-based and RJR-based searches. Also listed are the main targeted SR backgrounds in each case, the process used to model the background, and the main CR requirement(s) used to select this process. The transverse momenta of high-purity leptons (photons) used to select CR events must exceed 27 (150) GeV. The jet p_{T} thresholds and $m_{\mathrm{eff}}(\mathrm{incl})$ selections match those used in the corresponding SRs of the Meff-based search. For the RJR-based search, selections are based on the discriminating variables used in the SRs, as described in the text.

CR	SR background	CR process	CR selection (Meff-based)	CR selection (RJR-based)
Meff/RJR-CRγ	$Z(\to \nu\bar{\nu})+$jets	$\gamma+$jets	Isolated photon	Isolated photon
Meff/RJR-CRQ	Multi-jet	Multi-jet	SR with reversed requirements on (i) $\Delta\phi(\mathrm{jet}, \vec{E})_{\mathrm{min}}$ and (ii) $E_{\mathrm{T}}^{\mathrm{miss}}/m_{\mathrm{eff}}(N_j)$ or $E_{\mathrm{T}}^{\mathrm{miss}}/\sqrt{H_{\mathrm{T}}}$	$\Delta_{\mathrm{QCD}} < 0$ reversed requirement on $H_{1,1}^{PP}$ (RJR-S/G) or $R_{\mathrm{ISR}} < 0.5$ (RJR-C)
Meff/RJR-CRW	$W(\to \ell\nu)+$jets	$W(\to \ell\nu)+$jets	30 GeV $< m_{\mathrm{T}}(\ell, E_{\mathrm{T}}^{\mathrm{miss}}) <$ 100 GeV, b-veto	
Meff/RJR-CRT	$t\bar{t}(+\mathrm{EW})$ and single top	$t\bar{t} \to b\bar{b}qq'\ell\nu$	30 GeV $< m_{\mathrm{T}}(\ell, E_{\mathrm{T}}^{\mathrm{miss}}) <$ 100 GeV, b-tag	

the invariant mass lies within 25 GeV of the mass of the Z boson, satisfying $E_{\mathrm{T}}^{\mathrm{miss}} > 250$ GeV, $E_{\mathrm{T}}^{\mathrm{miss}}/\sqrt{H_{\mathrm{T}}} > 14\ \mathrm{GeV}^{1/2}$ and $m_{\mathrm{eff}}(\mathrm{incl}) > 1200$ GeV where two leptons are treated as contributing to $E_{\mathrm{T}}^{\mathrm{miss}}$.

The W and top regions in both searches (labeled as Meff/RJR-CRW and Meff/RJR-CRT in Table IV) aim to select samples rich in $W(\to \ell\nu)+\mathrm{jets}$ and semileptonic $t\bar{t}$ background events, respectively. They use events with one high-purity lepton with $p_{\mathrm{T}} > 27$ GeV and differ in their number of b-jets (zero or ≥ 1, respectively). In both searches, the requirement on the transverse mass m_{T} formed by the $E_{\mathrm{T}}^{\mathrm{miss}}$ and a selected lepton is applied, as indicated in Table IV. The lepton is treated as a jet with the same momentum to model background events in which a hadronically decaying τ-lepton is produced. This estimation procedure is used to try to get a better idea of the $W(\to \ell\nu)+\mathrm{jets}$ and $t\bar{t}$ cross section in a restricted kinematic phase space, by normalizing the MC to the data for the electron and muon channels, respectively. The propagation of the number of background events from the control region to the signal region is done purely by Monte Carlo which takes into account the impact of all the differences in selection criteria between the control and signal regions. The Meff-CRW and Meff-CRT criteria omit the SR selection requirements on $|\eta_{\mathrm{jet}}|$, $\Delta\phi(\mathrm{jet}, \vec{E})_{\mathrm{min}}$ and aplanarity for all SRs, while for the SRs requiring $m_{\mathrm{eff}}(\mathrm{incl}) > 2200$ GeV the requirements on $E_{\mathrm{T}}^{\mathrm{miss}}/m_{\mathrm{eff}}(N_{\mathrm{j}})$ are not applied. This is done in order to increase the number of CR data events without significantly increasing the theoretical uncertainties associated with the CR-to-SR extrapolation in the background estimation procedure.

The multijet background in both searches is estimated using a data-driven technique [90], which applies a resolution function to well-measured multijet events in order to estimate the impact of jet energy mismeasurement and heavy-flavor semileptonic decays on $E_{\mathrm{T}}^{\mathrm{miss}}$ and other variables. The resolution function of jets is initially estimated from MC simulation by matching "truth" jets reconstructed from generator-level particles including muons and neutrinos to detector-level jets with $\Delta R < 0.1$ in multijet samples, and then is modified to agree with data in dedicated samples to measure the resolution function. The Meff-CRQ region uses reversed selection requirements on $\Delta\phi(\mathrm{jet}, \vec{E})_{\mathrm{min}}$ and on $E_{\mathrm{T}}^{\mathrm{miss}}/m_{\mathrm{eff}}(N_{\mathrm{j}})$ (or $E_{\mathrm{T}}^{\mathrm{miss}}/\sqrt{H_{\mathrm{T}}}$ where appropriate) to produce samples enriched in multijet background events.

In the RJR-based search, all CRs corresponding to RJR-S (RJR-G) SRs are required to satisfy $H_{1,1}^{PP} > 800\,(700)$ GeV. Additionally, $H_{\mathrm{T2},1}^{PP} > 1000$ GeV (for RJR-S), $H_{\mathrm{T4},1}^{PP} > 1200$ GeV (for RJR-G), and $M_{TS} > 0$ (for RJR-C) are required for RJR-CRW, RJR-CRT and RJR-CRQ regions. In RJR-CRW and RJR-CRT, the requirements on all the other variables used for the RJR-SR selections are chosen such that the loosest value in the SR category (RJR-S, RJR-G, or RJR-C) indicated in Table III is used. No requirement on $p_{PP,z}^{\mathrm{lab}}/(p_{PP,z}^{\mathrm{lab}} + H_{\mathrm{TN},1}^{PP})$ is used for the RJR-CRQ selections in all RJR-SRs, where $N = 2$ or 4.

The normalization factors determined from the background-only fits in each CR for each background process are shown in Fig. 5. Some trends in these factors are observed, with the normalization factors for top background becoming smaller with increasingly tight m_{eff} requirements for the Meff-based regions. Similarly, the measured top normalization factors decrease with increasingly tight M_{TS} and N_{jet}^{V} requirements in the RJR-based

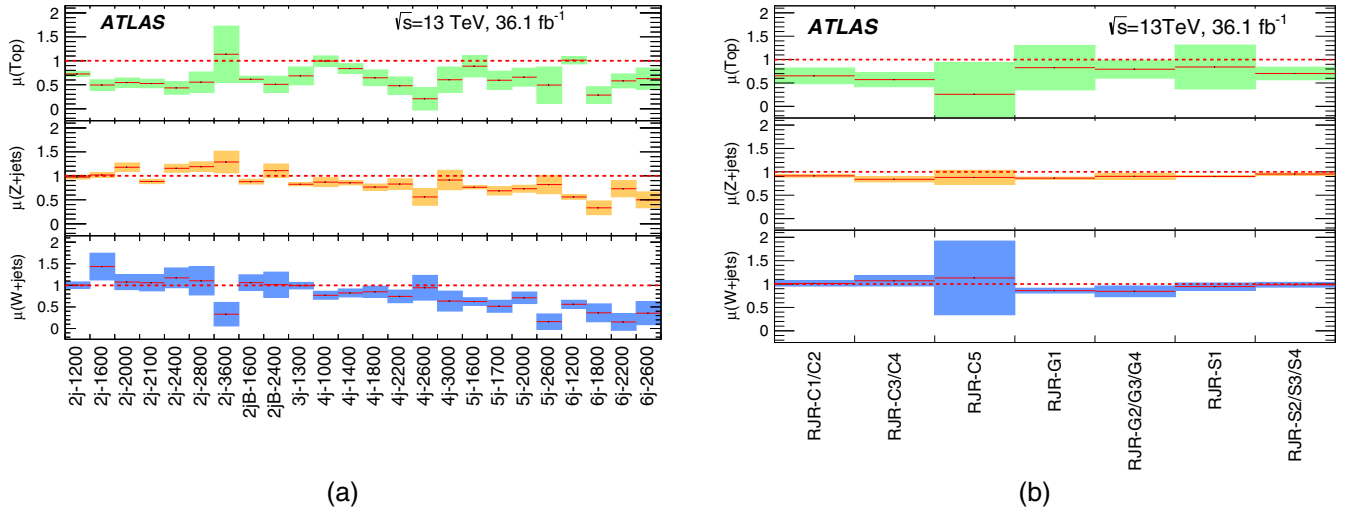

FIG. 5. Fitted normalization factor per process as a function of the channel considered in the (a) Meff-based and (b) RJR-based searches. The dashed horizontal lines at 1 correspond to pure MC estimates with the vertical size of the colored regions corresponding to the total uncertainty in each background source.

search. This behavior follows from the simulated top MC samples exhibiting generally harder kinematics than observed in data, as seen in Figs. 6(d) and 7(d). The normalization factors for $W+$ jets and $Z+$ jets processes are generally stable with changing kinematic selections but with a clear indication that they become systematically smaller with increasingly strict requirements on the jet multiplicity. This is due to the MC simulation

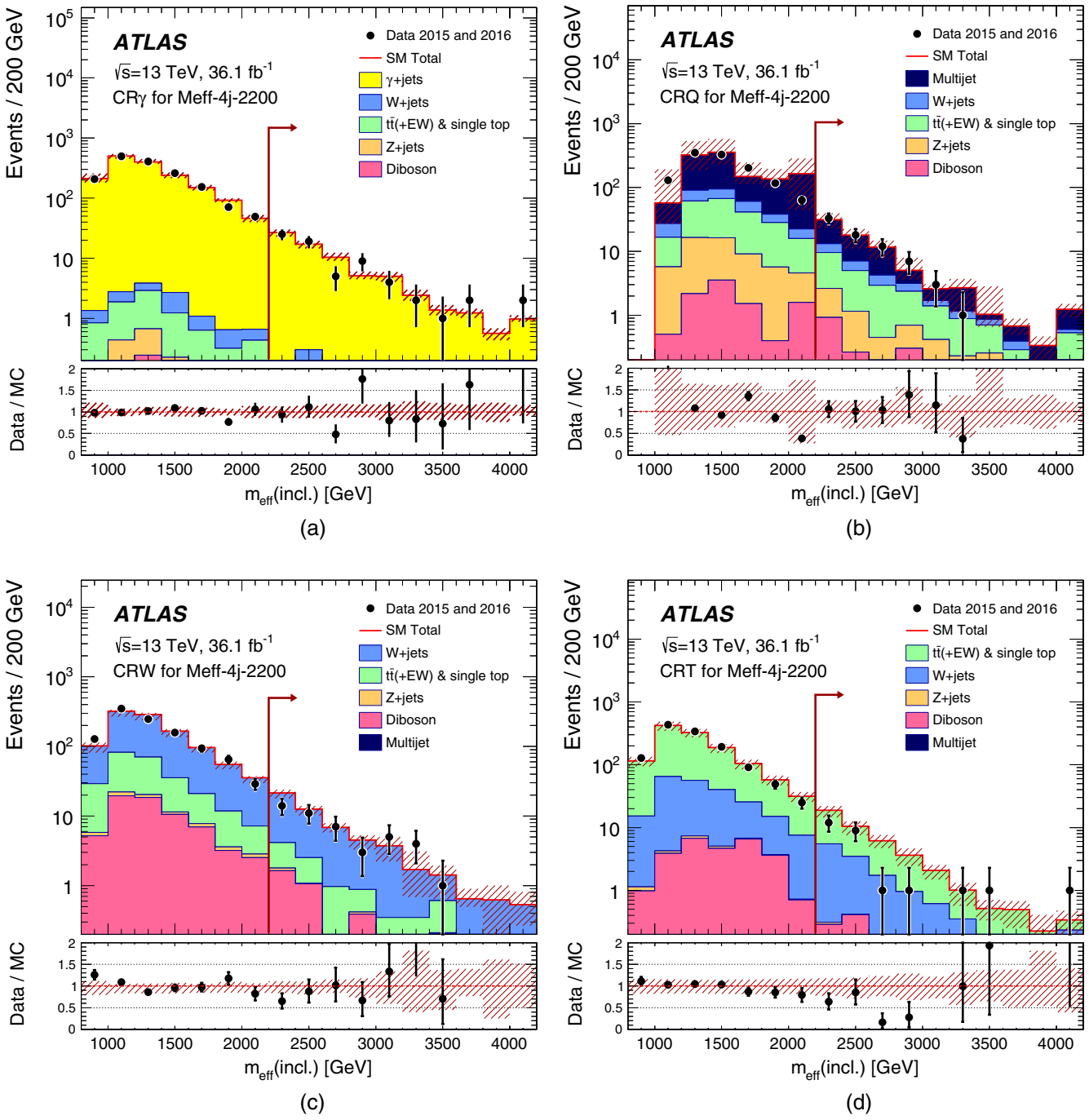

FIG. 6. Observed $m_{\mathrm{eff}}(\mathrm{incl})$ distributions in control regions (a) Meff-CRγ, (b) Meff-CRQ, (c) Meff-CRW, and (d) Meff-CRT after applying the Meff-4j-2200 selection requirements listed in Table II, except those on the plotted variable. No selection requirements on $\Delta\phi(\mathrm{jet}, \vec{E})_{\mathrm{min}}$ are applied in Meff-CRW and Meff-CRT regions. The arrows indicate the values at which the requirements on $m_{\mathrm{eff}}(\mathrm{incl})$ are applied. The histograms show the MC background predictions, normalized using cross section times integrated luminosity and the dominant process in each CR is normalized using data. In the case of the $\gamma+$ jets background, a κ factor described in the text is applied. The last bin includes overflow events. The hatched (red) error bands indicate the combined experimental, MC statistical and theoretical modeling uncertainties.

predicting jet multiplicities higher than observed in data events.

Example $m_{\text{eff}}(\text{incl})$ distributions in control regions associated with Meff-4j-2200 selections are shown in Fig. 6. Figure 7 shows the p_{TS}^{CM} discriminating variable distributions in control regions corresponding to RJR-C1 signal region selections. In all CRs, the data distributions are consistent with the MC background prediction within uncertainties after normalizing the dominant process in each CR.

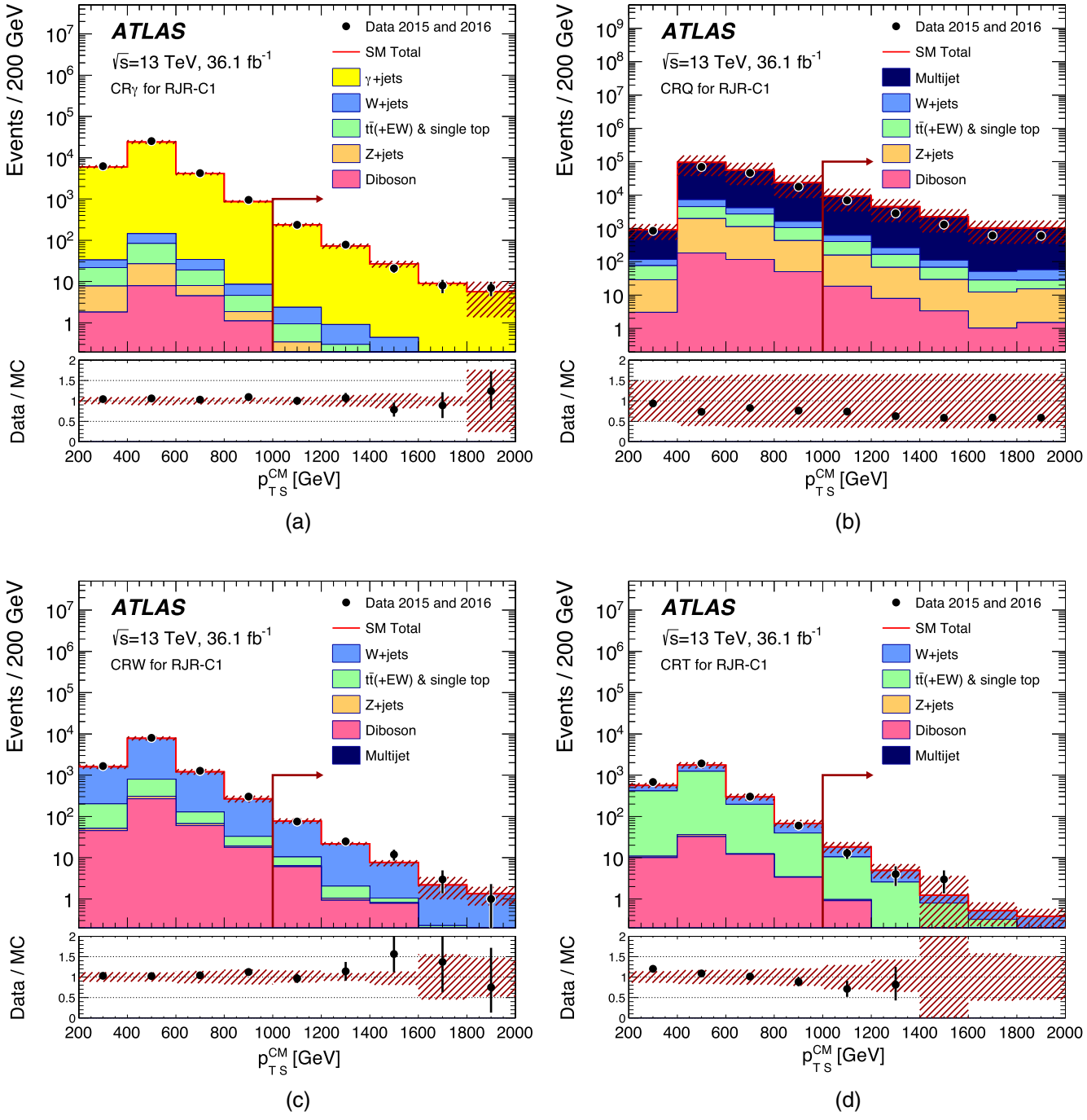

FIG. 7. Observed p_{TS}^{CM} distribution in control regions (a) RJR-CRγ, (b) RJR-CRQ, (c) RJR-CRW, and (d) RJR-CRT after selecting events for the corresponding control regions as explained in the text for RJR-C1 region and after applying all selection requirements except those on the plotted variable. The arrows indicate the values at which the requirements are applied. The histograms show the MC background predictions, normalized using cross section times integrated luminosity and the dominant process in each CR is normalized using data. In the case of γ + jets background, a κ factor described in the text is applied. The last bin includes overflow events. The hatched (red) error bands indicate the combined experimental, MC statistical and theoretical modeling uncertainties.

B. Validation regions

The background estimation procedure is validated by comparing the numbers of events observed in the VRs to the corresponding SM background predictions obtained from the background-only fits. Several VRs are defined in both searches, with requirements distinct from those used in the CRs and that maintain low expected signal contamination. Like the CRs, the majority of the VRs are defined in final states with leptons and photons, allowing the different expected background contributions to the SRs to be validated almost separately with high-purity selections.

The Meff/RJR-CRγ estimates of the $Z(\to \nu\bar{\nu}) + \text{jets}$ background are validated using samples of $Z(\to \ell\bar{\ell}) + \text{jets}$ events selected by requiring high-purity lepton pairs of opposite sign and identical flavor for which the dilepton invariant mass lies within 25 GeV of the Z boson mass (Meff/RJR-VRZ). In Meff/RJR-VRZ regions, the leptons are treated as contributing to $E_{\mathrm{T}}^{\mathrm{miss}}$. Additional VRs designed to validate the $Z(\to \nu\bar{\nu}) + \text{jets}$ estimate in the RJR-based search are also used: the VRZc region, which selects events with no leptons but inverts the $\Delta\phi_{\mathrm{ISR},I}$ requirement of the SR selection (Table III) and VRZca, which further loosens some other criteria to match the RJR-CRW and RJR-CRT regions. The VRZc regions have a purity of $Z(\to \nu\bar{\nu}) + \text{jets}$ of 50%–70%. In order to increase yields in the dilepton final state RJR-VRZ regions, two additional regions, RJR-VRZa and RJR-VRZb are constructed with $H_{1,1}^{PP}$ and $H_{\mathrm{T2},1}^{PP}$ (or $H_{\mathrm{T4},1}^{PP}$ where appropriate) loosened, respectively, relative to the values used for the RJR-CRW and RJR-CRT regions.

The Meff-CRW and Meff-CRT estimates of the $W + \text{jets}$ and top quark background are validated with the same Meff-CRW and Meff-CRT selections, but applying the $\Delta\phi(\text{jet}, \vec{E})_{\mathrm{min}}$ requirement and treating the lepton as a jet (Meff-VRW, Meff-VRT). To further validate the extrapolation over the $\Delta\phi(\text{jet}, \vec{E})_{\mathrm{min}}$ and aplanarity variables from the dedicated $W + \text{jets}$ and top quark CRs to the SRs, additional validation regions Meff-VRW$\Delta\Phi$ and Meff-VRT$\Delta\Phi$ as well as Meff-VRWAp and Meff-VRTAp are defined by relaxing $\Delta\phi(\text{jet}, \vec{E})_{\mathrm{min}}$ and aplanarity requirements, respectively, relative to Meff-VRW and Meff-VRT.

Similarly, the RJR-CRW and RJR-CRT estimates of the $W + \text{jets}$ and top quark backgrounds are validated using the same selections as for the corresponding CRs, except that the requirements on $H_{1,1}^{PP}$ and M_{TS} (RJR-VRWa, RJR-VRTa) or $H_{\mathrm{T2},1}^{PP}$ and $H_{\mathrm{T4},1}^{PP}$ (RJR-VRWb, RJR-VRTb) are omitted. Two additional VRs that require the presence of a high-purity lepton and either veto (RJR-VRW) or require the presence of at least one b-jet (RJR-VRT), and require no additional SR selection criteria, are also used in the analysis.

The Meff-CRQ estimates of the multijet background are validated with VRs for which the Meff-CRQ selection is applied, but with the SR $E_{\mathrm{T}}^{\mathrm{miss}}/m_{\mathrm{eff}}(N_{\mathrm{j}})$ $(E_{\mathrm{T}}^{\mathrm{miss}}/\sqrt{H_{\mathrm{T}}})$ requirement reinstated (Meff-VRQa), or with a requirement of an intermediate value of $\Delta\phi(\text{jet}, \vec{E})_{\mathrm{min}}$ applied (Meff-VRQb). The RJR-VRQ regions use the same selection as the corresponding RJR-CRQ, except that the requirements on $H_{1,1}^{PP}$, $H_{\mathrm{T2},1}^{PP}$ (or $H_{\mathrm{T4},1}^{PP}$ where appropriate) and M_{TS} are omitted depending on the region. Additional VRs with inverted Δ_{QCD} (RJR-VRQa), $H_{1,1}^{PP}$ (RJR-VRQb) for RJR-S and RJR-G signal regions, and with $0.5 < R_{\mathrm{ISR}} <$ SR requirement (RJR-VRQc) for the RJR-C region (Table III), are also used.

The results of the validation procedure are shown in Fig. 8, where the difference in each VR between the

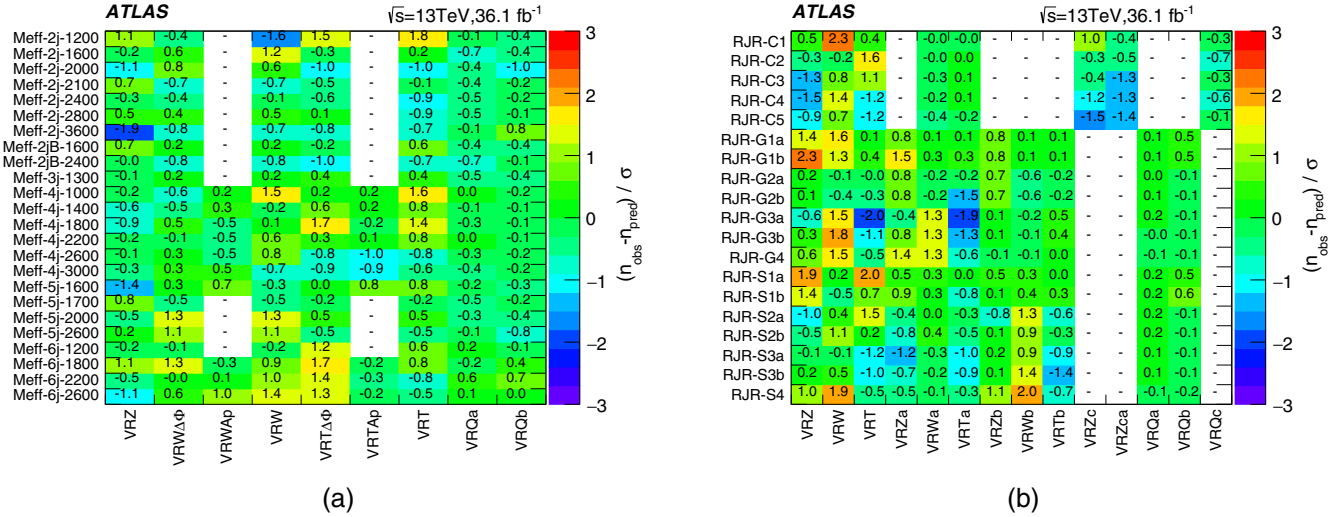

FIG. 8. Differences between the numbers of observed events in data and the SM background predictions for each VR used in the (a) Meff-based and (b) RJR-based searches, expressed as a fraction of the total uncertainty, which combines the uncertainty in the background predictions, and the expected statistical uncertainty of the test obtained from the number of expected events. Empty boxes (indicated by a "-") are when the VR is not used for the corresponding SR selection.

numbers of observed and expected events, expressed as fractions of the one-standard deviation (1σ) uncertainties in the latter, are summarized. No significant systematic biases are observed for both searches, with the largest discrepancies being 1.9σ in the Meff-VRZ associated with the SR Meff-2j-3600 out of 190 VRs and 2.3σ in RJR-VRW associated with the SR RJR-G1b out of 194 VRs.

IX. SYSTEMATIC UNCERTAINTIES

Systematic uncertainties in background estimates arise from the use of extrapolation factors that relate observations in the control regions to background predictions in the signal regions, and from the MC modeling of minor backgrounds.

The overall background uncertainties, detailed in Fig. 9, range from 6% in SR Meff-2j-1200 to 67% in SR Meff-6j-2600 and from 10% in SRs RJR-S1a, RJR-S2a, RJR-G1a, and RJR-C2 to 30% in SR RJR-G4.

For the backgrounds estimated with MC simulation-derived extrapolation factors, the primary common sources of systematic uncertainty are the jet energy scale (JES) calibration, jet energy resolution (JER), theoretical uncertainties, and limited event yields in the MC samples and data CRs. Correlations between uncertainties (for instance between JES or JER uncertainties in CRs and SRs) are taken into account where appropriate.

The JES and JER uncertainties are estimated using the methods discussed in Refs. [75,91,92]. An additional uncertainty in the modeling of energy not associated with reconstructed objects, used in the calculation of $E_{\mathrm{T}}^{\mathrm{miss}}$ and measured with unassociated charged tracks, is also included. The combined JES, JER and $E_{\mathrm{T}}^{\mathrm{miss}}$ uncertainty ranges from 1% of the expected background in 2-jet Meff-SRs to 12% in SR Meff-6j-2600. In the RJR-based search, the same uncertainties range from 1% in RJR-C4 to 14% in RJR-G4. Uncertainties in jet mass scale (JMS) and jet mass resolution (JMR) are additionally assigned to SR Meff-2jB-1600 and Meff-2jB-2400, which have requirements on the

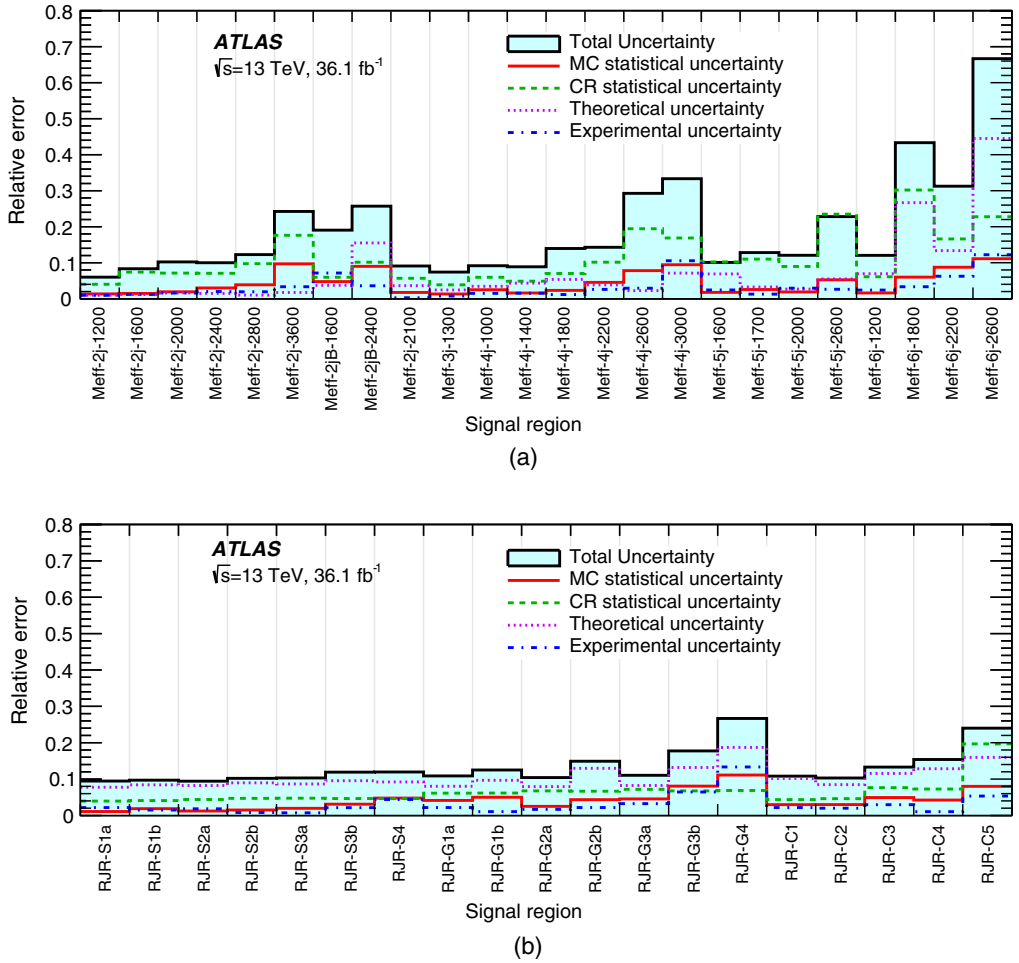

FIG. 9. Breakdown of the largest systematic uncertainties in the background estimates for the (a) Meff-based and (b) RJR-based searches. The individual uncertainties can be correlated, such that the total background uncertainty is not necessarily their sum in quadrature.

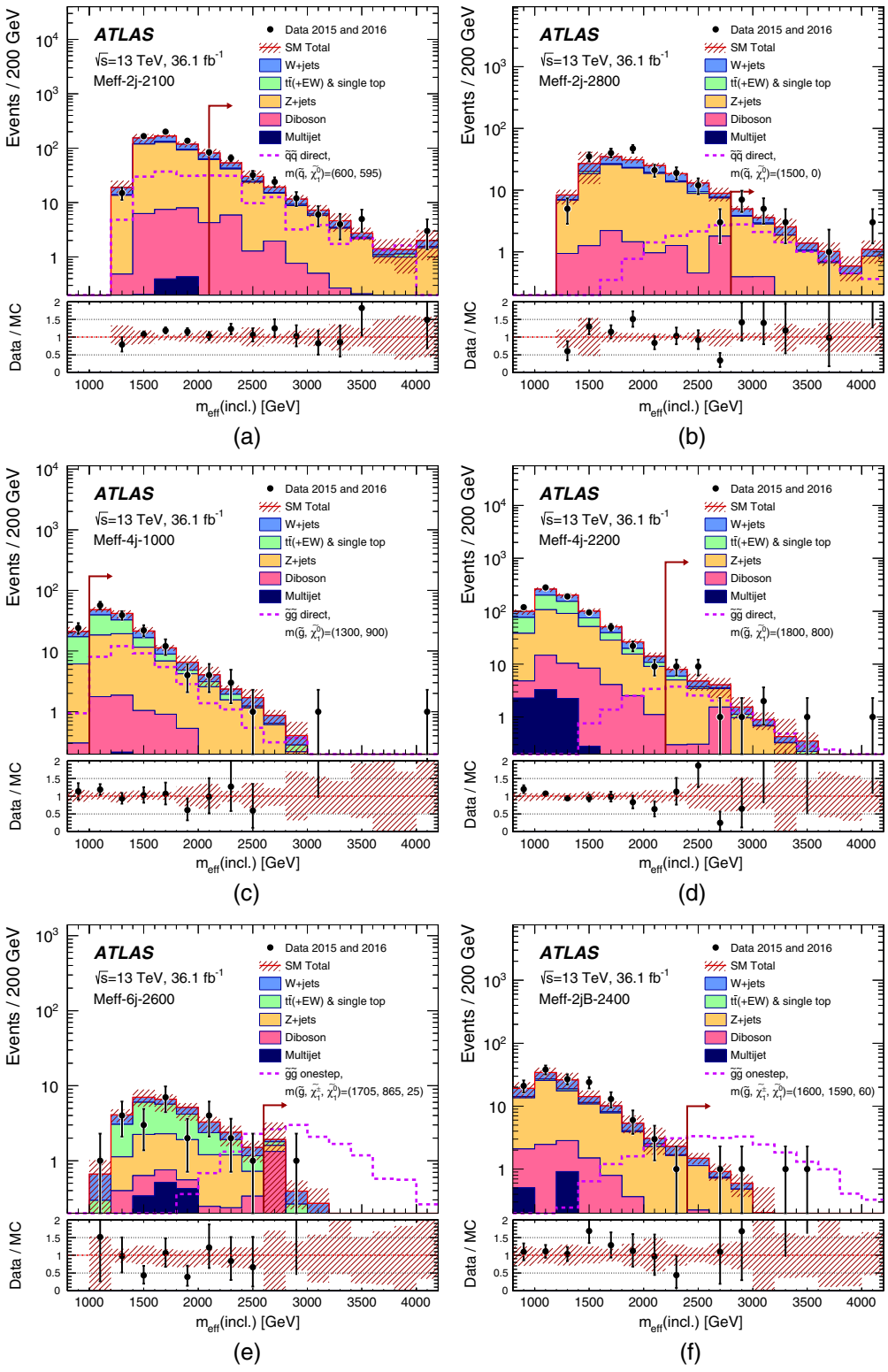

FIG. 10. Observed $m_{\mathrm{eff}}(\mathrm{incl})$ distributions for the (a) Meff-2j-2100, (b) Meff-2j-2800, (c) Meff-4j-1000, (d) Meff-4j-2200, (e) Meff-6j-2600, and (f) Meff-2jB-2400 signal regions, after applying all selection requirements except those on the plotted variable. The histograms show the MC background predictions prior to the fits described in the text, normalized using cross section times integrated luminosity. The last bin includes the overflow. The hatched (red) error bands indicate the combined experimental and MC statistical uncertainties. The arrows indicate the values at which the requirements on $m_{\mathrm{eff}}(\mathrm{incl})$ are applied. Expected distributions for benchmark signal model points, normalized using NLO + NLL cross section (Sec. III) times integrated luminosity, are also shown for comparison (masses in GeV).

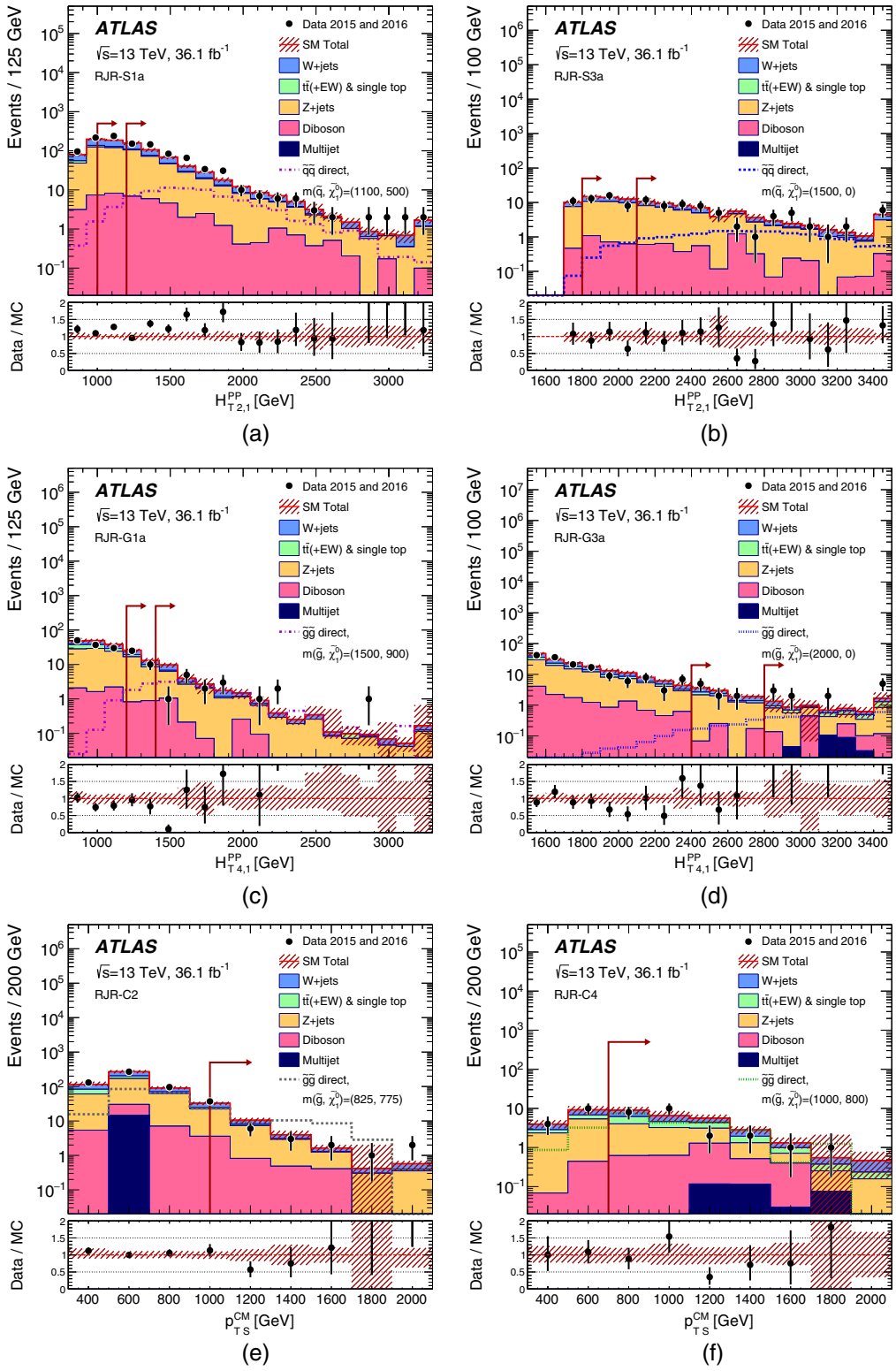

FIG. 11. Observed $H_{\mathrm{T2,1}}^{PP}$ distributions for the (a) RJR-S1a and (b) RJR-S3a signal regions, $H_{\mathrm{T4,1}}^{PP}$ distributions for the (c) RJR-G1a and (d) RJR-G3a signal regions, and p_{TS}^{CM} distributions for the (e) RJR-C2 and (f) RJR-C4 signal regions, after applying all selection requirements except those on the plotted variable. The histograms show the MC background predictions prior to the fits described in the text, normalized using cross section times integrated luminosity. The last bin includes the overflow. The hatched (red) error bands indicate the combined experimental and MC statistical uncertainties. The arrows indicate the values at which the requirements on the plotted variable are applied. When two arrows are shown, these correspond to the looser SR variation "a" and the tighter variation "b." Expected distributions for benchmark signal model points, normalized using NLO + NLL cross section (Sec. III) times integrated luminosity, are also shown for comparison (masses in GeV).

masses of large-radius jets. The JMS uncertainty is estimated using the same methodology as Ref. [93]. A 20% uncertainty is conservatively assigned to the JMR. The combined JMS and JMR uncertainty is 3.2% of the expected background in Meff-2j-1600 and 5.1% in Meff-2j-2400.

Uncertainties arising from theoretical modeling of background processes are estimated by comparing samples produced with different MC generators or by varying the scales. Uncertainties in $W/Z+$ jets production are estimated by increasing and decreasing the renormalization, factorization and resummation scales by a factor of 2, and by increasing and decreasing the nominal CKKW matching scale, 20 GeV, by 10 and 5 GeV, respectively. Uncertainties in the modeling of top quark pair production are estimated by comparing samples generated with POWHEG-BOX and MG5_aMC@NLO, and by comparing the nominal sample with samples generated using different shower tunes. Uncertainties associated with PDF modeling of top quark pair production are found to be negligible. Uncertainties in diboson production due to PDF, renormalization and factorization scale uncertainties (estimated by increasing and decreasing the scales used in the MC generators by a factor of 2 for all combinations and taking the envelope of them) are accounted for. The combined theoretical uncertainty ranges from 1% in Meff-2j-1200 to 45% in Meff-6j-2600 for Meff SRs. In the RJR-based search, the same uncertainties range from 8% in RJR-S1a to 18% in RJR-G4, with the smaller range largely due to the absence of 6-jet SRs. Uncertainties associated with the modeling of $Z+$ jets production are largest in the 2-jet Meff-SRs (7%). In the RJR-based search, these uncertainties are largest in RJR-S2b and RJR-S3b SR (8%). The impact of lepton reconstruction uncertainties, and of the uncertainties related to the b-tag/b-veto efficiency, on the overall background uncertainty is found to be negligible for all SRs.

The uncertainties arising from the data-driven correction procedure applied to events selected in the CRγ region, described in Sec. VIII, are included in Fig. 9 under "CR statistical uncertainty." Other uncertainties due to CR data sample size range from 4% to 30% for Meff SRs and from 4% to 20% for RJR SRs. The statistical uncertainty arising from the use of MC samples is largest in SRs Meff-6j-2600 (11%) and RJR-G4 (12%). Uncertainties related to the multijet background estimates are taken into account by applying a uniform 100% uncertainty to the multijet yield in all SRs. In most of the SRs these uncertainties are negligible, and the maximum resulting contribution to the overall background uncertainty is less than 1%.

Experimental uncertainties (JES, JER, JMS, JMR, and $E_{\mathrm{T}}^{\mathrm{miss}}$) and MC statistical uncertainty in the SUSY signals are estimated in the same way as for the background and are less than a few percent for most of the signals, except that 7% is assigned as JMS and JMR uncertainties in Meff-2jB-1600 and Meff-2jB-2400. The signal cross section uncertainty is estimated by computing the changes when the renormalization and factorization scale, PDF and the strong coupling constant (α_{s}) are varied. The uncertainties in the amount of ISR and FSR in the SUSY signals are estimated by varying generator tunes in the simulation as well as scales used in the matrix-element generator as a function of the mass difference, Δm, between gluino (or squark) and $\tilde{\chi}_1^0$. This uncertainty reaches 20% in the limit of no mass difference and is negligible for $\Delta m > 200$ GeV.

X. RESULTS, INTERPRETATION, AND LIMITS

Distributions of $m_{\mathrm{eff}}(\mathrm{incl})$ from the Meff-based search for selected signal regions, obtained before the final selections on this quantity (but after applying all other selections), are shown in Fig. 10 for data and the different MC samples normalized using the theoretical cross sections. Similarly, distributions of the final discriminating variables used in the RJR-based search, $H_{\mathrm{T2},1}^{PP}$ ($H_{\mathrm{T4},1}^{PP}$ where appropriate) in selected RJR-S and RJR-G regions, and p_{TS}^{CM} in selected RJR-C regions, after applying all other selection requirements except those based on the plotted variable, are shown in Fig. 11. Examples of SUSY signals are also shown for illustration. These signals correspond to the processes to which each SR is primarily sensitive: $\tilde{q}\,\tilde{q}$

TABLE V. Numbers of events observed in the signal regions used in the Meff-based analysis compared with background predictions obtained from the fits described in the text. The p-values (p_0) are the probabilities to obtain a value equal to or larger than that observed in the data. For an observed number of events lower than expected, the p-value is truncated at 0.5. In addition to p-values, the number of equivalent Gaussian standard deviations (Z) is given in parentheses. Also shown are 95% C.L. upper limits on the visible cross section ($\langle\epsilon\sigma\rangle_{\mathrm{obs}}^{95}$), the visible number of signal events (S_{obs}^{95}), and the number of signal events (S_{exp}^{95}) given the expected number of background events (and $\pm1\sigma$ excursions of the expected number).

Signal region [Meff-]	2j-1200	2j-1600	2j-2000	2j-2400	2j-2800	2j-3600	2j-B1600	2j-B2400
				MC expected events				
Diboson	28	14.8	5.6	3.4	1.2	0.21	1.9	0.41
Z/γ^*+ jets	345	140	54	24.2	10.2	2.3	16.6	2.5
$W+$ jets	141	47	18	8.2	3.4	1.11	5.2	0.7
$t\bar{t}(+\mathrm{EW})+$ single top	21.0	5.8	2.48	1.13	0.32	0.04	0.80	0.03

(Table continued)

TABLE V. *(Continued)*

Signal region [Meff-]	2j-1200	2j-1600	2j-2000	2j-2400	2j-2800	2j-3600	2j-B1600	2j-B2400
				Fitted background events				
Diboson	28 ± 4	14.8 ± 2.3	5.5 ± 1.2	3.4 ± 0.7	1.2 ± 0.2	0.21 ± 0.07	1.9 ± 0.5	0.41 ± 0.07
$Z/\gamma^* +$ jets	336 ± 19	143 ± 11	64 ± 8	28.0 ± 3.3	12.2 ± 1.5	2.9 ± 0.8	14.6 ± 1.9	2.8 ± 0.6
$W +$ jets	141 ± 24	68 ± 16	20 ± 4	9.6 ± 2.6	3.7 ± 1.2	0.37 ± 0.32	5.5 ± 3.1	0.7 ± 0.7
$t\bar{t}(+\mathrm{EW}) +$ single top	15 ± 4	2.9 ± 1.6	1.36 ± 1.0	0.5 ± 0.5	0.18 ± 0.15	$0.04^{+0.05}_{-0.04}$	0.5 ± 0.5	$0.02^{+0.67}_{-0.02}$
Multi-jet	6 ± 6	0.3 ± 0.3	0.07 ± 0.07	0.02 ± 0.02	< 0.004	$\cdots$	0.03 ± 0.03	< 0.002
Total MC	538	208	80	37	15.1	3.6	24	3.6
Total bkg	526 ± 31	228 ± 19	90 ± 10	42 ± 4	17.3 ± 2.0	3.6 ± 0.9	22 ± 4	3.9 ± 1.2
Observed	611	216	73	34	19	5	26	4
$\langle \epsilon\sigma \rangle^{95}_{\mathrm{obs}}$ [fb]	4.14	1.03	0.47	0.32	0.33	0.20	0.46	0.17
S^{95}_{obs}	149	37	17.0	11.4	11.9	7.2	16.7	6.1
S^{95}_{exp}	81^{+31}_{-25}	44^{+18}_{-12}	$25.2^{+9.0}_{-7.8}$	$15.3^{+5.7}_{-3.9}$	$10.6^{+3.9}_{-2.8}$	$5.5^{+2.5}_{-1.4}$	$13.1^{+5.5}_{-3.4}$	$5.7^{+2.3}_{-1.2}$
p_0 (Z)	0.02 (2.03)	0.50 (0.00)	0.50 (0.00)	0.50 (0.00)	0.31 (0.50)	0.21 (0.81)	0.28 (0.57)	0.32 (0.47)

Signal region [Meff-]	2j-2100	3j-1300	4j-1000	4j-1400	4j-1800	4j-2200	4j-2600	4j-3000
				MC expected events				
Diboson	12	37	6.4	18.1	6.0	2.4	1.8	0.24
$Z/\gamma^* +$ jets	116	268	60	100	33	12.0	4.1	1.4
$W +$ jets	34	107	29	52	15	4.5	1.66	0.6
$t\bar{t}(+\mathrm{EW}) +$ single top	5.0	36	43	42	7.7	1.6	0.64	0.21
				Fitted background events				
Diboson	12 ± 5	37 ± 6	6.4 ± 1.1	18.1 ± 3.0	6.0 ± 1.1	2.4 ± 0.7	1.8 ± 0.8	0.24 ± 0.07
$Z/\gamma^* +$ jets	102 ± 8	221 ± 20	52 ± 7	85 ± 10	25 ± 4	9.9 ± 2.0	2.3 ± 0.9	1.2 ± 0.5
$W +$ jets	35 ± 10	106 ± 19	22 ± 7	42 ± 10	12 ± 6	3.3 ± 1.1	1.57 ± 1.0	0.39 ± 0.3
$t\bar{t}(+\mathrm{EW}) +$ single top	2.6 ± 1.4	25 ± 9	43 ± 8	35 ± 10	5.0 ± 3.3	0.8 ± 0.4	$0.13^{+0.17}_{-0.13}$	0.12 ± 0.11
Multi-jet	0.11 ± 0.11	1.4 ± 1.4	0.39 ± 0.39	0.5 ± 0.5	0.10 ± 0.10	0.02 ± 0.02	0.03 ± 0.03	0.01 ± 0.01
Total MC	167	449	138	212	61	20.5	8.2	2.4
Total bkg	153 ± 14	390 ± 29	124 ± 12	182 ± 16	49 ± 7	16.5 ± 2.7	5.8 ± 2.0	2.0 ± 0.6
Observed	190	429	142	199	55	24	4	2
$\langle \epsilon\sigma \rangle^{95}_{\mathrm{obs}}$ [fb]	1.98	2.84	1.40	1.76	0.79	0.49	0.16	0.12
S^{95}_{obs}	72	103	50.6	64	28.3	17.6	5.8	4.5
S^{95}_{exp}	38^{+16}_{-10}	72^{+29}_{-21}	$37.1^{+12.5}_{-9.1}$	45^{+15}_{-12}	$22.2^{+6.9}_{-7.0}$	$11.3^{+4.8}_{-2.7}$	$6.7^{+2.7}_{-1.9}$	$4.6^{+1.6}_{-1.2}$
p_0 (Z)	0.02 (2.03)	0.13 (1.12)	0.10 (1.26)	0.08 (1.39)	0.18 (0.90)	0.09 (1.34)	0.50 (0.00)	0.50 (0.00)

Signal region [Meff-]	5j-1600	5j-1700	5j-2000	5j-2600	6j-1200	6j-1800	6j-2200	6j-2600
				MC expected events				
Diboson	10.8	6.6	8.9	2.6	20.5	1.9	1.7	1.3
$Z/\gamma^* +$ jets	56	31	50	7.4	109	3.3	1.3	0.76
$W +$ jets	42	15.5	18.6	2.57	81	2.2	0.67	0.44
$t\bar{t}(+\mathrm{EW}) +$ single top	45	12.0	9.9	0.8	144	4.3	0.63	0.39
				Fitted background events				
Diboson	10.8 ± 1.8	6.6 ± 1.1	8.9 ± 1.5	2.6 ± 0.7	20.5 ± 3.5	1.9 ± 0.7	1.7 ± 0.8	1.3 ± 0.9
$Z/\gamma^* +$ jets	42 ± 5	21 ± 4	37 ± 6	6.0 ± 1.7	61 ± 11	1.1 ± 0.7	0.9 ± 0.5	0.38 ± 0.29
$W +$ jets	26 ± 7	8.0 ± 2.6	13.3 ± 3.3	$0.41^{+0.45}_{-0.41}$	46 ± 22	$0.8^{+1.1}_{-0.8}$	$0.10^{+0.16}_{-0.10}$	$0.16^{+0.24}_{-0.16}$
$t\bar{t}(+\mathrm{EW}) +$ single top	40 ± 9	7.1 ± 2.8	6.5 ± 2.6	0.4 ± 0.4	145 ± 25	1.2 ± 1.0	0.37 ± 0.27	$0.24^{+0.41}_{-0.24}$
Multi-jet	9 ± 9	$0.08^{+0.09}_{-0.08}$	0.09 ± 0.09	0.01 ± 0.01	$1.29^{+1.30}_{-1.29}$	0.12 ± 0.12	$0.02^{+0.03}_{-0.02}$	0.06 ± 0.06
Total MC	158	65	88	13.3	355	11.7	4.3	2.9
Total bkg	128 ± 14	43 ± 5	65 ± 7	9.4 ± 2.1	274 ± 32	5.1 ± 1.8	3.1 ± 1.3	2.2 ± 1.4
Observed	135	49	59	10	276	9	3	1
$\langle \epsilon\sigma \rangle^{95}_{\mathrm{obs}}$ [fb]	1.26	0.64	0.49	0.24	2.19	0.33	0.15	0.11
S^{95}_{obs}	45.4	23.0	17.8	8.8	79	11.9	5.4	3.8
S^{95}_{exp}	39^{+14}_{-8}	$18.2^{+6.7}_{-5.6}$	$20.7^{+8.6}_{-5.3}$	$8.5^{+3.0}_{-2.1}$	70^{+19}_{-20}	$8.2^{+3.6}_{-1.7}$	$5.4^{+1.8}_{-1.2}$	$4.3^{+1.8}_{-0.6}$
p_0 (Z)	0.32 (0.46)	0.21 (0.82)	0.50 (0.00)	0.46 (0.09)	0.50 (0.00)	0.11 (1.25)	0.50 (0.00)	0.50 (0.00)

TABLE VI. Numbers of events observed in the signal regions used in the RJR-based analysis compared with background predictions obtained from the fits described in the text. The p-values (p_0) are the probabilities to obtain a value equal to or larger than that observed in the data. For an observed number of events lower than expected, the p-value is truncated at 0.5. In addition to p-values, the number of equivalent Gaussian standard deviations (Z) is given in parentheses. Also shown are 95% C.L. upper limits on the visible cross section ($\langle\epsilon\sigma\rangle^{95}_{\rm obs}$), the visible number of signal events ($S^{95}_{\rm obs}$) and the number of signal events ($S^{95}_{\rm exp}$) given the expected number of background events (and $\pm1\sigma$ excursions of the expected number).

Signal region	RJR-S1a	RJR-S1b	RJR-S2a	RJR-S2b	RJR-S3a	RJR-S3b	RJR-S4
				MC expected events			
Diboson	37	17	23	10.3	7.2	3.5	2.0
Z/γ^* + jets	495	189	222	102	70	30.5	17.9
W + jets	220	77	84	36	22.6	9.2	5.3
$t\bar{t}$(+EW) + single top	32	9.2	10.9	4.7	2.6	1.17	0.68
				Fitted background events			
Diboson	37 ± 8	17 ± 4	23 ± 5	10.3 ± 2.6	7.2 ± 1.5	3.5 ± 1.1	2.0 ± 0.5
Z/γ^* + jets	450 ± 40	170 ± 14	211 ± 17	97 ± 8	67 ± 5	29.0 ± 2.4	17.0 ± 1.5
W + jets	208 ± 27	73 ± 9	83 ± 12	35 ± 5	22.3 ± 3.0	9.0 ± 1.3	5.2 ± 0.9
$t\bar{t}$(+EW) + single top	27 ± 26	7.4 ± 2.0	7.6 ± 3.2	3.3 ± 1.2	1.9 ± 0.5	0.82 ± 0.34	$0.49^{+0.51}_{-0.49}$
Multi-jet	18 ± 17	1.3 ± 1.3	0.6 ± 0.6	0.31 ± 0.31	0.27 ± 0.27	0.03 ± 0.03	0.03 ± 0.03
Total MC	1830	370	378	172	120	45.9	27.7
Total bkg	740 ± 50	268 ± 18	326 ± 22	146 ± 10	98 ± 6	42.4 ± 3.0	24.7 ± 2.1
Observed	880	325	365	170	102	46	23
$\langle\epsilon\sigma\rangle^{95}_{\rm obs}$ [fb]	6.45	2.76	1.89	1.38	0.69	0.51	0.30
$S^{95}_{\rm obs}$	233	99.5	68.3	49.9	24.7	18.3	10.7
$S^{95}_{\rm exp}$	120^{+44}_{-34}	50^{+18}_{-13}	50^{+14}_{-10}	32^{+14}_{-8}	24^{+11}_{-6}	$15.5^{+5.9}_{-3.4}$	$11.6^{+4.5}_{-3.9}$
p_0 (Z)	0.01 (2.52)	0.01 (2.34)	0.14 (1.07)	0.10 (1.30)	0.50 (0.00)	0.50 (0.00)	0.50 (0.00)

Signal region	RJR-G1a	RJR-G1b	RJR-G2a	RJR-G2b	RJR-G3a	RJR-G3b	RJR-G4
				MC expected events			
Diboson	3.1	1.6	2.8	1.34	0.80	0.37	0.24
Z/γ^* + jets	28.7	13.1	28.1	9.4	8.8	3.0	2.09
W + jets	14.0	6.4	14.6	5.0	4.7	1.7	1.0
$t\bar{t}$(+EW) + single top	6.0	2.0	6.5	2.0	3.1	1.5	1.1
				Fitted background events			
Diboson	3.1 ± 0.7	1.6 ± 0.5	2.8 ± 0.8	1.34 ± 0.33	0.80 ± 0.27	0.36 ± 0.29	0.24 ± 0.11
Z/γ^* + jets	24.8 ± 2.7	11.3 ± 1.4	25.4 ± 2.9	8.4 ± 1.2	7.9 ± 1.1	2.7 ± 0.7	1.89 ± 0.35
W + jets	12.0 ± 1.7	5.5 ± 0.9	12.3 ± 2.1	4.2 ± 0.8	3.9 ± 0.7	1.5 ± 0.6	0.85 ± 0.29
$t\bar{t}$(+EW) + single top	4.8 ± 0.9	1.6 ± 1.4	5.2 ± 1.9	1.6 ± 0.6	2.4 ± 0.9	1.2 ± 1.0	0.9 ± 0.8
Multi-jet	0.25 ± 0.25	0.13 ± 0.13	0.5 ± 0.5	0.2 ± 0.2	0.5 ± 0.5	0.26 ± 0.25	$0.18^{+0.18}_{-0.18}$
Total MC	66.8	30.9	80.4	28.9	44.4	21.1	14.4
Total bkg	45 ± 4	20.1 ± 2.3	46 ± 4	15.8 ± 1.8	15.6 ± 1.7	6.0 ± 1.4	4.1 ± 0.9
Observed	42	16	52	15	21	12	6
$\langle\epsilon\sigma\rangle^{95}_{\rm obs}$ [fb]	0.44	0.25	0.63	0.26	0.42	0.38	0.22
$S^{95}_{\rm obs}$	15.9	8.9	22.7	9.4	15.2	13.9	7.8
$S^{95}_{\rm exp}$	$16.6^{+6.7}_{-5.0}$	$11.0^{+4.1}_{-2.7}$	$16.7^{+6.8}_{-4.8}$	$9.9^{+4.1}_{-2.5}$	$10.7^{+3.4}_{-3.1}$	$10.3^{+2.7}_{-2.1}$	$6.3^{+1.9}_{-2.1}$
p_0 (Z)	0.50 (0.00)	0.50 (0.00)	0.19 (0.89)	0.50 (0.00)	0.11 (1.21)	0.07 (1.50)	0.24 (0.72)

Signal region	RJR-C1	RJR-C2	RJR-C3	RJR-C4	RJR-C5
			MC expected events		
Diboson	4.5	3.4	1.6	2.7	0.8
Z/γ^* + jets	24.8	20.7	7.8	10.3	2.3
W + jets	9.8	7.4	8.3	8.0	2.4
$t\bar{t}$(+EW) + single top	1.32	1.6	5.5	6.9	3.39
			Fitted background events		
Diboson	4.5 ± 1.0	3.4 ± 0.8	1.6 ± 0.5	2.7 ± 0.7	0.8 ± 0.5
Z/γ^* + jets	22.6 ± 2.3	18.9 ± 2.0	6.5 ± 1.2	8.6 ± 1.2	2.1 ± 0.6
W + jets	9.9 ± 1.9	7.5 ± 1.4	8.9 ± 1.4	8.6 ± 1.4	2.7 ± 2.1

(Table continued)

TABLE VI. *(Continued)*

Signal region	RJR-C1	RJR-C2	RJR-C3	RJR-C4	RJR-C5
$t\bar{t}(+\mathrm{EW})$ + single top	$0.86^{+1.00}_{-0.86}$	1.0 ± 0.7	3.2 ± 1.5	4.0 ± 2.4	$0.89^{+2.17}_{-0.89}$
Multi-jet	0.06 ± 0.06	0.33 ± 0.33	0.5 ± 0.5	0.8 ± 0.8	$0.25^{+0.26}_{-0.25}$
Total MC	43.9	53.3	54.8	84.0	28.0
Total bkg	37.9 ± 3.5	31.2 ± 2.9	20.7 ± 2.6	24.8 ± 3.3	6.7 ± 1.3
Observed	36	29	12	24	10
$\langle \epsilon\sigma \rangle^{95}_{\mathrm{obs}}$ [fb]	0.38	0.35	0.18	0.42	0.30
S^{95}_{obs}	13.8	12.7	6.4	15.2	10.7
S^{95}_{exp}	$15.3^{+5.7}_{-4.7}$	$14.0^{+5.0}_{-4.2}$	$11.2^{+4.4}_{-3.5}$	$15.2^{+4.5}_{-3.5}$	$7.8^{+2.7}_{-2.0}$
p_0 (Z)	0.50 (0.00)	0.50 (0.00)	0.50 (0.00)	0.50 (0.00)	0.14 (1.06)

production for the lower jet-multiplicity SRs and $\tilde{g}\tilde{g}$ production for the higher jet-multiplicity SRs. In these figures, data and background distributions largely agree within uncertainties.

The number of events observed in the data and the number of SM events expected to enter each of the signal regions, determined using the background-only fit, are shown in Tables V and VI and in Fig. 12. The prefit background predictions are also shown in Tables V and VI for comparison.

The background normalizations for each SR are fit to reproduce the event yields observed in the CRs. This is in particular seen in Fig. 5, leading to agreement between data and postfit background predictions in most of the SRs. The most significant observed excess in the signal regions for the Meff-based search, with a p-value for the background-only hypothesis of 0.02, corresponding to a significance of 2.0 standard deviations, occurs in SR Meff-2j-1200 and Meff-2j-2100 (Table V). The most significant observed excess across the signal regions for RJR-based search, with a p-value for the background-only hypothesis of 0.01, corresponding to a significance of 2.5 standard deviations, occurs in SR RJR-S1a (Table VI).

In the absence of a statistically significant excess, limits are set on contributions to the SRs from BSM physics. Upper limits at 95% C.L. on the number of BSM signal events in each SR and the corresponding visible BSM cross section are derived from the model-independent fits described in Sec. V using the $\mathrm{CL_S}$ prescription. Limits are evaluated using MC pseudoexperiments. The results are presented in Tables V and VI.

The model-dependent fits in all the SRs are used to set limits on specific classes of SUSY models using asymptotic formulae [94]. The two searches presented in this paper are combined such that the final observed and expected 95% C.L. exclusion limits are obtained from the signal regions with the best expected $\mathrm{CL_S}$ value. Fine structures in the limit lines arise due to transitions between best SR's which then also have an impact on the interpolations between grid points.

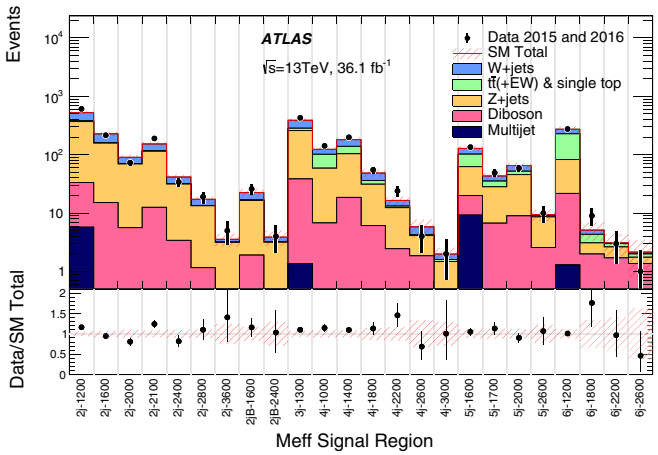

(a)

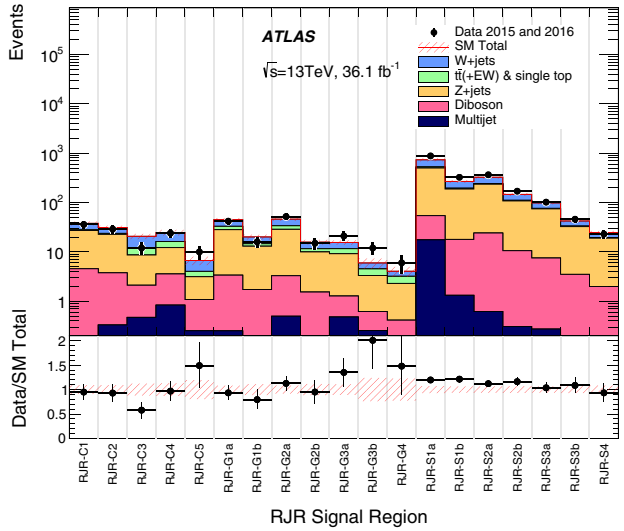

(b)

FIG. 12. Comparison of the observed and expected event yields as a function of signal region in the (a) Meff-based and (b) RJR-based searches. The background predictions are those obtained from the background-only fits, presented in Tables V and VI. The bottom graph shows the ratio of observed data yields to the total predicted background. The hatched (red) error bands indicate the combined experimental and MC statistical uncertainties.

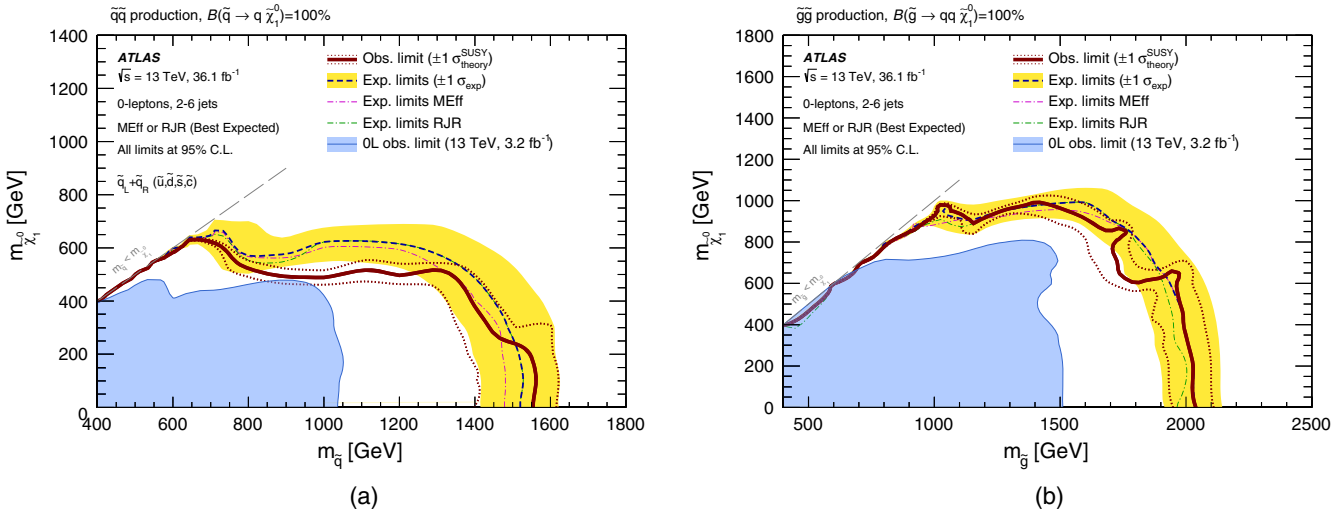

FIG. 13. Exclusion limits for direct production of (a) first- and second-generation squark pairs with decoupled gluinos and (b) gluino pairs with decoupled squarks. Gluinos (first- and second-generation squarks) are required to decay to two quarks (one quark) and a neutralino LSP. Exclusion limits are obtained by using the signal region with the best expected sensitivity at each point. Expected limits from the Meff- and RJR-based searches separately are also shown for comparison. The blue dashed lines show the expected limits at 95% C.L., with the light (yellow) bands indicating the 1σ excursions due to experimental and background-only theoretical uncertainties. Observed limits are indicated by medium dark (maroon) curves where the solid contour represents the nominal limit, and the dotted lines are obtained by varying the signal cross section by the renormalization and factorization scale and PDF uncertainties. Results are compared with the observed limits obtained by the previous ATLAS searches with jets, missing transverse momentum, and no leptons [11].

In Fig. 13, limits are shown for two classes of simplified models in which only direct production of first- and second-generation mass-degenerate squark or gluino pairs are considered. Limits are obtained by using the signal region with the best expected sensitivity at each point. In these simplified-model scenarios, the upper limit of the excluded first- and second-generation squark mass region is 1.55 TeV assuming massless $\tilde{\chi}_1^0$, as obtained from the signal region RJR-S4. The observed exclusion limit is worse than the expected limit in the region with squark ($\tilde{\chi}_1^0$) mass of 1 TeV (500 GeV) due to a 2σ excess in SR Meff-2j-1200. The corresponding limit on the gluino mass is 2.03 TeV, if the $\tilde{\chi}_1^0$ is massless, as obtained from the signal region Meff-4j-3000. The best sensitivity in the region of parameter space where the mass difference between the squark (gluino) and the lightest neutralino is small, is obtained from the dedicated RJR-C signal regions. In these regions with very compressed spectra and where the mass difference is less than 50 GeV, squark (gluino) masses up to 650 GeV (1 TeV) are excluded. In Fig. 13(b), the compressed-mass region with a gluino mass below 700 GeV is fully excluded by this analysis; small deviations in the exclusion contour in this region, suggesting nonexcluded areas, are due to interpolation effects. The observed exclusion limit is worse than the expected limit in the region with gluino ($\tilde{\chi}_1^0$) mass of 1800 (700) GeV due to a moderate excess (1.3σ) in SR Meff-4j-2200.

In Fig. 14, limits are shown for pair-produced first- and second-generation squarks or gluinos each decaying via an intermediate $\tilde{\chi}_1^\pm$ to a quark (for squarks) or two quarks (for gluinos), a W boson and a $\tilde{\chi}_1^0$. Two sets of models of mass spectra are considered for each case. One is with a fixed $m_{\tilde{\chi}_1^\pm} = (m_{\tilde{q}} + m_{\tilde{\chi}_1^0})/2$ [or $(m_{\tilde{g}} + m_{\tilde{\chi}_1^0})/2$], the other is with a fixed $m_{\tilde{\chi}_1^0} = 60$ GeV. In the former models with squark pair production, $m_{\tilde{q}}$ up to 1.15 TeV are excluded for a massless $\tilde{\chi}_1^0$, as is $m_{\tilde{g}}$ up to 1.98 TeV with gluino pair production. These limits are obtained from the signal region RJR-G2b and Meff-6j-2600, respectively. In the regions with very compressed spectra with mass difference between the gluino (or squark) and $\tilde{\chi}_1^0$ less than 50 GeV, RJR-C signal regions also exclude squark (gluino) masses up to 600 GeV (1 TeV). In the latter models, Meff-2jB-1600 and Meff-2jB-2400 extend the limits on squark (gluino) masses up to 1.1 TeV (1.85 TeV) in the regions with small mass difference between the squark (gluino) and $\tilde{\chi}_1^\pm$.

In Fig. 15, limits are shown for gluino pair production decaying via an intermediate $\tilde{\chi}_2^0$ to two quarks, a Z boson and a $\tilde{\chi}_1^0$. The mass of the $\tilde{\chi}_1^0$ is set to 1 GeV. In these models, gluino masses below 2.0 TeV are excluded for $\tilde{\chi}_2^0$ masses of $\sim$1 TeV, as obtained from the signal region Meff-6j-2600.

In Fig. 16, results are presented in the models with mixed decays of intermediate $\tilde{\chi}_1^\pm$ and $\tilde{\chi}_2^0$ for squark pair and gluino

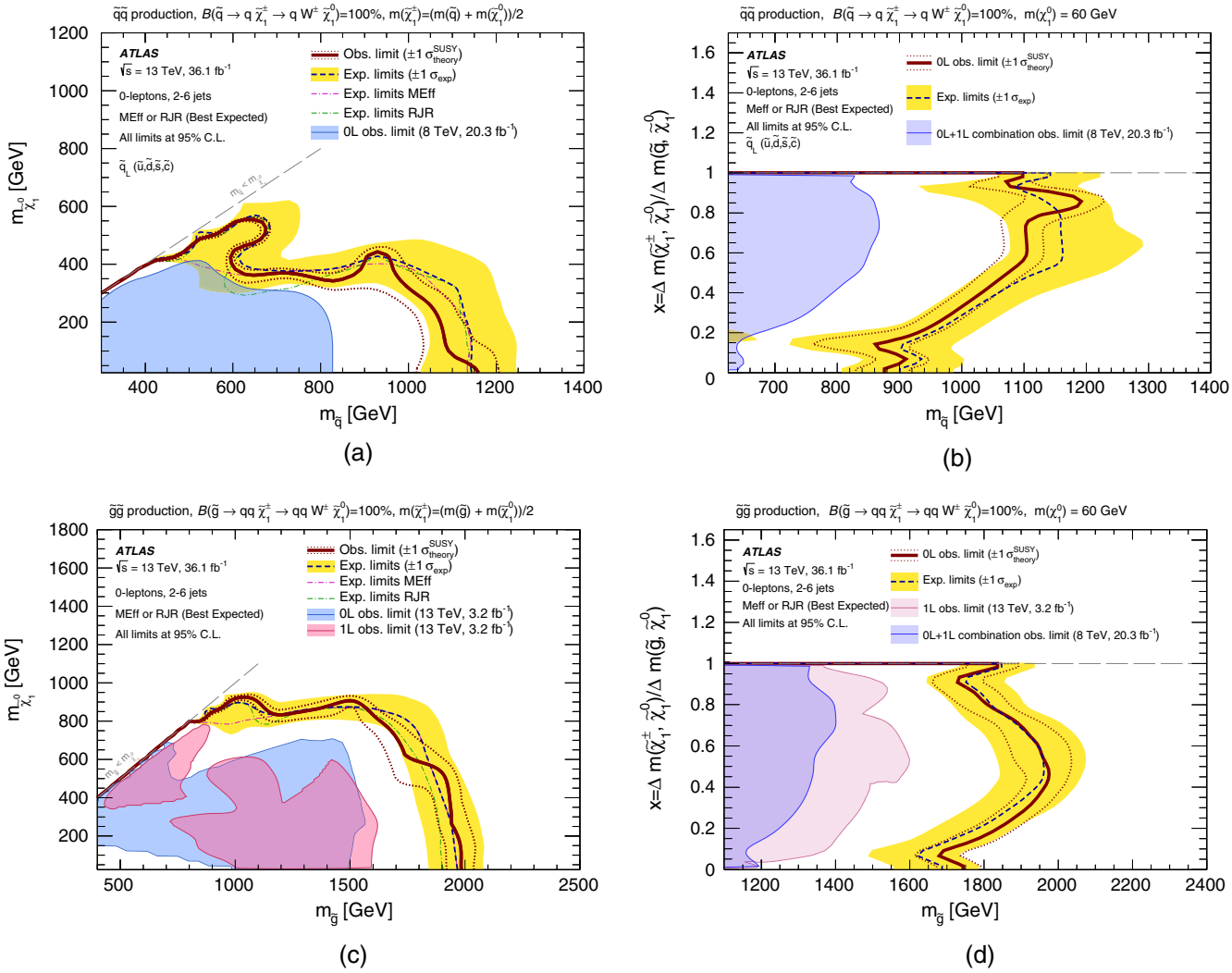

FIG. 14. Exclusion limits for direct production of (a),(b) first- and second-generation left-handed squark pairs with decoupled gluinos and (c),(d) gluino pairs with decoupled squarks. Gluinos (first- and second-generation squarks) are required to decay to two quarks (one quark) and an intermediate $\tilde{\chi}_1^{\pm}$, decaying to a W boson and a $\tilde{\chi}_1^0$. Models with (a),(c) a fixed $m_{\tilde{\chi}_1^{\pm}} = (m_{\tilde{g}} + m_{\tilde{\chi}_1^0})/2$ [or $(m_{\tilde{q}} + m_{\tilde{\chi}_1^0})/2$] and varying values of $m_{\tilde{g}}$ (or $m_{\tilde{q}}$) and $m_{\tilde{\chi}_1^0}$, and (b),(d) a fixed $m_{\tilde{\chi}_1^0} = 60$ GeV and varying values of $m_{\tilde{g}}$ (or $m_{\tilde{q}}$) and $m_{\tilde{\chi}_1^{\pm}}$ are considered. Exclusion limits are obtained by using the signal region with the best expected sensitivity at each point. Expected limits from the Meff- and RJR-based searches separately are also shown for comparison in (a),(c). The blue dashed lines show the expected limits at 95% C.L., with the light (yellow) bands indicating the 1σ excursions due to experimental and background-only theoretical uncertainties. Observed limits are indicated by medium dark (maroon) curves where the solid contour represents the nominal limit, and the dotted lines are obtained by varying the signal cross section by the renormalization and factorization scale and PDF uncertainties. Results are compared with the observed limits obtained by the previous ATLAS searches with one or no leptons, jets and missing transverse momentum [11,19,95].

pair production. The highest limits on the squark mass are 1.34 TeV and on the gluino mass are 2.02 TeV, which are similar to the models with 100% branching fraction for $\tilde{\chi}_1^{\pm}$ ($\tilde{\chi}_2^0$) to a W (Z) boson and $\tilde{\chi}_1^0$. In Fig. 16(b), the limits are extended by the SR Meff-2jet in the region with small mass differences between the gluino and $\tilde{\chi}_2^0$.

In Fig. 17, results are interpreted in simplified pMSSM models assuming only first- and second-generation squarks, gluino and $\tilde{\chi}_1^0$. The $\tilde{\chi}_1^0$ is assumed to be purely bino. Models with a fixed $m_{\tilde{\chi}_1^0} = 0, 695, 995$ GeV are considered while varying $m_{\tilde{g}}$ and $m_{\tilde{q}}$. In the limit of high squark mass, gluino masses up to 2 TeV are excluded for massless $\tilde{\chi}_1^0$, which is consistent with the simplified models of gluino pair production with decoupled squarks. With a gluino mass of 6 TeV, squark masses up to 2.2 TeV are excluded for a massless $\tilde{\chi}_1^0$, much higher than in the simplified models of squark pair production with decoupled gluinos. This is due to the large cross section of squark pair production via gluino exchange diagrams.

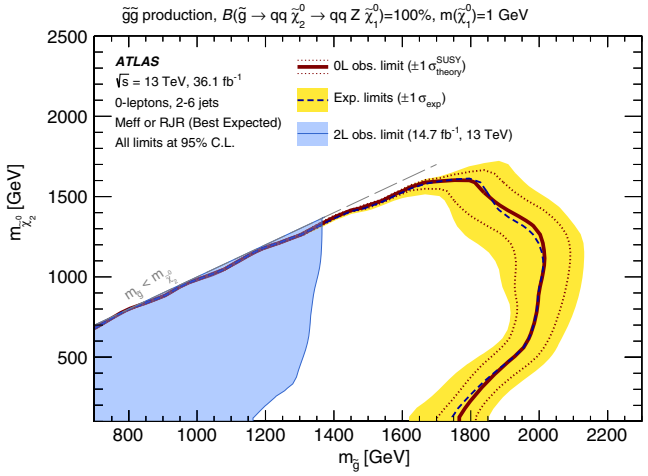

FIG. 15. Exclusion limits for pair-produced gluinos each decaying via an intermediate $\tilde{\chi}_2^0$ to two quarks, a Z boson and a $\tilde{\chi}_1^0$ for models with a fixed $m_{\tilde{\chi}_1^0} = 1$ GeV and varying values of $m_{\tilde{g}}$ and $m_{\tilde{\chi}_2^0}$. Exclusion limits are obtained by using the signal region with the best expected sensitivity at each point. The blue dashed lines show the expected limits at 95% C.L., with the light (yellow) bands indicating the 1σ excursions due to experimental and background-only theoretical uncertainties. Observed limits are indicated by medium dark (maroon) curves where the solid contour represents the nominal limit, and the dotted lines are obtained by varying the signal cross section by the renormalization and factorization scale and PDF uncertainties. Results are compared with the observed limits obtained by the previous ATLAS search in events containing a leptonically decaying Z boson, jets and missing transverse momentum [96].

A comparison of the Meff-based and RJR-based results highlights some notable features. The RJR-Cx signal regions provide additional sensitivity in the most compressed mass regions beyond their Meff-based counterparts, extending exclusion limits up to 200 GeV in $\tilde{\chi}_1^0$ mass for the smallest mass splitting, as is the case in Fig. 14(a) for first- and second-generation squarks decaying via an intermediate $\tilde{\chi}_1^\pm$. In general, the RJR-Cx regions are only mildly sensitive to the specific decays of squarks and gluinos, resulting in similar sensitivity as a function of $\tilde{q}/\tilde{g}$ and $\tilde{\chi}_1^0$ masses between signal models with direct decays in Fig. 13 and those with intermediate sparticle decays as in Fig. 14.

Despite being largely orthogonal, the RJR-based and Meff-based SRs targeting squark and gluino direct decay signals tend to result in similar sensitivity, with the RJR-based regions generally performing better for intermediate mass splittings. This is the result of tighter restrictions placed on dimensionless variables in the RJR-based regions, resulting in generally lower background yields.

For models with additional jets in the final state expected from intermediate sparticle decays, the Meff-5j-x and Meff-6j-x provide significant additional sensitivity with respect to lower multiplicity SRs, extending exclusion limits by close to 100 GeV in gluino mass when intermediate $\tilde{\chi}_1^\pm$ decays are considered. These more stringent jet multiplicity requirements compensate for the modest $E_{\mathrm{T}}^{\mathrm{miss}}/m_{\mathrm{eff}}(N_{\mathrm{j}})$ values characteristic of these models.

With requirements aimed at tagging hadronic decays of W/Z bosons, the Meff-2jB-x SRs provide higher

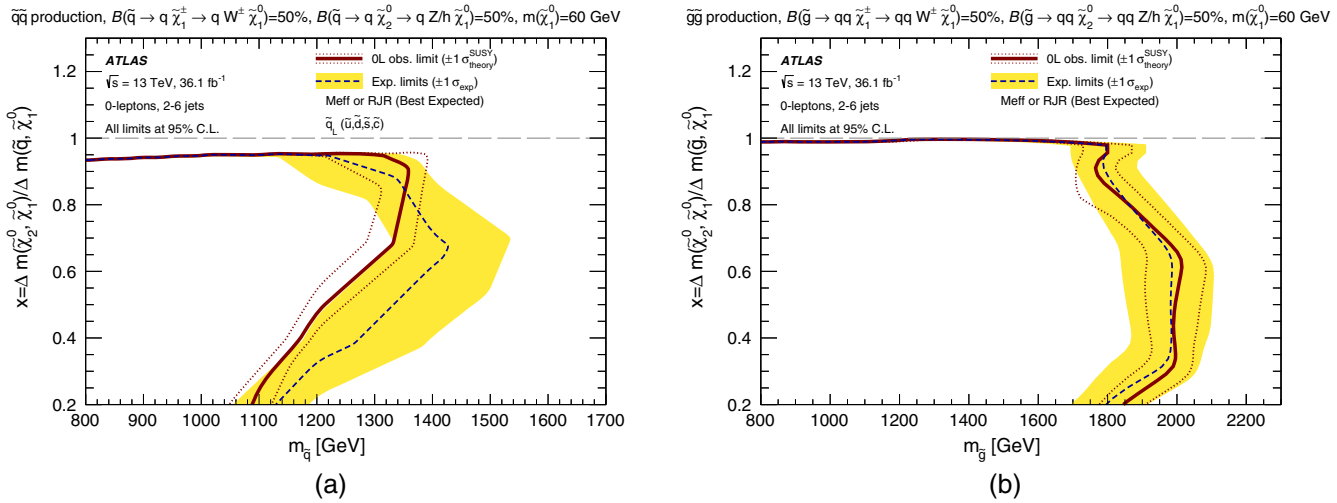

FIG. 16. Exclusion limits for direct production of (a) first- and second-generation left-handed squark pairs with decoupled gluinos and (b) gluino pairs with decoupled squarks. Gluinos (first- and second-generation squarks) are required to decay to two quarks (one quark) and a intermediate $\tilde{\chi}_1^\pm$ or $\tilde{\chi}_2^0$ with a 50% branching fraction, respectively, with $\tilde{\chi}_1^\pm$ decays to a W boson and a $\tilde{\chi}_1^0$, and $\tilde{\chi}_2^0$ decays to a Z or a h boson and $\tilde{\chi}_1^0$. Models with fixed $m_{\tilde{\chi}_1^0} = 60$ GeV are considered while varying $m_{\tilde{g}}$ (or $m_{\tilde{q}}$) and $m_{\tilde{\chi}_1^0}$. Exclusion limits are obtained by using the signal region with the best expected sensitivity at each point. The blue dashed lines show the expected limits at 95% C.L., with the light (yellow) bands indicating the 1σ excursions due to experimental and background-only theoretical uncertainties. Observed limits are indicated by medium dark (maroon) curves where the solid contour represents the nominal limit, and the dotted lines are obtained by varying the signal cross section by the renormalization and factorization scale and PDF uncertainties.

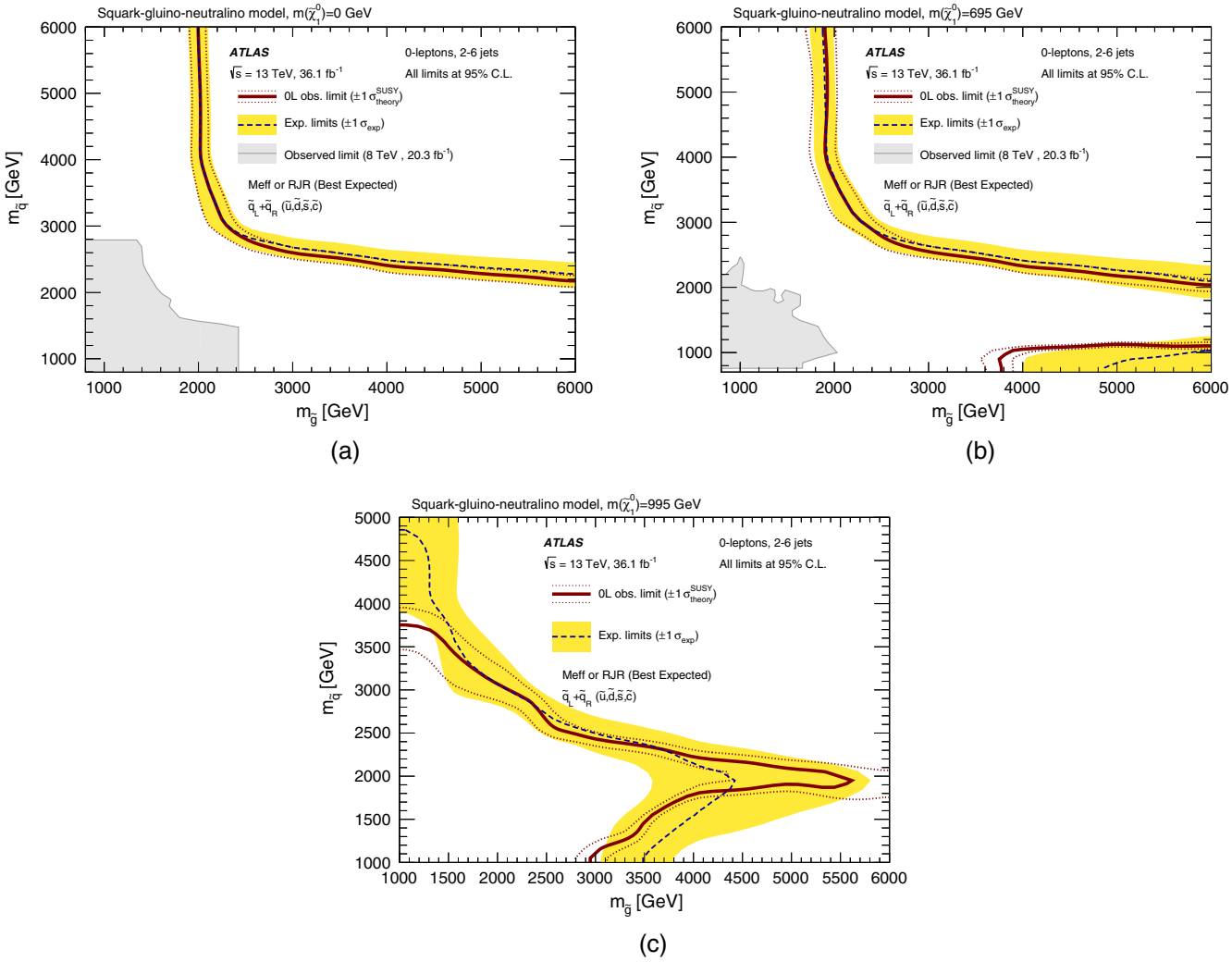

FIG. 17. Exclusion limits for inclusive squark-gluino production in pMSSM models with (a) $m_{\tilde{\chi}_1^0} = 0$ GeV, (b) $m_{\tilde{\chi}_1^0} = 695$ GeV, and (c) $m_{\tilde{\chi}_1^0} = 995$ GeV varying values of $m_{\tilde{g}}$ and $m_{\tilde{q}}$ and assuming purely bino $\tilde{\chi}_1^0$. Exclusion limits are obtained by using the signal region with the best expected sensitivity at each point. The blue dashed lines show the expected limits at 95% C.L., with the light (yellow) bands indicating the 1σ excursions due to experimental and background-only theoretical uncertainties. Observed limits are indicated by medium dark (maroon) curves where the solid contour represents the nominal limit, and the dotted lines are obtained by varying the signal cross section by the renormalization and factorization scale and PDF uncertainties. Results (a),(b) are compared with the observed limits obtained by the previous ATLAS searches with no leptons, jets, and missing transverse momentum [97].

sensitivity to models with intermediate $\tilde{\chi}_1^{\pm}$ and $\tilde{\chi}_2^0$ decays when these sparticles are almost degenerate in mass with their parent squarks and gluinos, corresponding to Figs. 14(b), 14(d), 15, and 16. In these cases, the sensitivity of the Meff-2jB-x regions far surpasses those of the RJR-based and other Meff-based SRs.

XI. CONCLUSION

This paper presents results of two selection strategies to search for squarks and gluinos in final states containing high-p_{T} jets, large missing transverse momentum but no electrons or muons, based on a 36.1 fb^{-1} dataset of $\sqrt{s} =$ 13 TeV proton-proton collisions recorded by the ATLAS experiment at the LHC in 2015 and 2016. No significant deviation from the background expectation is found.

Results are interpreted in terms of simplified models or pMSSM models with only first- and second-generation squarks, or gluinos, together with a neutralino LSP, with the masses of all the other SUSY particles set such that the particles are effectively decoupled. For a massless lightest neutralino, gluino masses below 2.03 TeV are excluded at the 95% confidence level in a simplified model with only gluinos and the lightest neutralino. For a simplified model involving the strong production of squarks of the first and second generations, with decays to a massless lightest neutralino, squark masses below 1.55 TeV are excluded, assuming mass-degenerate

squarks of the first two generations. No exclusion is obtained for simplified models of squark (gluino) pair production with lightest neutralino masses above 630 GeV (970 GeV). In simplified models with pair-produced squarks and gluinos, each decaying via an intermediate $\tilde{\chi}_1^{\pm}$ to one quark or two quarks, a W boson and a $\tilde{\chi}_1^0$, squark masses below 1.15 TeV and gluino masses below 1.98 TeV are excluded for massless $\tilde{\chi}_1^0$. In pMSSM models assuming squarks, gluinos and $\tilde{\chi}_1^0$, gluino masses below 2.0 TeV are excluded for a squark mass of 6 TeV or squark masses below 2.2 TeV are excluded for a gluino mass of 6 TeV for massless $\tilde{\chi}_1^0$.

These results substantially extend the region of supersymmetric parameter space previously excluded by ATLAS searches.

ACKNOWLEDGMENTS

We thank CERN for the very successful operation of the LHC, as well as the support staff from our institutions without whom ATLAS could not be operated efficiently. We acknowledge the support of ANPCyT, Argentina; YerPhI, Armenia; ARC, Australia; BMWFW and FWF, Austria; ANAS, Azerbaijan; SSTC, Belarus; CNPq and FAPESP, Brazil; NSERC, NRC and CFI, Canada; CERN; CONICYT, Chile; CAS, MOST and NSFC, China; COLCIENCIAS, Colombia; MSMT CR, MPO CR and VSC CR, Czech Republic; DNRF and DNSRC, Denmark; IN2P3-CNRS, CEA-DRF/IRFU, France; SRNSF, Georgia; BMBF, HGF, and MPG, Germany; GSRT, Greece; RGC, Hong Kong SAR, China; ISF, I-CORE and Benoziyo Center, Israel; INFN, Italy; MEXT and JSPS, Japan; CNRST, Morocco; NWO, Netherlands; RCN, Norway; MNiSW and NCN, Poland; FCT, Portugal; MNE/IFA, Romania; MES of Russia and NRC KI, Russian Federation; JINR; MESTD, Serbia; MSSR, Slovakia; ARRS and MIZŠ, Slovenia; DST/NRF, South Africa; MINECO, Spain; SRC and Wallenberg Foundation, Sweden; SERI, SNSF and Cantons of Bern and Geneva, Switzerland; MOST, Taiwan; TAEK, Turkey; STFC, United Kingdom; DOE and NSF, United States of America. In addition, individual groups and members have received support from BCKDF, the Canada Council, CANARIE, CRC, Compute Canada, FQRNT, and the Ontario Innovation Trust, Canada; EPLANET, ERC, ERDF, FP7, Horizon 2020 and Marie Skłodowska-Curie Actions, European Union; Investissements d'Avenir Labex and Idex, ANR, Région Auvergne and Fondation Partager le Savoir, France; DFG and AvH Foundation, Germany; Herakleitos, Thales and Aristeia programmes co-financed by EU-ESF and the Greek NSRF; BSF, GIF and Minerva, Israel; BRF, Norway; CERCA Programme Generalitat de Catalunya, Generalitat Valenciana, Spain; the Royal Society and Leverhulme Trust, United Kingdom. The crucial computing support from all WLCG partners is acknowledged gratefully, in particular from CERN, the ATLAS Tier-1 facilities at TRIUMF (Canada), NDGF (Denmark, Norway, Sweden), CC-IN2P3 (France), KIT/GridKA (Germany), INFN-CNAF (Italy), NL-T1 (Netherlands), PIC (Spain), ASGC (Taiwan), RAL (UK) and BNL (USA), the Tier-2 facilities worldwide and large non-WLCG resource providers. Major contributors of computing resources are listed in Ref. [98].

[1] Y. A. Golfand and E. P. Likhtman, Extension of the algebra of Poincare group generators and violation of p invariance, JETP Lett. **13**, 452 (1971).
[2] D. V. Volkov and V. P. Akulov, Is the neutrino a Goldstone particle?, Phys. Lett. B **46**, 109 (1973).
[3] J. Wess and B. Zumino, Supergauge transformations in four-dimensions, Nucl. Phys. **B70**, 39 (1974).
[4] J. Wess and B. Zumino, Supergauge invariant extension of quantum electrodynamics, Nucl. Phys. **B78**, 1 (1974).
[5] S. Ferrara and B. Zumino, Supergauge invariant Yang-Mills theories, Nucl. Phys. **B79**, 413 (1974).
[6] A. Salam and J. A. Strathdee, Supersymmetry and non-Abelian gauges, Phys. Lett. B **51**, 353 (1974).
[7] G. R. Farrar and P. Fayet, Phenomenology of the production, decay, and detection of new hadronic states associated with supersymmetry, Phys. Lett. **76B**, 575 (1978).
[8] L. Evans and P. Bryant, LHC machine, J. Instrum. **3**, S08001 (2008).
[9] P. Fayet, Supersymmetry and weak, electromagnetic and strong interactions, Phys. Lett. **64B**, 159 (1976).
[10] P. Fayet, Spontaneously broken supersymmetric theories of weak, electromagnetic and strong interactions, Phys. Lett. **69B**, 489 (1977).
[11] ATLAS Collaboration, Search for squarks and gluinos in final states with jets and missing transverse momentum at $\sqrt{s} = 13$ TeV with the ATLAS detector, Eur. Phys. J. C **76**, 392 (2016).
[12] M. R. Buckley, J. D. Lykken, C. Rogan, and M. Spiropulu, Super-razor and searches for sleptons and charginos at the LHC, Phys. Rev. D **89**, 055020 (2014).
[13] P. Jackson, C. Rogan, and M. Santoni, Sparticles in motion: Analyzing compressed SUSY scenarios with a new method of event reconstruction, Phys. Rev. D **95**, 035031 (2017).
[14] P. Jackson and C. Rogan, Recursive jigsaw reconstruction: HEP event analysis in the presence of kinematic and combinatoric ambiguities, Phys. Rev. D **96**, 112007 (2017).

[15] CMS Collaboration, Searches for Supersymmetry using the M_{T2} Variable in Hadronic Events Produced in pp Collisions at 8 TeV, J. High Energy Phys. 05 (2015) 078.

[16] CMS Collaboration, A search for new phenomena in pp collisions at $\sqrt{s} = 13$ TeV in final states with missing transverse momentum and at least one jet using the α_T variable, Eur. Phys. J. C **77**, 294 (2017).

[17] CMS Collaboration, Inclusive search for supersymmetry using razor variables in pp collisions at $\sqrt{s} = 13$ TeV, Phys. Rev. D **95**, 012003 (2017).

[18] CMS Collaboration, Search for new physics with the MT2 variable in all-jets final states produced in pp collisions at $\sqrt{s} = 13$ TeV, J. High Energy Phys. 10 (2016) 006.

[19] ATLAS Collaboration, Search for gluinos in events with an isolated lepton, jets and missing transverse momentum at $\sqrt{s} = 13$ TeV with the ATLAS detector, Eur. Phys. J. C **76**, 565 (2016).

[20] J. Alwall, M. Le, M. Lisanti, and J. G. Wacker, Searching for directly decaying gluinos at the tevatron, Phys. Lett. B **666**, 34 (2008).

[21] J. Alwall, P. Schuster, and N. Toro, Simplified models for a first characterization of new physics at the LHC, Phys. Rev. D **79**, 075020 (2009).

[22] D. Alves *et al.*, Simplified models for LHC new physics searches, J. Phys. G **39**, 105005 (2012).

[23] A. Djouadi *et al.*, The minimal supersymmetric standard model: Group summary report, arXiv:hep-ph/9901246.

[24] C. F. Berger, J. S. Gainer, J. Hewett, and T. G. Rizzo, Supersymmetry without prejudice, J. High Energy Phys. 02 (2009) 023.

[25] ATLAS Collaboration, The ATLAS experiment at the CERN Large Hadron Collider, J. Instrum. **3**, S08003 (2008).

[26] ATLAS Collaboration, ATLAS insertable B-layer technical design report, Report No. ATLAS-TDR-19, 2010, https://cdsweb.cern.ch/record/1291633; ATLAS insertable B-layer technical design report addendum, Report No. ATLAS-TDR-19-ADD-1, 2012, https://cds.cern.ch/record/1451888.

[27] ATLAS Collaboration, Performance of the ATLAS trigger system in 2015, Eur. Phys. J. C **77**, 317 (2017).

[28] ATLAS Collaboration, Improved luminosity determination in pp collisions at $\sqrt{s} = 7$ TeV using the ATLAS detector at the LHC, Eur. Phys. J. C **73**, 2518 (2013).

[29] J. Alwall, R. Frederix, S. Frixione, V. Hirschi, F. Maltoni, O. Mattelaer, H.-S. Shao, T. Stelzer, P. Torrielli, and M. Zaro, The automated computation of tree-level and next-to-leading order differential cross sections, and their matching to parton shower simulations, J. High Energy Phys. 07 (2014) 079.

[30] T. Sjöstrand, S. Ask, J. R. Christiansen, R. Corke, N. Desai, P. Ilten, S. Mrenna, S. Prestel, C. O. Rasmussen, and P. Z. Skands, An introduction to PYTHIA 8.2, Comput. Phys. Commun. **191**, 159 (2015).

[31] L. Lönnblad and S. Prestel, Matching tree-level matrix elements with interleaved showers, J. High Energy Phys. 03 (2012) 019.

[32] ATLAS Collaboration, Summary of ATLAS Pythia 8 tunes, Report No. ATL-PHYS-PUB-2012-003, 2012, https://cdsweb.cern.ch/record/1474107.

[33] R. D. Ball *et al.*, Parton distributions with LHC data, Nucl. Phys. **B867**, 244 (2013).

[34] W. Beenakker, R. Höpker, M. Spira, and P.M. Zerwas, Squark and gluino production at hadron colliders, Nucl. Phys. **B492**, 51 (1997).

[35] A. Kulesza and L. Motyka, Threshold Resummation for Squark-Antisquark and Gluino-Pair Production at the LHC, Phys. Rev. Lett. **102**, 111802 (2009).

[36] A. Kulesza and L. Motyka, Soft gluon resummation for the production of gluino-gluino and squark-antisquark pairs at the LHC, Phys. Rev. D **80**, 095004 (2009).

[37] W. Beenakker, S. Brensing, M. Krämer, A. Kulesza, E. Laenen, and I. Niessen, Soft-gluon resummation for squark and gluino hadroproduction, J. High Energy Phys. 12 (2009) 041.

[38] W. Beenakker, S. Brensing, M. Krämer, A. Kulesza, E. Laenen, L. Motyka, and I. Niessen, Squark and gluino hadroproduction, Int. J. Mod. Phys. A **26**, 2637 (2011).

[39] C. Borschensky, M. Krämer, A. Kulesza, M. Mangano, S. Padhi, T. Plehn, and X. Portell, Squark and gluino production cross sections in pp collisions at $\sqrt{s} = 13$, 14, 33 and 100 TeV, Eur. Phys. J. C **74**, 3174 (2014).

[40] ATLAS Collaboration, Monte Carlo generators for the production of a W or Z/γ^* boson in association with jets at ATLAS in Run 2, Report No. ATL-PHYS-PUB-2016-003, 2016, https://cds.cern.ch/record/2120133.

[41] T. Gleisberg, S. Höche, F. Krauss, M. Schönherr, S. Schumann, F. Siegert, and J. Winter, Event generation with SHERPA 1.1, J. High Energy Phys. 02 (2009) 007.

[42] T. Gleisberg and S. Höche, Comix, A new matrix element generator, J. High Energy Phys. 12 (2008) 039.

[43] F. Cascioli, P. Maierhofer, and S. Pozzorini, Scattering Amplitudes with Open Loops, Phys. Rev. Lett. **108**, 111601 (2012).

[44] S. Schumann and F. Krauss, A Parton shower algorithm based on Catani-Seymour dipole factorisation, J. High Energy Phys. 03 (2008) 038.

[45] S. Höche, F. Krauss, M. Schönherr, and F. Siegert, QCD matrix elements + parton showers: The NLO case, J. High Energy Phys. 04 (2013) 027.

[46] S. Höche, F. Krauss, S. Schumann, and F. Siegert, QCD matrix elements and truncated showers, J. High Energy Phys. 05 (2009) 053.

[47] R. Gavin, Y. Li, F. Petriello, and S. Quackenbush, FEWZ 2.0: A code for hadronic Z production at next-to-next-to-leading order, Comput. Phys. Commun. **182**, 2388 (2011).

[48] ATLAS Collaboration, Simulation of top quark production for the ATLAS experiment at $\sqrt{s} = 13$ TeV, Report No. ATL-PHYS-PUB-2016-004, 2016, https://cds.cern.ch/record/2120417.

[49] S. Alioli, P. Nason, C. Oleari, and E. Re, A general framework for implementing NLO calculations in shower Monte Carlo programs: The POWHEG BOX, J. High Energy Phys. 06 (2010) 043.

[50] H.-L. Lai, M. Guzzi, J. Huston, Z. Li, P. M. Nadolsky, J. Pumplin, and C.-P. Yuan, New parton distributions for collider physics, Phys. Rev. D **82**, 074024 (2010).

[51] P. Artoisenet, R. Frederix, O. Mattelaer, and R. Rietkerk, Automatic spin-entangled decays of heavy resonances in Monte Carlo simulations, J. High Energy Phys. 03 (2013) 015.

[52] T. Sjöstrand, S. Mrenna, and P. Skands, PYTHIA 6.4 Physics and Manual, J. High Energy Phys. 05 (2006) 026.
[53] J. Pumplin, D. R. Stump, J. Huston, H.-L. Lai, P. Nadolsky, and W.-K. Tung, New generation of parton distributions with uncertainties from global QCD analysis, J. High Energy Phys. 07 (2002) 012.
[54] P. Z. Skands, Tuning Monte Carlo generators: The Perugia Tunes, Phys. Rev. D **82**, 074018 (2010).
[55] M. Czakon, P. Fiedler, and A. Mitov, Total Top-Quark Pair-Production Cross Section at Hadron Colliders Through $O(\alpha_S^4)$, Phys. Rev. Lett. **110**, 252004 (2013).
[56] M. Czakon and A. Mitov, Top++: A program for the calculation of the top-pair cross section at Hadron colliders, Comput. Phys. Commun. **185**, 2930 (2014).
[57] M. Aliev, H. Lacker, U. Langenfeld, S. Moch, P. Uwer, and M. Wiedermann, HATHOR: HAdronic top and heavy quarks cross section calculator, Comput. Phys. Commun. **182**, 1034 (2011).
[58] P. Kant, O. M. Kind, T. Kintscher, T. Lohse, T. Martini, S. Mölbitz, P. Rieck, and P. Uwer, HatHor for single top-quark production: Updated predictions and uncertainty estimates for single top-quark production in hadronic collisions, Comput. Phys. Commun. **191**, 74 (2015).
[59] N. Kidonakis, Two-loop soft anomalous dimensions for single top quark associated production with a W^- or H^-, Phys. Rev. D **82**, 054018 (2010).
[60] N. Kidonakis, Next-to-next-to-leading-order collinear and soft gluon corrections for t-channel single top quark production, Phys. Rev. D **83**, 091503 (2011).
[61] ATLAS Collaboration, Modelling of the $t\bar{t}H$ and $t\bar{t}V$ ($V = W, Z$) processes for $\sqrt{s} = 13$ TeV ATLAS analyses, Report No. ATL-PHYS-PUB-2016-005, 2016 https://cds.cern.ch/record/2120826.
[62] A. Lazopoulos, T. McElmurry, K. Melnikov, and F. Petriello, Next-to-leading order QCD corrections to $t\bar{t}Z$ production at the LHC, Phys. Lett. B **666**, 62 (2008).
[63] J. M. Campbell and R. K. Ellis, $t\bar{t}W^{\pm}$ production and decay at NLO, J. High Energy Phys. 07 (2012) 052.
[64] ATLAS Collaboration, Multi-boson simulation for 13 TeV ATLAS analyses, Report No. ATL-PHYS-PUB-2016-002, 2016, https://cds.cern.ch/record/2119986.
[65] ATLAS Collaboration, The ATLAS simulation infrastructure, Eur. Phys. J. C **70**, 823 (2010).
[66] S. Agostinelli *et al.*, GEANT4: A simulation toolkit, Nucl. Instrum. Methods Phys. Res., Sect. A **506**, 250 (2003).
[67] ATLAS Collaboration, The simulation principle and performance of the ATLAS fast calorimeter simulation FastCaloSim, Report No. ATL-PHYS-PUB-2010-013, 2010, https://cds.cern.ch/record/1300517.
[68] D. J. Lange, The EvtGen particle decay simulation package, Nucl. Instrum. Methods Phys. Res, Sect. A **462**, 152 (2001).
[69] A. D. Martin, W. J. Stirling, R. S. Thorne, and G. Watt, Parton distributions for the LHC, Eur. Phys. J. C **63**, 189 (2009).
[70] M. Cacciari, G. P. Salam, and G. Soyez, The anti-k_t jet clustering algorithm, J. High Energy Phys. 04 (2008) 063.
[71] M. Cacciari, G. P. Salam, and G. Soyez, FastJet User Manual, Eur. Phys. J. C **72**, 1896 (2012).
[72] ATLAS Collaboration, Topological cell clustering in the ATLAS calorimeters and its performance in LHC Run 1, Eur. Phys. J. C **77**, 490 (2017).
[73] M. Cacciari and G. P. Salam, Pileup subtraction using jet areas, Phys. Lett. B **659**, 119 (2008).
[74] ATLAS Collaboration, Performance of pile-up mitigation techniques for jets in pp collisions at $\sqrt{s} = 8$ TeV using the ATLAS detector, Eur. Phys. J. C **76**, 581 (2016).
[75] ATLAS Collaboration, Jet energy scale measurements and their systematic uncertainties in proton-proton collisions at $\sqrt{s} = 13$ TeV with the ATLAS detector, Phys. Rev. D **96**, 072002 (2017).
[76] ATLAS Collaboration, Performance of b-Jet Identification in the ATLAS Experiment, J. Instrum. **11**, P04008 (2016).
[77] ATLAS Collaboration, Optimisation of the ATLAS b-tagging performance for the 2016 LHC Run, Report No. ATL-PHYS-PUB-2016-012, 2016, https://cds.cern.ch/record/2160731.
[78] ATLAS Collaboration, Characterisation and mitigation of beam-induced backgrounds observed in the ATLAS detector during the 2011 proton-proton run, J. Instrum. **8**, P07004 (2013).
[79] ATLAS Collaboration, Tagging and suppression of pileup jets with the ATLAS detector, Report No. ATLAS-CONF-2014-018, 2014, https://cds.cern.ch/record/1700870.
[80] ATLAS Collaboration, Muon reconstruction performance of the ATLAS detector in proton-proton collision data at $\sqrt{s} = 13$ TeV, Eur. Phys. J. C **76**, 292 (2016).
[81] ATLAS Collaboration, Electron efficiency measurements with the ATLAS detector using 2012 LHC proton-proton collision data, Eur. Phys. J. C **77**, 195 (2017).
[82] ATLAS Collaboration, Measurement of the photon identification efficiencies with the ATLAS detector using LHC Run-1 data, Eur. Phys. J. C **76**, 666 (2016).
[83] ATLAS Collaboration, Expected performance of missing transverse momentum reconstruction for the ATLAS detector at $\sqrt{s} = 13$ TeV, Report No. ATL-PHYS-PUB-2015-023, 2015, https://cdsweb.cern.ch/record/2037700.
[84] B. Nachman, P. Nef, A. Schwartzman, M. Swiatlowski, and C. Wanotayaroj, Jets from Jets: Re-clustering as a tool for large radius jet reconstruction and grooming at the LHC, J. High Energy Phys. 02 (2015) 075.
[85] M. Baak, G. Besjes, D. Cote, A. Koutsman, J. Lorenz, and D. Short, HistFitter software framework for statistical data analysis, Eur. Phys. J. C **75**, 153 (2015).
[86] A. L. Read, Presentation of Search Results: The CL(s) Technique, J. Phys. G **28**, 2693 (2002).
[87] ATLAS Collaboration, HepData record for this publication, http://dx.doi.org/10.17182/hepdata.77891.v3.
[88] I. Hinchliffe, F. E. Paige, M. D. Shapiro, J. Soderqvist, and W. Yao, Precision SUSY measurements at CERN LHC, Phys. Rev. D **55**, 5520 (1997).
[89] C. Chen, New approach to identifying boosted hadronically decaying particles using jet substructure in its center-of-mass frame, Phys. Rev. D **85**, 034007 (2012).
[90] ATLAS Collaboration, Search for squarks and gluinos with the ATLAS detector in final states with jets and missing transverse momentum using 4.7 fb^{-1} of $\sqrt{s} = 7$ TeV proton-proton collision data, Phys. Rev. D **87**, 012008 (2013).

[91] ATLAS Collaboration, Jet energy measurement with the ATLAS detector in proton-proton collisions at $\sqrt{s} = 7$ TeV, Eur. Phys. J. C **73**, 2304 (2013).
[92] ATLAS Collaboration, Measurements of top quark pair relative differential cross sections with ATLAS in pp collisions at $\sqrt{s} = 7$ TeV, Eur. Phys. J. C **73**, 2261 (2013).
[93] ATLAS Collaboration, Jet mass reconstruction with the ATLAS Detector in early Run 2 data, ATLAS-CONF-2016-035, 2016, https://cds.cern.ch/record/2200211.
[94] G. Cowan, K. Cranmer, E. Gross, and O. Vitells, Asymptotic formulae for likelihood-based tests of new physics, Eur. Phys. J. C **71**, 1554 (2011).
[95] ATLAS Collaboration, Summary of the searches for squarks and gluinos using $\sqrt{s} = 8$ TeV pp collisions with the ATLAS experiment at the LHC, J. High Energy Phys. 10 (2015) 054.
[96] ATLAS Collaboration, Search for new phenomena in events containing a same-flavour opposite-sign dilepton pair, jets, and large missing transverse momentum in $\sqrt{s} = 13$ pp collisions with the ATLAS detector, Eur. Phys. J. C **77**, 144 (2017).
[97] ATLAS Collaboration, Search for squarks and gluinos with the ATLAS detector in final states with jets and missing transverse momentum using $\sqrt{s} = 8$ TeV proton-proton collision data, J. High Energy Phys. 09 (2014) 176.
[98] ATLAS Collaboration, ATLAS Computing Acknowledgements 2016–2017, Report No. ATL-GEN-PUB-2016-002, https://cds.cern.ch/record/2202407.

M. Aaboud,[137d] G. Aad,[88] B. Abbott,[115] O. Abdinov,[12,a] B. Abeloos,[119] S. H. Abidi,[161] O. S. AbouZeid,[139] N. L. Abraham,[151] H. Abramowicz,[155] H. Abreu,[154] R. Abreu,[118] Y. Abulaiti,[148a,148b] B. S. Acharya,[167a,167b,b] S. Adachi,[157] L. Adamczyk,[41a] J. Adelman,[110] M. Adersberger,[102] T. Adye,[133] A. A. Affolder,[139] T. Agatonovic-Jovin,[14] C. Agheorghiesei,[28c] J. A. Aguilar-Saavedra,[128a,128f] S. P. Ahlen,[24] F. Ahmadov,[68,c] G. Aielli,[135a,135b] S. Akatsuka,[71] H. Akerstedt,[148a,148b] T. P. A. Åkesson,[84] E. Akilli,[52] A. V. Akimov,[98] G. L. Alberghi,[22a,22b] J. Albert,[172] P. Albicocco,[50] M. J. Alconada Verzini,[74] S. C. Alderweireldt,[108] M. Aleksa,[32] I. N. Aleksandrov,[68] C. Alexa,[28b] G. Alexander,[155] T. Alexopoulos,[10] M. Alhroob,[115] B. Ali,[130] M. Aliev,[76a,76b] G. Alimonti,[94a] J. Alison,[33] S. P. Alkire,[38] B. M. M. Allbrooke,[151] B. W. Allen,[118] P. P. Allport,[19] A. Aloisio,[106a,106b] A. Alonso,[39] F. Alonso,[74] C. Alpigiani,[140] A. A. Alshehri,[56] M. I. Alstaty,[88] B. Alvarez Gonzalez,[32] D. Álvarez Piqueras,[170] M. G. Alviggi,[106a,106b] B. T. Amadio,[16] Y. Amaral Coutinho,[26a] C. Amelung,[25] D. Amidei,[92] S. P. Amor Dos Santos,[128a,128c] A. Amorim,[128a,128b] S. Amoroso,[32] G. Amundsen,[25] C. Anastopoulos,[141] L. S. Ancu,[52] N. Andari,[19] T. Andeen,[11] C. F. Anders,[60b] J. K. Anders,[77] K. J. Anderson,[33] A. Andreazza,[94a,94b] V. Andrei,[60a] S. Angelidakis,[9] I. Angelozzi,[109] A. Angerami,[38] A. V. Anisenkov,[111,d] N. Anjos,[13] A. Annovi,[126a,126b] C. Antel,[60a] M. Antonelli,[50] A. Antonov,[100,a] D. J. Antrim,[166] F. Anulli,[134a] M. Aoki,[69] L. Aperio Bella,[32] G. Arabidze,[93] Y. Arai,[69] J. P. Araque,[128a] V. Araujo Ferraz,[26a] A. T. H. Arce,[48] R. E. Ardell,[80] F. A. Arduh,[74] J-F. Arguin,[97] S. Argyropoulos,[66] M. Arik,[20a] A. J. Armbruster,[32] L. J. Armitage,[79] O. Arnaez,[161] H. Arnold,[51] M. Arratia,[30] O. Arslan,[23] A. Artamonov,[99] G. Artoni,[122] S. Artz,[86] S. Asai,[157] N. Asbah,[45] A. Ashkenazi,[155] L. Asquith,[151] K. Assamagan,[27] R. Astalos,[146a] M. Atkinson,[169] N. B. Atlay,[143] K. Augsten,[130] G. Avolio,[32] B. Axen,[16] M. K. Ayoub,[119] G. Azuelos,[97,e] A. E. Baas,[60a] M. J. Baca,[19] H. Bachacou,[138] K. Bachas,[76a,76b] M. Backes,[122] M. Backhaus,[32] P. Bagnaia,[134a,134b] M. Bahmani,[42] H. Bahrasemani,[144] J. T. Baines,[133] M. Bajic,[39] O. K. Baker,[179] E. M. Baldin,[111,d] P. Balek,[175] F. Balli,[138] W. K. Balunas,[124] E. Banas,[42] A. Bandyopadhyay,[23] Sw. Banerjee,[176,f] A. A. E. Bannoura,[178] L. Barak,[32] E. L. Barberio,[91] D. Barberis,[53a,53b] M. Barbero,[88] T. Barillari,[103] M-S Barisits,[32] J. T. Barkeloo,[118] T. Barklow,[145] N. Barlow,[30] S. L. Barnes,[36c] B. M. Barnett,[133] R. M. Barnett,[16] Z. Barnovska-Blenessy,[36a] A. Baroncelli,[136a] G. Barone,[25] A. J. Barr,[122] L. Barranco Navarro,[170] F. Barreiro,[85] J. Barreiro Guimarães da Costa,[35a] R. Bartoldus,[145] A. E. Barton,[75] P. Bartos,[146a] A. Basalaev,[125] A. Bassalat,[119,g] R. L. Bates,[56] S. J. Batista,[161] J. R. Batley,[30] M. Battaglia,[139] M. Bauce,[134a,134b] F. Bauer,[138] H. S. Bawa,[145,h] J. B. Beacham,[113] M. D. Beattie,[75] T. Beau,[83] P. H. Beauchemin,[165] P. Bechtle,[23] H. P. Beck,[18,i] H. C. Beck,[57] K. Becker,[122] M. Becker,[86] M. Beckingham,[173] C. Becot,[112] A. J. Beddall,[20d] A. Beddall,[20b] V. A. Bednyakov,[68] M. Bedognetti,[109] C. P. Bee,[150] T. A. Beermann,[32] M. Begalli,[26a] M. Begel,[27] J. K. Behr,[45] A. S. Bell,[81] G. Bella,[155] L. Bellagamba,[22a] A. Bellerive,[31] M. Bellomo,[154] K. Belotskiy,[100] O. Beltramello,[32] N. L. Belyaev,[100] O. Benary,[155,a] D. Benchekroun,[137a] M. Bender,[102] K. Bendtz,[148a,148b] N. Benekos,[10] Y. Benhammou,[155] E. Benhar Noccioli,[179] J. Benitez,[66] D. P. Benjamin,[48] M. Benoit,[52] J. R. Bensinger,[25] S. Bentvelsen,[109] L. Beresford,[122] M. Beretta,[50] D. Berge,[109] E. Bergeaas Kuutmann,[168] N. Berger,[5] J. Beringer,[16] S. Berlendis,[58] N. R. Bernard,[89] G. Bernardi,[83] C. Bernius,[145] F. U. Bernlochner,[23] T. Berry,[80] P. Berta,[131] C. Bertella,[35a] G. Bertoli,[148a,148b] F. Bertolucci,[126a,126b] I. A. Bertram,[75] C. Bertsche,[45] D. Bertsche,[115]

G. J. Besjes,[39] O. Bessidskaia Bylund,[148a,148b] M. Bessner,[45] N. Besson,[138] C. Betancourt,[51] A. Bethani,[87] S. Bethke,[103] A. J. Bevan,[79] J. Beyer,[103] R. M. Bianchi,[127] O. Biebel,[102] D. Biedermann,[17] R. Bielski,[87] K. Bierwagen,[86] N. V. Biesuz,[126a,126b] M. Biglietti,[136a] T. R. V. Billoud,[97] H. Bilokon,[50] M. Bindi,[57] A. Bingul,[20b] C. Bini,[134a,134b] S. Biondi,[22a,22b] T. Bisanz,[57] C. Bittrich,[47] D. M. Bjergaard,[48] C. W. Black,[152] J. E. Black,[145] K. M. Black,[24] R. E. Blair,[6] T. Blazek,[146a] I. Bloch,[45] C. Blocker,[25] A. Blue,[56] W. Blum,[86,a] U. Blumenschein,[79] S. Blunier,[34a] G. J. Bobbink,[109] V. S. Bobrovnikov,[111,d] S. S. Bocchetta,[84] A. Bocci,[48] C. Bock,[102] M. Boehler,[51] D. Boerner,[178] D. Bogavac,[102] A. G. Bogdanchikov,[111] C. Bohm,[148a] V. Boisvert,[80] P. Bokan,[168,j] T. Bold,[41a] A. S. Boldyrev,[101] A. E. Bolz,[60b] M. Bomben,[83] M. Bona,[79] M. Boonekamp,[138] A. Borisov,[132] G. Borissov,[75] J. Bortfeldt,[32] D. Bortoletto,[122] V. Bortolotto,[62a,62b,62c] D. Boscherini,[22a] M. Bosman,[13] J. D. Bossio Sola,[29] J. Boudreau,[127] J. Bouffard,[2] E. V. Bouhova-Thacker,[75] D. Boumediene,[37] C. Bourdarios,[119] S. K. Boutle,[56] A. Boveia,[113] J. Boyd,[32] I. R. Boyko,[68] J. Bracinik,[19] A. Brandt,[8] G. Brandt,[57] O. Brandt,[60a] U. Bratzler,[158] B. Brau,[89] J. E. Brau,[118] W. D. Breaden Madden,[56] K. Brendlinger,[45] A. J. Brennan,[91] L. Brenner,[109] R. Brenner,[168] S. Bressler,[175] D. L. Briglin,[19] T. M. Bristow,[49] D. Britton,[56] D. Britzger,[45] F. M. Brochu,[30] I. Brock,[23] R. Brock,[93] G. Brooijmans,[38] T. Brooks,[80] W. K. Brooks,[34b] J. Brosamer,[16] E. Brost,[110] J. H Broughton,[19] P. A. Bruckman de Renstrom,[42] D. Bruncko,[146b] A. Bruni,[22a] G. Bruni,[22a] L. S. Bruni,[109] BH Brunt,[30] M. Bruschi,[22a] N. Bruscino,[23] P. Bryant,[33] L. Bryngemark,[45] T. Buanes,[15] Q. Buat,[144] P. Buchholz,[143] A. G. Buckley,[56] I. A. Budagov,[68] F. Buehrer,[51] M. K. Bugge,[121] O. Bulekov,[100] D. Bullock,[8] T. J. Burch,[110] S. Burdin,[77] C. D. Burgard,[51] A. M. Burger,[5] B. Burghgrave,[110] K. Burka,[42] S. Burke,[133] I. Burmeister,[46] J. T. P. Burr,[122] E. Busato,[37] D. Büscher,[51] V. Büscher,[86] P. Bussey,[56] J. M. Butler,[24] C. M. Buttar,[56] J. M. Butterworth,[81] P. Butti,[32] W. Buttinger,[27] A. Buzatu,[35c] A. R. Buzykaev,[111,d] S. Cabrera Urbán,[170] D. Caforio,[130] V. M. Cairo,[40a,40b] O. Cakir,[4a] N. Calace,[52] P. Calafiura,[16] A. Calandri,[88] G. Calderini,[83] P. Calfayan,[64] G. Callea,[40a,40b] L. P. Caloba,[26a] S. Calvente Lopez,[85] D. Calvet,[37] S. Calvet,[37] T. P. Calvet,[88] R. Camacho Toro,[33] S. Camarda,[32] P. Camarri,[135a,135b] D. Cameron,[121] R. Caminal Armadans,[169] C. Camincher,[58] S. Campana,[32] M. Campanelli,[81] A. Camplani,[94a,94b] A. Campoverde,[143] V. Canale,[106a,106b] M. Cano Bret,[36c] J. Cantero,[116] T. Cao,[155] M. D. M. Capeans Garrido,[32] I. Caprini,[28b] M. Caprini,[28b] M. Capua,[40a,40b] R. M. Carbone,[38] R. Cardarelli,[135a] F. Cardillo,[51] I. Carli,[131] T. Carli,[32] G. Carlino,[106a] B. T. Carlson,[127] L. Carminati,[94a,94b] R. M. D. Carney,[148a,148b] S. Caron,[108] E. Carquin,[34b] S. Carrá,[94a,94b] G. D. Carrillo-Montoya,[32] J. Carvalho,[128a,128c] D. Casadei,[19] M. P. Casado,[13,k] M. Casolino,[13] D. W. Casper,[166] R. Castelijn,[109] V. Castillo Gimenez,[170] N. F. Castro,[128a,l] A. Catinaccio,[32] J. R. Catmore,[121] A. Cattai,[32] J. Caudron,[23] V. Cavaliere,[169] E. Cavallaro,[13] D. Cavalli,[94a] M. Cavalli-Sforza,[13] V. Cavasinni,[126a,126b] E. Celebi,[20c] F. Ceradini,[136a,136b] L. Cerda Alberich,[170] A. S. Cerqueira,[26b] A. Cerri,[151] L. Cerrito,[135a,135b] F. Cerutti,[16] A. Cervelli,[18] S. A. Cetin,[20c] A. Chafaq,[137a] D. Chakraborty,[110] S. K. Chan,[59] W. S. Chan,[109] Y. L. Chan,[62a] P. Chang,[169] J. D. Chapman,[30] D. G. Charlton,[19] C. C. Chau,[161] C. A. Chavez Barajas,[151] S. Che,[113] S. Cheatham,[167a,167c] A. Chegwidden,[93] S. Chekanov,[6] S. V. Chekulaev,[163a] G. A. Chelkov,[68,m] M. A. Chelstowska,[32] C. Chen,[67] H. Chen,[27] J. Chen,[36a] S. Chen,[35b] S. Chen,[157] X. Chen,[35c,n] Y. Chen,[70] H. C. Cheng,[92] H. J. Cheng,[35a] A. Cheplakov,[68] E. Cheremushkina,[132] R. Cherkaoui El Moursli,[137e] E. Cheu,[7] K. Cheung,[63] L. Chevalier,[138] V. Chiarella,[50] G. Chiarelli,[126a,126b] G. Chiodini,[76a] A. S. Chisholm,[32] A. Chitan,[28b] Y. H. Chiu,[172] M. V. Chizhov,[68] K. Choi,[64] A. R. Chomont,[37] S. Chouridou,[156] V. Christodoulou,[81] D. Chromek-Burckhart,[32] M. C. Chu,[62a] J. Chudoba,[129] A. J. Chuinard,[90] J. J. Chwastowski,[42] L. Chytka,[117] A. K. Ciftci,[4a] D. Cinca,[46] V. Cindro,[78] I. A. Cioara,[23] C. Ciocca,[22a,22b] A. Ciocio,[16] F. Cirotto,[106a,106b] Z. H. Citron,[175] M. Citterio,[94a] M. Ciubancan,[28b] A. Clark,[52] B. L. Clark,[59] M. R. Clark,[38] P. J. Clark,[49] R. N. Clarke,[16] C. Clement,[148a,148b] Y. Coadou,[88] M. Cobal,[167a,167c] A. Coccaro,[52] J. Cochran,[67] L. Colasurdo,[108] B. Cole,[38] A. P. Colijn,[109] J. Collot,[58] T. Colombo,[166] P. Conde Muiño,[128a,128b] E. Coniavitis,[51] S. H. Connell,[147b] I. A. Connelly,[87] S. Constantinescu,[28b] G. Conti,[32] F. Conventi,[106a,o] M. Cooke,[16] A. M. Cooper-Sarkar,[122] F. Cormier,[171] K. J. R. Cormier,[161] M. Corradi,[134a,134b] F. Corriveau,[90,p] A. Cortes-Gonzalez,[32] G. Cortiana,[103] G. Costa,[94a] M. J. Costa,[170] D. Costanzo,[141] G. Cottin,[30] G. Cowan,[80] B. E. Cox,[87] K. Cranmer,[112] S. J. Crawley,[56] R. A. Creager,[124] G. Cree,[31] S. Crépé-Renaudin,[58] F. Crescioli,[83] W. A. Cribbs,[148a,148b] M. Cristinziani,[23] V. Croft,[108] G. Crosetti,[40a,40b] A. Cueto,[85] T. Cuhadar Donszelmann,[141] A. R. Cukierman,[145] J. Cummings,[179] M. Curatolo,[50] J. Cúth,[86] P. Czodrowski,[32] G. D'amen,[22a,22b] S. D'Auria,[56] L. D'eramo,[83] M. D'Onofrio,[77] M. J. Da Cunha Sargedas De Sousa,[128a,128b] C. Da Via,[87] W. Dabrowski,[41a] T. Dado,[146a] T. Dai,[92] O. Dale,[15] F. Dallaire,[97] C. Dallapiccola,[89] M. Dam,[39] J. R. Dandoy,[124] M. F. Daneri,[29] N. P. Dang,[176] A. C. Daniells,[19] N. S. Dann,[87] M. Danninger,[171] M. Dano Hoffmann,[138] V. Dao,[150] G. Darbo,[53a] S. Darmora,[8] J. Dassoulas,[3] A. Dattagupta,[118] T. Daubney,[45] W. Davey,[23] C. David,[45] T. Davidek,[131] D. R. Davis,[48] P. Davison,[81] E. Dawe,[91] I. Dawson,[141] K. De,[8] R. de Asmundis,[106a] A. De Benedetti,[115] S. De Castro,[22a,22b]

S. De Cecco,[83] N. De Groot,[108] P. de Jong,[109] H. De la Torre,[93] F. De Lorenzi,[67] A. De Maria,[57] D. De Pedis,[134a] A. De Salvo,[134a] U. De Sanctis,[135a,135b] A. De Santo,[151] K. De Vasconcelos Corga,[88] J. B. De Vivie De Regie,[119] W. J. Dearnaley,[75] R. Debbe,[27] C. Debenedetti,[139] D. V. Dedovich,[68] N. Dehghanian,[3] I. Deigaard,[109] M. Del Gaudio,[40a,40b] J. Del Peso,[85] D. Delgove,[119] F. Deliot,[138] C. M. Delitzsch,[52] A. Dell'Acqua,[32] L. Dell'Asta,[24] M. Dell'Orso,[126a,126b] M. Della Pietra,[106a,106b] D. della Volpe,[52] M. Delmastro,[5] C. Delporte,[119] P. A. Delsart,[58] D. A. DeMarco,[161] S. Demers,[179] M. Demichev,[68] A. Demilly,[83] S. P. Denisov,[132] D. Denysiuk,[138] D. Derendarz,[42] J. E. Derkaoui,[137d] F. Derue,[83] P. Dervan,[77] K. Desch,[23] C. Deterre,[45] K. Dette,[46] M. R. Devesa,[29] P. O. Deviveiros,[32] A. Dewhurst,[133] S. Dhaliwal,[25] F. A. Di Bello,[52] A. Di Ciaccio,[135a,135b] L. Di Ciaccio,[5] W. K. Di Clemente,[124] C. Di Donato,[106a,106b] A. Di Girolamo,[32] B. Di Girolamo,[32] B. Di Micco,[136a,136b] R. Di Nardo,[32] K. F. Di Petrillo,[59] A. Di Simone,[51] R. Di Sipio,[161] D. Di Valentino,[31] C. Diaconu,[88] M. Diamond,[161] F. A. Dias,[39] M. A. Diaz,[34a] E. B. Diehl,[92] J. Dietrich,[17] S. Díez Cornell,[45] A. Dimitrievska,[14] J. Dingfelder,[23] P. Dita,[28b] S. Dita,[28b] F. Dittus,[32] F. Djama,[88] T. Djobava,[54b] J. I. Djuvsland,[60a] M. A. B. do Vale,[26c] D. Dobos,[32] M. Dobre,[28b] C. Doglioni,[84] J. Dolejsi,[131] Z. Dolezal,[131] M. Donadelli,[26d] S. Donati,[126a,126b] P. Dondero,[123a,123b] J. Donini,[37] J. Dopke,[133] A. Doria,[106a] M. T. Dova,[74] A. T. Doyle,[56] E. Drechsler,[57] M. Dris,[10] Y. Du,[36b] J. Duarte-Campderros,[155] A. Dubreuil,[52] E. Duchovni,[175] G. Duckeck,[102] A. Ducourthial,[83] O. A. Ducu,[97,q] D. Duda,[109] A. Dudarev,[32] A. Chr. Dudder,[86] E. M. Duffield,[16] L. Duflot,[119] M. Dührssen,[32] M. Dumancic,[175] A. E. Dumitriu,[28b] A. K. Duncan,[56] M. Dunford,[60a] H. Duran Yildiz,[4a] M. Düren,[55] A. Durglishvili,[54b] D. Duschinger,[47] B. Dutta,[45] D. Duvnjak,[1] M. Dyndal,[45] B. S. Dziedzic,[42] C. Eckardt,[45] K. M. Ecker,[103] R. C. Edgar,[92] T. Eifert,[32] G. Eigen,[15] K. Einsweiler,[16] T. Ekelof,[168] M. El Kacimi,[137c] R. El Kosseifi,[88] V. Ellajosyula,[88] M. Ellert,[168] S. Elles,[5] F. Ellinghaus,[178] A. A. Elliot,[172] N. Ellis,[32] J. Elmsheuser,[27] M. Elsing,[32] D. Emeliyanov,[133] Y. Enari,[157] O. C. Endner,[86] J. S. Ennis,[173] J. Erdmann,[46] A. Ereditato,[18] M. Ernst,[27] S. Errede,[169] M. Escalier,[119] C. Escobar,[170] B. Esposito,[50] O. Estrada Pastor,[170] A. I. Etienvre,[138] E. Etzion,[155] H. Evans,[64] A. Ezhilov,[125] M. Ezzi,[137e] F. Fabbri,[22a,22b] L. Fabbri,[22a,22b] V. Fabiani,[108] G. Facini,[81] R. M. Fakhrutdinov,[132] S. Falciano,[134a] R. J. Falla,[81] J. Faltova,[32] Y. Fang,[35a] M. Fanti,[94a,94b] A. Farbin,[8] A. Farilla,[136a] C. Farina,[127] E. M. Farina,[123a,123b] T. Farooque,[93] S. Farrell,[16] S. M. Farrington,[173] P. Farthouat,[32] F. Fassi,[137e] P. Fassnacht,[32] D. Fassouliotis,[9] M. Faucci Giannelli,[80] A. Favareto,[53a,53b] W. J. Fawcett,[122] L. Fayard,[119] O. L. Fedin,[125,r] W. Fedorko,[171] S. Feigl,[121] L. Feligioni,[88] C. Feng,[36b] E. J. Feng,[32] H. Feng,[92] M. J. Fenton,[56] A. B. Fenyuk,[132] L. Feremenga,[8] P. Fernandez Martinez,[170] S. Fernandez Perez,[13] J. Ferrando,[45] A. Ferrari,[168] P. Ferrari,[109] R. Ferrari,[123a] D. E. Ferreira de Lima,[60b] A. Ferrer,[170] D. Ferrere,[52] C. Ferretti,[92] F. Fiedler,[86] A. Filipčič,[78] M. Filipuzzi,[45] F. Filthaut,[108] M. Fincke-Keeler,[172] K. D. Finelli,[152] M. C. N. Fiolhais,[128a,128c,s] L. Fiorini,[170] A. Fischer,[2] C. Fischer,[13] J. Fischer,[178] W. C. Fisher,[93] N. Flaschel,[45] I. Fleck,[143] P. Fleischmann,[92] R. R. M. Fletcher,[124] T. Flick,[178] B. M. Flierl,[102] L. R. Flores Castillo,[62a] M. J. Flowerdew,[103] G. T. Forcolin,[87] A. Formica,[138] F. A. Förster,[13] A. Forti,[87] A. G. Foster,[19] D. Fournier,[119] H. Fox,[75] S. Fracchia,[141] P. Francavilla,[83] M. Franchini,[22a,22b] S. Franchino,[60a] D. Francis,[32] L. Franconi,[121] M. Franklin,[59] M. Frate,[166] M. Fraternali,[123a,123b] D. Freeborn,[81] S. M. Fressard-Batraneanu,[32] B. Freund,[97] D. Froidevaux,[32] J. A. Frost,[122] C. Fukunaga,[158] T. Fusayasu,[104] J. Fuster,[170] C. Gabaldon,[58] O. Gabizon,[154] A. Gabrielli,[22a,22b] A. Gabrielli,[16] G. P. Gach,[41a] S. Gadatsch,[32] S. Gadomski,[80] G. Gagliardi,[53a,53b] L. G. Gagnon,[97] C. Galea,[108] B. Galhardo,[128a,128c] E. J. Gallas,[122] B. J. Gallop,[133] P. Gallus,[130] G. Galster,[39] K. K. Gan,[113] S. Ganguly,[37] Y. Gao,[77] Y. S. Gao,[145,h] F. M. Garay Walls,[49] C. García,[170] J. E. García Navarro,[170] J. A. García Pascual,[35a] M. Garcia-Sciveres,[16] R. W. Gardner,[33] N. Garelli,[145] V. Garonne,[121] A. Gascon Bravo,[45] K. Gasnikova,[45] C. Gatti,[50] A. Gaudiello,[53a,53b] G. Gaudio,[123a] I. L. Gavrilenko,[98] C. Gay,[171] G. Gaycken,[23] E. N. Gazis,[10] C. N. P. Gee,[133] J. Geisen,[57] M. Geisen,[86] M. P. Geisler,[60a] K. Gellerstedt,[148a,148b] C. Gemme,[53a] M. H. Genest,[58] C. Geng,[92] S. Gentile,[134a,134b] C. Gentsos,[156] S. George,[80] D. Gerbaudo,[13] A. Gershon,[155] G. Geßner,[46] S. Ghasemi,[143] M. Ghneimat,[23] B. Giacobbe,[22a] S. Giagu,[134a,134b] N. Giangiacomi,[22a,22b] P. Giannetti,[126a,126b] S. M. Gibson,[80] M. Gignac,[171] M. Gilchriese,[16] D. Gillberg,[31] G. Gilles,[178] D. M. Gingrich,[3,e] N. Giokaris,[9,a] M. P. Giordani,[167a,167c] F. M. Giorgi,[22a] P. F. Giraud,[138] P. Giromini,[59] G. Giugliarelli,[167a,167c] D. Giugni,[94a] F. Giuli,[122] C. Giuliani,[103] M. Giulini,[60b] B. K. Gjelsten,[121] S. Gkaitatzis,[156] I. Gkialas,[9,t] E. L. Gkougkousis,[139] P. Gkountoumis,[10] L. K. Gladilin,[101] C. Glasman,[85] J. Glatzer,[13] P. C. F. Glaysher,[45] A. Glazov,[45] M. Goblirsch-Kolb,[25] J. Godlewski,[42] S. Goldfarb,[91] T. Golling,[52] D. Golubkov,[132] A. Gomes,[128a,128b,128d] R. Gonçalo,[128a] R. Goncalves Gama,[26a] J. Goncalves Pinto Firmino Da Costa,[138] G. Gonella,[51] L. Gonella,[19] A. Gongadze,[68] S. González de la Hoz,[170] S. Gonzalez-Sevilla,[52] L. Goossens,[32] P. A. Gorbounov,[99] H. A. Gordon,[27] I. Gorelov,[107] B. Gorini,[32] E. Gorini,[76a,76b] A. Gorišek,[78] A. T. Goshaw,[48] C. Gössling,[46] M. I. Gostkin,[68] C. A. Gottardo,[23] C. R. Goudet,[119] D. Goujdami,[137c] A. G. Goussiou,[140] N. Govender,[147b,u] E. Gozani,[154] L. Graber,[57] I. Grabowska-Bold,[41a] P. O. J. Gradin,[168]

J. Gramling,[166] E. Gramstad,[121] S. Grancagnolo,[17] V. Gratchev,[125] P. M. Gravila,[28f] C. Gray,[56] H. M. Gray,[16] Z. D. Greenwood,[82,v] C. Grefe,[23] K. Gregersen,[81] I. M. Gregor,[45] P. Grenier,[145] K. Grevtsov,[5] J. Griffiths,[8] A. A. Grillo,[139] K. Grimm,[75] S. Grinstein,[13,w] Ph. Gris,[37] J.-F. Grivaz,[119] S. Groh,[86] E. Gross,[175] J. Grosse-Knetter,[57] G. C. Grossi,[82] Z. J. Grout,[81] A. Grummer,[107] L. Guan,[92] W. Guan,[176] J. Guenther,[65] F. Guescini,[163a] D. Guest,[166] O. Gueta,[155] B. Gui,[113] E. Guido,[53a,53b] T. Guillemin,[5] S. Guindon,[2] U. Gul,[56] C. Gumpert,[32] J. Guo,[36c] W. Guo,[92] Y. Guo,[36a] R. Gupta,[43] S. Gupta,[122] G. Gustavino,[134a,134b] P. Gutierrez,[115] N. G. Gutierrez Ortiz,[81] C. Gutschow,[81] C. Guyot,[138] M. P. Guzik,[41a] C. Gwenlan,[122] C. B. Gwilliam,[77] A. Haas,[112] C. Haber,[16] H. K. Hadavand,[8] N. Haddad,[137e] A. Hadef,[88] S. Hageböck,[23] M. Hagihara,[164] H. Hakobyan,[180,a] M. Haleem,[45] J. Haley,[116] G. Halladjian,[93] G. D. Hallewell,[88] K. Hamacher,[178] P. Hamal,[117] K. Hamano,[172] A. Hamilton,[147a] G. N. Hamity,[141] P. G. Hamnett,[45] L. Han,[36a] S. Han,[35a] K. Hanagaki,[69,x] K. Hanawa,[157] M. Hance,[139] B. Haney,[124] P. Hanke,[60a] J. B. Hansen,[39] J. D. Hansen,[39] M. C. Hansen,[23] P. H. Hansen,[39] K. Hara,[164] A. S. Hard,[176] T. Harenberg,[178] F. Hariri,[119] S. Harkusha,[95] R. D. Harrington,[49] P. F. Harrison,[173] N. M. Hartmann,[102] M. Hasegawa,[70] Y. Hasegawa,[142] A. Hasib,[49] S. Hassani,[138] S. Haug,[18] R. Hauser,[93] L. Hauswald,[47] L. B. Havener,[38] M. Havranek,[130] C. M. Hawkes,[19] R. J. Hawkings,[32] D. Hayakawa,[159] D. Hayden,[93] C. P. Hays,[122] J. M. Hays,[79] H. S. Hayward,[77] S. J. Haywood,[133] S. J. Head,[19] T. Heck,[86] V. Hedberg,[84] L. Heelan,[8] S. Heer,[23] K. K. Heidegger,[51] S. Heim,[45] T. Heim,[16] B. Heinemann,[45,y] J. J. Heinrich,[102] L. Heinrich,[112] C. Heinz,[55] J. Hejbal,[129] L. Helary,[32] A. Held,[171] S. Hellman,[148a,148b] C. Helsens,[32] R. C. W. Henderson,[75] Y. Heng,[176] S. Henkelmann,[171] A. M. Henriques Correia,[32] S. Henrot-Versille,[119] G. H. Herbert,[17] H. Herde,[25] V. Herget,[177] Y. Hernández Jiménez,[147c] H. Herr,[86] G. Herten,[51] R. Hertenberger,[102] L. Hervas,[32] T. C. Herwig,[124] G. G. Hesketh,[81] N. P. Hessey,[163a] J. W. Hetherly,[43] S. Higashino,[69] E. Higón-Rodriguez,[170] K. Hildebrand,[33] E. Hill,[172] J. C. Hill,[30] K. H. Hiller,[45] S. J. Hillier,[19] M. Hils,[47] I. Hinchliffe,[16] M. Hirose,[51] D. Hirschbuehl,[178] B. Hiti,[78] O. Hladik,[129] X. Hoad,[49] J. Hobbs,[150] N. Hod,[163a] M. C. Hodgkinson,[141] P. Hodgson,[141] A. Hoecker,[32] M. R. Hoeferkamp,[107] F. Hoenig,[102] D. Hohn,[23] T. R. Holmes,[33] M. Homann,[46] S. Honda,[164] T. Honda,[69] T. M. Hong,[127] B. H. Hooberman,[169] W. H. Hopkins,[118] Y. Horii,[105] A. J. Horton,[144] J-Y. Hostachy,[58] S. Hou,[153] A. Hoummada,[137a] J. Howarth,[87] J. Hoya,[74] M. Hrabovsky,[117] J. Hrdinka,[32] I. Hristova,[17] J. Hrivnac,[119] T. Hryn'ova,[5] A. Hrynevich,[96] P. J. Hsu,[63] S.-C. Hsu,[140] Q. Hu,[36a] S. Hu,[36c] Y. Huang,[35a] Z. Hubacek,[130] F. Hubaut,[88] F. Huegging,[23] T. B. Huffman,[122] E. W. Hughes,[38] G. Hughes,[75] M. Huhtinen,[32] P. Huo,[150] N. Huseynov,[68,c] J. Huston,[93] J. Huth,[59] G. Iacobucci,[52] G. Iakovidis,[27] I. Ibragimov,[143] L. Iconomidou-Fayard,[119] Z. Idrissi,[137e] P. Iengo,[32] O. Igonkina,[109,z] T. Iizawa,[174] Y. Ikegami,[69] M. Ikeno,[69] Y. Ilchenko,[11,aa] D. Iliadis,[156] N. Ilic,[145] G. Introzzi,[123a,123b] P. Ioannou,[9,a] M. Iodice,[136a] K. Iordanidou,[38] V. Ippolito,[59] M. F. Isacson,[168] N. Ishijima,[120] M. Ishino,[157] M. Ishitsuka,[159] C. Issever,[122] S. Istin,[20a] F. Ito,[164] J. M. Iturbe Ponce,[62a] R. Iuppa,[162a,162b] H. Iwasaki,[69] J. M. Izen,[44] V. Izzo,[106a] S. Jabbar,[3] P. Jackson,[1] R. M. Jacobs,[23] V. Jain,[2] K. B. Jakobi,[86] K. Jakobs,[51] S. Jakobsen,[65] T. Jakoubek,[129] D. O. Jamin,[116] D. K. Jana,[82] R. Jansky,[52] J. Janssen,[23] M. Janus,[57] P. A. Janus,[41a] G. Jarlskog,[84] N. Javadov,[68,c] T. Javůrek,[51] M. Javurkova,[51] F. Jeanneau,[138] L. Jeanty,[16] J. Jejelava,[54a,bb] A. Jelinskas,[173] P. Jenni,[51,cc] C. Jeske,[173] S. Jézéquel,[5] H. Ji,[176] J. Jia,[150] H. Jiang,[67] Y. Jiang,[36a] Z. Jiang,[145] S. Jiggins,[81] J. Jimenez Pena,[170] S. Jin,[35a] A. Jinaru,[28b] O. Jinnouchi,[159] H. Jivan,[147c] P. Johansson,[141] K. A. Johns,[7] C. A. Johnson,[64] W. J. Johnson,[140] K. Jon-And,[148a,148b] R. W. L. Jones,[75] S. D. Jones,[151] S. Jones,[7] T. J. Jones,[77] J. Jongmanns,[60a] P. M. Jorge,[128a,128b] J. Jovicevic,[163a] X. Ju,[176] A. Juste Rozas,[13,w] M. K. Köhler,[175] A. Kaczmarska,[42] M. Kado,[119] H. Kagan,[113] M. Kagan,[145] S. J. Kahn,[88] T. Kaji,[174] E. Kajomovitz,[48] C. W. Kalderon,[84] A. Kaluza,[86] S. Kama,[43] A. Kamenshchikov,[132] N. Kanaya,[157] L. Kanjir,[78] V. A. Kantserov,[100] J. Kanzaki,[69] B. Kaplan,[112] L. S. Kaplan,[176] D. Kar,[147c] K. Karakostas,[10] N. Karastathis,[10] M. J. Kareem,[57] E. Karentzos,[10] S. N. Karpov,[68] Z. M. Karpova,[68] K. Karthik,[112] V. Kartvelishvili,[75] A. N. Karyukhin,[132] K. Kasahara,[164] L. Kashif,[176] R. D. Kass,[113] A. Kastanas,[149] Y. Kataoka,[157] C. Kato,[157] A. Katre,[52] J. Katzy,[45] K. Kawade,[70] K. Kawagoe,[73] T. Kawamoto,[157] G. Kawamura,[57] E. F. Kay,[77] V. F. Kazanin,[111,d] R. Keeler,[172] R. Kehoe,[43] J. S. Keller,[31] J. J. Kempster,[80] J Kendrick,[19] H. Keoshkerian,[161] O. Kepka,[129] B. P. Kerševan,[78] S. Kersten,[178] R. A. Keyes,[90] M. Khader,[169] F. Khalil-zada,[12] A. Khanov,[116] A. G. Kharlamov,[111,d] T. Kharlamova,[111,d] A. Khodinov,[160] T. J. Khoo,[52] V. Khovanskiy,[99,a] E. Khramov,[68] J. Khubua,[54b,dd] S. Kido,[70] C. R. Kilby,[80] H. Y. Kim,[8] S. H. Kim,[164] Y. K. Kim,[33] N. Kimura,[156] O. M. Kind,[17] B. T. King,[77] D. Kirchmeier,[47] J. Kirk,[133] A. E. Kiryunin,[103] T. Kishimoto,[157] D. Kisielewska,[41a] V. Kitali,[45] K. Kiuchi,[164] O. Kivernyk,[5] E. Kladiva,[146b] T. Klapdor-Kleingrothaus,[51] M. H. Klein,[92] M. Klein,[77] U. Klein,[77] K. Kleinknecht,[86] P. Klimek,[110] A. Klimentov,[27] R. Klingenberg,[46] T. Klingl,[23] T. Klioutchnikova,[32] E.-E. Kluge,[60a] P. Kluit,[109] S. Kluth,[103] E. Kneringer,[65] E. B. F. G. Knoops,[88] A. Knue,[103] A. Kobayashi,[157] D. Kobayashi,[159] T. Kobayashi,[157] M. Kobel,[47] M. Kocian,[145] P. Kodys,[131] T. Koffas,[31] E. Koffeman,[109] N. M. Köhler,[103] T. Koi,[145] M. Kolb,[60b] I. Koletsou,[5] A. A. Komar,[98,a]

Y. Komori,[157] T. Kondo,[69] N. Kondrashova,[36c] K. Köneke,[51] A. C. König,[108] T. Kono,[69,ee] R. Konoplich,[112,ff] N. Konstantinidis,[81] R. Kopeliansky,[64] S. Koperny,[41a] A. K. Kopp,[51] K. Korcyl,[42] K. Kordas,[156] A. Korn,[81] A. A. Korol,[111,d] I. Korolkov,[13] E. V. Korolkova,[141] O. Kortner,[103] S. Kortner,[103] T. Kosek,[131] V. V. Kostyukhin,[23] A. Kotwal,[48] A. Koulouris,[10] A. Kourkoumeli-Charalampidi,[123a,123b] C. Kourkoumelis,[9] E. Kourlitis,[141] V. Kouskoura,[27] A. B. Kowalewska,[42] R. Kowalewski,[172] T. Z. Kowalski,[41a] C. Kozakai,[157] W. Kozanecki,[138] A. S. Kozhin,[132] V. A. Kramarenko,[101] G. Kramberger,[78] D. Krasnopevtsev,[100] M. W. Krasny,[83] A. Krasznahorkay,[32] D. Krauss,[103] J. A. Kremer,[41a] J. Kretzschmar,[77] K. Kreutzfeldt,[55] P. Krieger,[161] K. Krizka,[33] K. Kroeninger,[46] H. Kroha,[103] J. Kroll,[129] J. Kroll,[124] J. Kroseberg,[23] J. Krstic,[14] U. Kruchonak,[68] H. Krüger,[23] N. Krumnack,[67] M. C. Kruse,[48] T. Kubota,[91] H. Kucuk,[81] S. Kuday,[4b] J. T. Kuechler,[178] S. Kuehn,[32] A. Kugel,[60a] F. Kuger,[177] T. Kuhl,[45] V. Kukhtin,[68] R. Kukla,[88] Y. Kulchitsky,[95] S. Kuleshov,[34b] Y. P. Kulinich,[169] M. Kuna,[134a,134b] T. Kunigo,[71] A. Kupco,[129] T. Kupfer,[46] O. Kuprash,[155] H. Kurashige,[70] L. L. Kurchaninov,[163a] Y. A. Kurochkin,[95] M. G. Kurth,[35a] V. Kus,[129] E. S. Kuwertz,[172] M. Kuze,[159] J. Kvita,[117] T. Kwan,[172] D. Kyriazopoulos,[141] A. La Rosa,[103] J. L. La Rosa Navarro,[26d] L. La Rotonda,[40a,40b] F. La Ruffa,[40a,40b] C. Lacasta,[170] F. Lacava,[134a,134b] J. Lacey,[45] H. Lacker,[17] D. Lacour,[83] E. Ladygin,[68] R. Lafaye,[5] B. Laforge,[83] T. Lagouri,[179] S. Lai,[57] S. Lammers,[64] W. Lampl,[7] E. Lançon,[27] U. Landgraf,[51] M. P. J. Landon,[79] M. C. Lanfermann,[52] V. S. Lang,[60a] J. C. Lange,[13] R. J. Langenberg,[32] A. J. Lankford,[166] F. Lanni,[27] K. Lantzsch,[23] A. Lanza,[123a] A. Lapertosa,[53a,53b] S. Laplace,[83] J. F. Laporte,[138] T. Lari,[94a] F. Lasagni Manghi,[22a,22b] M. Lassnig,[32] P. Laurelli,[50] W. Lavrijsen,[16] A. T. Law,[139] P. Laycock,[77] T. Lazovich,[59] M. Lazzaroni,[94a,94b] B. Le,[91] O. Le Dortz,[83] E. Le Guirriec,[88] E. P. Le Quilleuc,[138] M. LeBlanc,[172] T. LeCompte,[6] F. Ledroit-Guillon,[58] C. A. Lee,[27] G. R. Lee,[133,gg] S. C. Lee,[153] L. Lee,[59] B. Lefebvre,[90] G. Lefebvre,[83] M. Lefebvre,[172] F. Legger,[102] C. Leggett,[16] G. Lehmann Miotto,[32] X. Lei,[7] W. A. Leight,[45] M. A. L. Leite,[26d] R. Leitner,[131] D. Lellouch,[175] B. Lemmer,[57] K. J. C. Leney,[81] T. Lenz,[23] B. Lenzi,[32] R. Leone,[7] S. Leone,[126a,126b] C. Leonidopoulos,[49] G. Lerner,[151] C. Leroy,[97] A. A. J. Lesage,[138] C. G. Lester,[30] M. Levchenko,[125] J. Levêque,[5] D. Levin,[92] L. J. Levinson,[175] M. Levy,[19] D. Lewis,[79] B. Li,[36a,hh] C.-Q. Li,[36a] H. Li,[150] L. Li,[36c] Q. Li,[35a] S. Li,[48] X. Li,[36c] Y. Li,[143] Z. Liang,[35a] B. Liberti,[135a] A. Liblong,[161] K. Lie,[62c] J. Liebal,[23] W. Liebig,[15] A. Limosani,[152] S. C. Lin,[182] T. H. Lin,[86] R. A. Linck,[64] B. E. Lindquist,[150] A. E. Lionti,[52] E. Lipeles,[124] A. Lipniacka,[15] M. Lisovyi,[60b] T. M. Liss,[169,ii] A. Lister,[171] A. M. Litke,[139] B. Liu,[153,jj] H. Liu,[92] H. Liu,[27] J. K. K. Liu,[122] J. Liu,[36b] J. B. Liu,[36a] K. Liu,[88] L. Liu,[169] M. Liu,[36a] Y. L. Liu,[36a] Y. Liu,[36a] M. Livan,[123a,123b] A. Lleres,[58] J. Llorente Merino,[35a] S. L. Lloyd,[79] C. Y. Lo,[62b] F. Lo Sterzo,[153] E. M. Lobodzinska,[45] P. Loch,[7] F. K. Loebinger,[87] A. Loesle,[51] K. M. Loew,[25] A. Loginov,[179,a] T. Lohse,[17] K. Lohwasser,[141] M. Lokajicek,[129] B. A. Long,[24] J. D. Long,[169] R. E. Long,[75] L. Longo,[76a,76b] K. A. Looper,[113] J. A. Lopez,[34b] D. Lopez Mateos,[59] I. Lopez Paz,[13] A. Lopez Solis,[83] J. Lorenz,[102] N. Lorenzo Martinez,[5] M. Losada,[21] P. J. Lösel,[102] X. Lou,[35a] A. Lounis,[119] J. Love,[6] P. A. Love,[75] H. Lu,[62a] N. Lu,[92] Y. J. Lu,[63] H. J. Lubatti,[140] C. Luci,[134a,134b] A. Lucotte,[58] C. Luedtke,[51] F. Luehring,[64] W. Lukas,[65] L. Luminari,[134a] O. Lundberg,[148a,148b] B. Lund-Jensen,[149] M. S. Lutz,[89] P. M. Luzi,[83] D. Lynn,[27] R. Lysak,[129] E. Lytken,[84] F. Lyu,[35a] V. Lyubushkin,[68] H. Ma,[27] L. L. Ma,[36b] Y. Ma,[36b] G. Maccarrone,[50] A. Macchiolo,[103] C. M. Macdonald,[141] B. Maček,[78] J. Machado Miguens,[124,128b] D. Madaffari,[170] R. Madar,[37] W. F. Mader,[47] A. Madsen,[45] J. Maeda,[70] S. Maeland,[15] T. Maeno,[27] A. S. Maevskiy,[101] V. Magerl,[51] J. Mahlstedt,[109] C. Maiani,[119] C. Maidantchik,[26a] A. A. Maier,[103] T. Maier,[102] A. Maio,[128a,128b,128d] O. Majersky,[146a] S. Majewski,[118] Y. Makida,[69] N. Makovec,[119] B. Malaescu,[83] Pa. Malecki,[42] V. P. Maleev,[125] F. Malek,[58] U. Mallik,[66] D. Malon,[6] C. Malone,[30] S. Maltezos,[10] S. Malyukov,[32] J. Mamuzic,[170] G. Mancini,[50] I. Mandić,[78] J. Maneira,[128a,128b] L. Manhaes de Andrade Filho,[26b] J. Manjarres Ramos,[47] K. H. Mankinen,[84] A. Mann,[102] A. Manousos,[32] B. Mansoulie,[138] J. D. Mansour,[35a] R. Mantifel,[90] M. Mantoani,[57] S. Manzoni,[94a,94b] L. Mapelli,[32] G. Marceca,[29] L. March,[52] L. Marchese,[122] G. Marchiori,[83] M. Marcisovsky,[129] M. Marjanovic,[37] D. E. Marley,[92] F. Marroquim,[26a] S. P. Marsden,[87] Z. Marshall,[16] M. U. F Martensson,[168] S. Marti-Garcia,[170] C. B. Martin,[113] T. A. Martin,[173] V. J. Martin,[49] B. Martin dit Latour,[15] M. Martinez,[13,w] V. I. Martinez Outschoorn,[169] S. Martin-Haugh,[133] V. S. Martoiu,[28b] A. C. Martyniuk,[81] A. Marzin,[32] L. Masetti,[86] T. Mashimo,[157] R. Mashinistov,[98] J. Masik,[87] A. L. Maslennikov,[111,d] L. Massa,[135a,135b] P. Mastrandrea,[5] A. Mastroberardino,[40a,40b] T. Masubuchi,[157] P. Mättig,[178] J. Maurer,[28b] S. J. Maxfield,[77] D. A. Maximov,[111,d] R. Mazini,[153] I. Maznas,[156] S. M. Mazza,[94a,94b] N. C. Mc Fadden,[107] G. Mc Goldrick,[161] S. P. Mc Kee,[92] A. McCarn,[92] R. L. McCarthy,[150] T. G. McCarthy,[103] L. I. McClymont,[81] E. F. McDonald,[91] J. A. Mcfayden,[81] G. Mchedlidze,[57] S. J. McMahon,[133] P. C. McNamara,[91] R. A. McPherson,[172,p] S. Meehan,[140] T. J. Megy,[51] S. Mehlhase,[102] A. Mehta,[77] T. Meideck,[58] K. Meier,[60a] B. Meirose,[44] D. Melini,[170,kk] B. R. Mellado Garcia,[147c] J. D. Mellenthin,[57] M. Melo,[146a] F. Meloni,[18] A. Melzer,[23] S. B. Menary,[87] L. Meng,[77] X. T. Meng,[92] A. Mengarelli,[22a,22b] S. Menke,[103]

E. Meoni,[40a,40b] S. Mergelmeyer,[17] P. Mermod,[52] L. Merola,[106a,106b] C. Meroni,[94a] F. S. Merritt,[33] A. Messina,[134a,134b] J. Metcalfe,[6] A. S. Mete,[166] C. Meyer,[124] J-P. Meyer,[138] J. Meyer,[109] H. Meyer Zu Theenhausen,[60a] F. Miano,[151] R. P. Middleton,[133] S. Miglioranzi,[53a,53b] L. Mijović,[49] G. Mikenberg,[175] M. Mikestikova,[129] M. Mikuž,[78] M. Milesi,[91] A. Milic,[161] D. W. Miller,[33] C. Mills,[49] A. Milov,[175] D. A. Milstead,[148a,148b] A. A. Minaenko,[132] Y. Minami,[157] I. A. Minashvili,[54b] A. I. Mincer,[112] B. Mindur,[41a] M. Mineev,[68] Y. Minegishi,[157] Y. Ming,[176] L. M. Mir,[13] K. P. Mistry,[124] T. Mitani,[174] J. Mitrevski,[102] V. A. Mitsou,[170] A. Miucci,[18] P. S. Miyagawa,[141] A. Mizukami,[69] J. U. Mjörnmark,[84] T. Mkrtchyan,[180] M. Mlynarikova,[131] T. Moa,[148a,148b] K. Mochizuki,[97] P. Mogg,[51] S. Mohapatra,[38] S. Molander,[148a,148b] R. Moles-Valls,[23] R. Monden,[71] M. C. Mondragon,[93] K. Mönig,[45] J. Monk,[39] E. Monnier,[88] A. Montalbano,[150] J. Montejo Berlingen,[32] F. Monticelli,[74] S. Monzani,[94a,94b] R. W. Moore,[3] N. Morange,[119] D. Moreno,[21] M. Moreno Llácer,[32] P. Morettini,[53a] S. Morgenstern,[32] D. Mori,[144] T. Mori,[157] M. Morii,[59] M. Morinaga,[157] V. Morisbak,[121] A. K. Morley,[32] G. Mornacchi,[32] J. D. Morris,[79] L. Morvaj,[150] P. Moschovakos,[10] M. Mosidze,[54b] H. J. Moss,[141] J. Moss,[145,ll] K. Motohashi,[159] R. Mount,[145] E. Mountricha,[27] E. J. W. Moyse,[89] S. Muanza,[88] F. Mueller,[103] J. Mueller,[127] R. S. P. Mueller,[102] D. Muenstermann,[75] P. Mullen,[56] G. A. Mullier,[18] F. J. Munoz Sanchez,[87] W. J. Murray,[173,133] H. Musheghyan,[32] M. Muškinja,[78] A. G. Myagkov,[132,mm] M. Myska,[130] B. P. Nachman,[16] O. Nackenhorst,[52] K. Nagai,[122] R. Nagai,[69,ee] K. Nagano,[69] Y. Nagasaka,[61] K. Nagata,[164] M. Nagel,[51] E. Nagy,[88] A. M. Nairz,[32] Y. Nakahama,[105] K. Nakamura,[69] T. Nakamura,[157] I. Nakano,[114] R. F. Naranjo Garcia,[45] R. Narayan,[11] D. I. Narrias Villar,[60a] I. Naryshkin,[125] T. Naumann,[45] G. Navarro,[21] R. Nayyar,[7] H. A. Neal,[92] P. Yu. Nechaeva,[98] T. J. Neep,[138] A. Negri,[123a,123b] M. Negrini,[22a] S. Nektarijevic,[108] C. Nellist,[119] A. Nelson,[166] M. E. Nelson,[122] S. Nemecek,[129] P. Nemethy,[112] M. Nessi,[32,nn] M. S. Neubauer,[169] M. Neumann,[178] P. R. Newman,[19] T. Y. Ng,[62c] T. Nguyen Manh,[97] R. B. Nickerson,[122] R. Nicolaidou,[138] J. Nielsen,[139] V. Nikolaenko,[132,mm] I. Nikolic-Audit,[83] K. Nikolopoulos,[19] J. K. Nilsen,[121] P. Nilsson,[27] Y. Ninomiya,[157] A. Nisati,[134a] N. Nishu,[35c] R. Nisius,[103] I. Nitsche,[46] T. Nitta,[174] T. Nobe,[157] Y. Noguchi,[71] M. Nomachi,[120] I. Nomidis,[31] M. A. Nomura,[27] T. Nooney,[79] M. Nordberg,[32] N. Norjoharuddeen,[122] O. Novgorodova,[47] M. Nozaki,[69] L. Nozka,[117] K. Ntekas,[166] E. Nurse,[81] F. Nuti,[91] K. O'connor,[25] D. C. O'Neil,[144] A. A. O'Rourke,[45] V. O'Shea,[56] F. G. Oakham,[31,e] H. Oberlack,[103] T. Obermann,[23] J. Ocariz,[83] A. Ochi,[70] I. Ochoa,[38] J. P. Ochoa-Ricoux,[34a] S. Oda,[73] S. Odaka,[69] A. Oh,[87] S. H. Oh,[48] C. C. Ohm,[16] H. Ohman,[168] H. Oide,[53a,53b] H. Okawa,[164] Y. Okumura,[157] T. Okuyama,[69] A. Olariu,[28b] L. F. Oleiro Seabra,[128a] S. A. Olivares Pino,[49] D. Oliveira Damazio,[27] A. Olszewski,[42] J. Olszowska,[42] A. Onofre,[128a,128e] K. Onogi,[105] P. U. E. Onyisi,[11,aa] H. Oppen,[121] M. J. Oreglia,[33] Y. Oren,[155] D. Orestano,[136a,136b] N. Orlando,[62b] R. S. Orr,[161] B. Osculati,[53a,53b,a] R. Ospanov,[36a] G. Otero y Garzon,[29] H. Otono,[73] M. Ouchrif,[137d] F. Ould-Saada,[121] A. Ouraou,[138] K. P. Oussoren,[109] Q. Ouyang,[35a] M. Owen,[56] R. E. Owen,[19] V. E. Ozcan,[20a] N. Ozturk,[8] K. Pachal,[144] A. Pacheco Pages,[13] L. Pacheco Rodriguez,[138] C. Padilla Aranda,[13] S. Pagan Griso,[16] M. Paganini,[179] F. Paige,[27] G. Palacino,[64] S. Palazzo,[40a,40b] S. Palestini,[32] M. Palka,[41b] D. Pallin,[37] E. St. Panagiotopoulou,[10] I. Panagoulias,[10] C. E. Pandini,[83] J. G. Panduro Vazquez,[80] P. Pani,[32] S. Panitkin,[27] D. Pantea,[28b] L. Paolozzi,[52] Th. D. Papadopoulou,[10] K. Papageorgiou,[9,t] A. Paramonov,[6] D. Paredes Hernandez,[179] A. J. Parker,[75] M. A. Parker,[30] K. A. Parker,[45] F. Parodi,[53a,53b] J. A. Parsons,[38] U. Parzefall,[51] V. R. Pascuzzi,[161] J. M. Pasner,[139] E. Pasqualucci,[134a] S. Passaggio,[53a] Fr. Pastore,[80] S. Pataraia,[86] J. R. Pater,[87] T. Pauly,[32] B. Pearson,[103] S. Pedraza Lopez,[170] R. Pedro,[128a,128b] S. V. Peleganchuk,[111,d] O. Penc,[129] C. Peng,[35a] H. Peng,[36a] J. Penwell,[64] B. S. Peralva,[26b] M. M. Perego,[138] D. V. Perepelitsa,[27] F. Peri,[17] L. Perini,[94a,94b] H. Pernegger,[32] S. Perrella,[106a,106b] R. Peschke,[45] V. D. Peshekhonov,[68,a] K. Peters,[45] R. F. Y. Peters,[87] B. A. Petersen,[32] T. C. Petersen,[39] E. Petit,[58] A. Petridis,[1] C. Petridou,[156] P. Petroff,[119] E. Petrolo,[134a] M. Petrov,[122] F. Petrucci,[136a,136b] N. E. Pettersson,[89] A. Peyaud,[138] R. Pezoa,[34b] F. H. Phillips,[93] P. W. Phillips,[133] G. Piacquadio,[150] E. Pianori,[173] A. Picazio,[89] E. Piccaro,[79] M. A. Pickering,[122] R. Piegaia,[29] J. E. Pilcher,[33] A. D. Pilkington,[87] A. W. J. Pin,[87] M. Pinamonti,[135a,135b] J. L. Pinfold,[3] H. Pirumov,[45] M. Pitt,[175] L. Plazak,[146a] M.-A. Pleier,[27] V. Pleskot,[86] E. Plotnikova,[68] D. Pluth,[67] P. Podberezko,[111] R. Poettgen,[148a,148b] R. Poggi,[123a,123b] L. Poggioli,[119] D. Pohl,[23] G. Polesello,[123a] A. Poley,[45] A. Policicchio,[40a,40b] R. Polifka,[32] A. Polini,[22a] C. S. Pollard,[56] V. Polychronakos,[27] K. Pommès,[32] D. Ponomarenko,[100] L. Pontecorvo,[134a] G. A. Popeneciu,[28d] A. Poppleton,[32] S. Pospisil,[130] K. Potamianos,[16] I. N. Potrap,[68] C. J. Potter,[30] G. Poulard,[32] T. Poulsen,[84] J. Poveda,[32] M. E. Pozo Astigarraga,[32] P. Pralavorio,[88] A. Pranko,[16] S. Prell,[67] D. Price,[87] M. Primavera,[76a] S. Prince,[90] N. Proklova,[100] K. Prokofiev,[62c] F. Prokoshin,[34b] S. Protopopescu,[27] J. Proudfoot,[6] M. Przybycien,[41a] A. Puri,[169] P. Puzo,[119] J. Qian,[92] G. Qin,[56] Y. Qin,[87] A. Quadt,[57] M. Queitsch-Maitland,[45] D. Quilty,[56] S. Raddum,[121] V. Radeka,[27] V. Radescu,[122] S. K. Radhakrishnan,[150] P. Radloff,[118] P. Rados,[91] F. Ragusa,[94a,94b] G. Rahal,[181] J. A. Raine,[87] S. Rajagopalan,[27] C. Rangel-Smith,[168] T. Rashid,[119] S. Raspopov,[5] M. G. Ratti,[94a,94b] D. M. Rauch,[45] F. Rauscher,[102] S. Rave,[86]

I. Ravinovich,[175] J. H. Rawling,[87] M. Raymond,[32] A. L. Read,[121] N. P. Readioff,[58] M. Reale,[76a,76b] D. M. Rebuzzi,[123a,123b] A. Redelbach,[177] G. Redlinger,[27] R. Reece,[139] R. G. Reed,[147c] K. Reeves,[44] L. Rehnisch,[17] J. Reichert,[124] A. Reiss,[86] C. Rembser,[32] H. Ren,[35a] M. Rescigno,[134a] S. Resconi,[94a] E. D. Resseguie,[124] S. Rettie,[171] E. Reynolds,[19] O. L. Rezanova,[111,d] P. Reznicek,[131] R. Rezvani,[97] R. Richter,[103] S. Richter,[81] E. Richter-Was,[41b] O. Ricken,[23] M. Ridel,[83] P. Rieck,[103] C. J. Riegel,[178] J. Rieger,[57] O. Rifki,[115] M. Rijssenbeek,[150] A. Rimoldi,[123a,123b] M. Rimoldi,[18] L. Rinaldi,[22a] G. Ripellino,[149] B. Ristić,[32] E. Ritsch,[32] I. Riu,[13] F. Rizatdinova,[116] E. Rizvi,[79] C. Rizzi,[13] R. T. Roberts,[87] S. H. Robertson,[90,p] A. Robichaud-Veronneau,[90] D. Robinson,[30] J. E. M. Robinson,[45] A. Robson,[56] E. Rocco,[86] C. Roda,[126a,126b] Y. Rodina,[88,oo] S. Rodriguez Bosca,[170] A. Rodriguez Perez,[13] D. Rodriguez Rodriguez,[170] S. Roe,[32] C. S. Rogan,[59] O. Røhne,[121] J. Roloff,[59] A. Romaniouk,[100] M. Romano,[22a,22b] S. M. Romano Saez,[37] E. Romero Adam,[170] N. Rompotis,[77] M. Ronzani,[51] L. Roos,[83] S. Rosati,[134a] K. Rosbach,[51] P. Rose,[139] N.-A. Rosien,[57] E. Rossi,[106a,106b] L. P. Rossi,[53a] J. H. N. Rosten,[30] R. Rosten,[140] M. Rotaru,[28b] J. Rothberg,[140] D. Rousseau,[119] A. Rozanov,[88] Y. Rozen,[154] X. Ruan,[147c] F. Rubbo,[145] F. Rühr,[51] A. Ruiz-Martinez,[31] Z. Rurikova,[51] N. A. Rusakovich,[68] H. L. Russell,[90] J. P. Rutherfoord,[7] N. Ruthmann,[32] Y. F. Ryabov,[125] M. Rybar,[169] G. Rybkin,[119] S. Ryu,[6] A. Ryzhov,[132] G. F. Rzehorz,[57] A. F. Saavedra,[152] G. Sabato,[109] S. Sacerdoti,[29] H. F-W. Sadrozinski,[139] R. Sadykov,[68] F. Safai Tehrani,[134a] P. Saha,[110] M. Sahinsoy,[60a] M. Saimpert,[45] M. Saito,[157] T. Saito,[157] H. Sakamoto,[157] Y. Sakurai,[174] G. Salamanna,[136a,136b] J. E. Salazar Loyola,[34b] D. Salek,[109] P. H. Sales De Bruin,[168] D. Salihagic,[103] A. Salnikov,[145] J. Salt,[170] D. Salvatore,[40a,40b] F. Salvatore,[151] A. Salvucci,[62a,62b,62c] A. Salzburger,[32] D. Sammel,[51] D. Sampsonidis,[156] D. Sampsonidou,[156] J. Sánchez,[170] V. Sanchez Martinez,[170] A. Sanchez Pineda,[167a,167c] H. Sandaker,[121] R. L. Sandbach,[79] C. O. Sander,[45] M. Sandhoff,[178] C. Sandoval,[21] D. P. C. Sankey,[133] M. Sannino,[53a,53b] Y. Sano,[105] A. Sansoni,[50] C. Santoni,[37] H. Santos,[128a] I. Santoyo Castillo,[151] A. Sapronov,[68] J. G. Saraiva,[128a,128d] B. Sarrazin,[23] O. Sasaki,[69] K. Sato,[164] E. Sauvan,[5] G. Savage,[80] P. Savard,[161,e] N. Savic,[103] C. Sawyer,[133] L. Sawyer,[82,v] J. Saxon,[33] C. Sbarra,[22a] A. Sbrizzi,[22a,22b] T. Scanlon,[81] D. A. Scannicchio,[166] M. Scarcella,[152] J. Schaarschmidt,[140] P. Schacht,[103] B. M. Schachtner,[102] D. Schaefer,[32] L. Schaefer,[124] R. Schaefer,[45] J. Schaeffer,[86] S. Schaepe,[23] S. Schaetzel,[60b] U. Schäfer,[86] A. C. Schaffer,[119] D. Schaile,[102] R. D. Schamberger,[150] V. A. Schegelsky,[125] D. Scheirich,[131] M. Schernau,[166] C. Schiavi,[53a,53b] S. Schier,[139] L. K. Schildgen,[23] C. Schillo,[51] M. Schioppa,[40a,40b] S. Schlenker,[32] K. R. Schmidt-Sommerfeld,[103] K. Schmieden,[32] C. Schmitt,[86] S. Schmitt,[45] S. Schmitz,[86] U. Schnoor,[51] L. Schoeffel,[138] A. Schoening,[60b] B. D. Schoenrock,[93] E. Schopf,[23] M. Schott,[86] J. F. P. Schouwenberg,[108] J. Schovancova,[32] S. Schramm,[52] N. Schuh,[86] A. Schulte,[86] M. J. Schultens,[23] H.-C. Schultz-Coulon,[60a] H. Schulz,[17] M. Schumacher,[51] B. A. Schumm,[139] Ph. Schune,[138] A. Schwartzman,[145] T. A. Schwarz,[92] H. Schweiger,[87] Ph. Schwemling,[138] R. Schwienhorst,[93] J. Schwindling,[138] A. Sciandra,[23] G. Sciolla,[25] M. Scornajenghi,[40a,40b] F. Scuri,[126a,126b] F. Scutti,[91] J. Searcy,[92] P. Seema,[23] S. C. Seidel,[107] A. Seiden,[139] J. M. Seixas,[26a] G. Sekhniaidze,[106a] K. Sekhon,[92] S. J. Sekula,[43] N. Semprini-Cesari,[22a,22b] S. Senkin,[37] C. Serfon,[121] L. Serin,[119] L. Serkin,[167a,167b] M. Sessa,[136a,136b] R. Seuster,[172] H. Severini,[115] T. Sfiligoj,[78] F. Sforza,[32] A. Sfyrla,[52] E. Shabalina,[57] N. W. Shaikh,[148a,148b] L. Y. Shan,[35a] R. Shang,[169] J. T. Shank,[24] M. Shapiro,[16] P. B. Shatalov,[99] K. Shaw,[167a,167b] S. M. Shaw,[87] A. Shcherbakova,[148a,148b] C. Y. Shehu,[151] Y. Shen,[115] N. Sherafati,[31] P. Sherwood,[81] L. Shi,[153,pp] S. Shimizu,[70] C. O. Shimmin,[179] M. Shimojima,[104] I. P. J. Shipsey,[122] S. Shirabe,[73] M. Shiyakova,[68,qq] J. Shlomi,[175] A. Shmeleva,[98] D. Shoaleh Saadi,[97] M. J. Shochet,[33] S. Shojaii,[94a] D. R. Shope,[115] S. Shrestha,[113] E. Shulga,[100] M. A. Shupe,[7] P. Sicho,[129] A. M. Sickles,[169] P. E. Sidebo,[149] E. Sideras Haddad,[147c] O. Sidiropoulou,[177] A. Sidoti,[22a,22b] F. Siegert,[47] Dj. Sijacki,[14] J. Silva,[128a,128d] S. B. Silverstein,[148a] V. Simak,[130] Lj. Simic,[14] S. Simion,[119] E. Simioni,[86] B. Simmons,[81] M. Simon,[86] P. Sinervo,[161] N. B. Sinev,[118] M. Sioli,[22a,22b] G. Siragusa,[177] I. Siral,[92] S. Yu. Sivoklokov,[101] J. Sjölin,[148a,148b] M. B. Skinner,[75] P. Skubic,[115] M. Slater,[19] T. Slavicek,[130] M. Slawinska,[42] K. Sliwa,[165] R. Slovak,[131] V. Smakhtin,[175] B. H. Smart,[5] J. Smiesko,[146a] N. Smirnov,[100] S. Yu. Smirnov,[100] Y. Smirnov,[100] L. N. Smirnova,[101,rr] O. Smirnova,[84] J. W. Smith,[57] M. N. K. Smith,[38] R. W. Smith,[38] M. Smizanska,[75] K. Smolek,[130] A. A. Snesarev,[98] I. M. Snyder,[118] S. Snyder,[27] R. Sobie,[172,p] F. Socher,[47] A. Soffer,[155] A. Søgaard,[49] D. A. Soh,[153] G. Sokhrannyi,[78] C. A. Solans Sanchez,[32] M. Solar,[130] E. Yu. Soldatov,[100] U. Soldevila,[170] A. A. Solodkov,[132] A. Soloshenko,[68] O. V. Solovyanov,[132] V. Solovyev,[125] P. Sommer,[51] H. Son,[165] A. Sopczak,[130] D. Sosa,[60b] C. L. Sotiropoulou,[126a,126b] R. Soualah,[167a,167c] A. M. Soukharev,[111,d] D. South,[45] B. C. Sowden,[80] S. Spagnolo,[76a,76b] M. Spalla,[126a,126b] M. Spangenberg,[173] F. Spanò,[80] D. Sperlich,[17] F. Spettel,[103] T. M. Spieker,[60a] R. Spighi,[22a] G. Spigo,[32] L. A. Spiller,[91] M. Spousta,[131] R. D. St. Denis,[56,a] A. Stabile,[94a] R. Stamen,[60a] S. Stamm,[17] E. Stanecka,[42] R. W. Stanek,[6] C. Stanescu,[136a] M. M. Stanitzki,[45] B. S. Stapf,[109] S. Stapnes,[121] E. A. Starchenko,[132] G. H. Stark,[33] J. Stark,[58] S. H Stark,[39] P. Staroba,[129] P. Starovoitov,[60a] S. Stärz,[32] R. Staszewski,[42]

P. Steinberg,[27] B. Stelzer,[144] H. J. Stelzer,[32] O. Stelzer-Chilton,[163a] H. Stenzel,[55] G. A. Stewart,[56] M. C. Stockton,[118] M. Stoebe,[90] G. Stoicea,[28b] P. Stolte,[57] S. Stonjek,[103] A. R. Stradling,[8] A. Straessner,[47] M. E. Stramaglia,[18] J. Strandberg,[149] S. Strandberg,[148a,148b] M. Strauss,[115] P. Strizenec,[146b] R. Ströhmer,[177] D. M. Strom,[118] R. Stroynowski,[43] A. Strubig,[49] S. A. Stucci,[27] B. Stugu,[15] N. A. Styles,[45] D. Su,[145] J. Su,[127] S. Suchek,[60a] Y. Sugaya,[120] M. Suk,[130] V. V. Sulin,[98] DMS Sultan,[162a,162b] S. Sultansoy,[4c] T. Sumida,[71] S. Sun,[59] X. Sun,[3] K. Suruliz,[151] C. J. E. Suster,[152] M. R. Sutton,[151] S. Suzuki,[69] M. Svatos,[129] M. Swiatlowski,[33] S. P. Swift,[2] I. Sykora,[146a] T. Sykora,[131] D. Ta,[51] K. Tackmann,[45] J. Taenzer,[155] A. Taffard,[166] R. Tafirout,[163a] N. Taiblum,[155] H. Takai,[27] R. Takashima,[72] E. H. Takasugi,[103] T. Takeshita,[142] Y. Takubo,[69] M. Talby,[88] A. A. Talyshev,[111,d] J. Tanaka,[157] M. Tanaka,[159] R. Tanaka,[119] S. Tanaka,[69] R. Tanioka,[70] B. B. Tannenwald,[113] S. Tapia Araya,[34b] S. Tapprogge,[86] S. Tarem,[154] G. F. Tartarelli,[94a] P. Tas,[131] M. Tasevsky,[129] T. Tashiro,[71] E. Tassi,[40a,40b] A. Tavares Delgado,[128a,128b] Y. Tayalati,[137e] A. C. Taylor,[107] G. N. Taylor,[91] P. T. E. Taylor,[91] W. Taylor,[163b] P. Teixeira-Dias,[80] D. Temple,[144] H. Ten Kate,[32] P. K. Teng,[153] J. J. Teoh,[120] F. Tepel,[178] S. Terada,[69] K. Terashi,[157] J. Terron,[85] S. Terzo,[13] M. Testa,[50] R. J. Teuscher,[161,p] T. Theveneaux-Pelzer,[88] F. Thiele,[39] J. P. Thomas,[19] J. Thomas-Wilsker,[80] P. D. Thompson,[19] A. S. Thompson,[56] L. A. Thomsen,[179] E. Thomson,[124] M. J. Tibbetts,[16] R. E. Ticse Torres,[88] V. O. Tikhomirov,[98,ss] Yu. A. Tikhonov,[111,d] S. Timoshenko,[100] P. Tipton,[179] S. Tisserant,[88] K. Todome,[159] S. Todorova-Nova,[5] S. Todt,[47] J. Tojo,[73] S. Tokár,[146a] K. Tokushuku,[69] E. Tolley,[59] L. Tomlinson,[87] M. Tomoto,[105] L. Tompkins,[145,tt] K. Toms,[107] B. Tong,[59] P. Tornambe,[51] E. Torrence,[118] H. Torres,[144] E. Torró Pastor,[140] J. Toth,[88,uu] F. Touchard,[88] D. R. Tovey,[141] C. J. Treado,[112] T. Trefzger,[177] F. Tresoldi,[151] A. Tricoli,[27] I. M. Trigger,[163a] S. Trincaz-Duvoid,[83] M. F. Tripiana,[13] W. Trischuk,[161] B. Trocmé,[58] A. Trofymov,[45] C. Troncon,[94a] M. Trottier-McDonald,[16] M. Trovatelli,[172] L. Truong,[147b] M. Trzebinski,[42] A. Trzupek,[42] K. W. Tsang,[62a] J. C-L. Tseng,[122] P. V. Tsiareshka,[95] G. Tsipolitis,[10] N. Tsirintanis,[9] S. Tsiskaridze,[13] V. Tsiskaridze,[51] E. G. Tskhadadze,[54a] K. M. Tsui,[62a] I. I. Tsukerman,[99] V. Tsulaia,[16] S. Tsuno,[69] D. Tsybychev,[150] Y. Tu,[62b] A. Tudorache,[28b] V. Tudorache,[28b] T. T. Tulbure,[28a] A. N. Tuna,[59] S. A. Tupputi,[22a,22b] S. Turchikhin,[68] D. Turgeman,[175] I. Turk Cakir,[4b,vv] R. Turra,[94a] P. M. Tuts,[38] G. Ucchielli,[22a,22b] I. Ueda,[69] M. Ughetto,[148a,148b] F. Ukegawa,[164] G. Unal,[32] A. Undrus,[27] G. Unel,[166] F. C. Ungaro,[91] Y. Unno,[69] C. Unverdorben,[102] J. Urban,[146b] P. Urquijo,[91] P. Urrejola,[86] G. Usai,[8] J. Usui,[69] L. Vacavant,[88] V. Vacek,[130] B. Vachon,[90] K. O. H. Vadla,[121] A. Vaidya,[81] C. Valderanis,[102] E. Valdes Santurio,[148a,148b] S. Valentinetti,[22a,22b] A. Valero,[170] L. Valéry,[13] S. Valkar,[131] A. Vallier,[5] J. A. Valls Ferrer,[170] W. Van Den Wollenberg,[109] H. van der Graaf,[109] P. van Gemmeren,[6] J. Van Nieuwkoop,[144] I. van Vulpen,[109] M. C. van Woerden,[109] M. Vanadia,[135a,135b] W. Vandelli,[32] A. Vaniachine,[160] P. Vankov,[109] G. Vardanyan,[180] R. Vari,[134a] E. W. Varnes,[7] C. Varni,[53a,53b] T. Varol,[43] D. Varouchas,[119] A. Vartapetian,[8] K. E. Varvell,[152] J. G. Vasquez,[179] G. A. Vasquez,[34b] F. Vazeille,[37] T. Vazquez Schroeder,[90] J. Veatch,[57] V. Veeraraghavan,[7] L. M. Veloce,[161] F. Veloso,[128a,128c] S. Veneziano,[134a] A. Ventura,[76a,76b] M. Venturi,[172] N. Venturi,[32] A. Venturini,[25] V. Vercesi,[123a] M. Verducci,[136a,136b] W. Verkerke,[109] A. T. Vermeulen,[109] J. C. Vermeulen,[109] M. C. Vetterli,[144,e] N. Viaux Maira,[34b] O. Viazlo,[84] I. Vichou,[169,a] T. Vickey,[141] O. E. Vickey Boeriu,[141] G. H. A. Viehhauser,[122] S. Viel,[16] L. Vigani,[122] M. Villa,[22a,22b] M. Villaplana Perez,[94a,94b] E. Vilucchi,[50] M. G. Vincter,[31] V. B. Vinogradov,[68] A. Vishwakarma,[45] C. Vittori,[22a,22b] I. Vivarelli,[151] S. Vlachos,[10] M. Vogel,[178] P. Vokac,[130] G. Volpi,[126a,126b] H. von der Schmitt,[103] E. von Toerne,[23] V. Vorobel,[131] K. Vorobev,[100] M. Vos,[170] R. Voss,[32] J. H. Vossebeld,[77] N. Vranjes,[14] M. Vranjes Milosavljevic,[14] V. Vrba,[130] M. Vreeswijk,[109] R. Vuillermet,[32] I. Vukotic,[33] P. Wagner,[23] W. Wagner,[178] J. Wagner-Kuhr,[102] H. Wahlberg,[74] S. Wahrmund,[47] J. Wakabayashi,[105] J. Walder,[75] R. Walker,[102] W. Walkowiak,[143] V. Wallangen,[148a,148b] A. M. Wang,[59] C. Wang,[35b] C. Wang,[36b,ww] F. Wang,[176] H. Wang,[16] H. Wang,[3] J. Wang,[45] J. Wang,[152] Q. Wang,[115] R. Wang,[6] S. M. Wang,[153] T. Wang,[38] W. Wang,[153,xx] W. Wang,[36a] Z. Wang,[36c] C. Wanotayaroj,[118] A. Warburton,[90] C. P. Ward,[30] D. R. Wardrope,[81] A. Washbrook,[49] P. M. Watkins,[19] A. T. Watson,[19] M. F. Watson,[19] G. Watts,[140] S. Watts,[87] B. M. Waugh,[81] A. F. Webb,[11] S. Webb,[86] M. S. Weber,[18] S. W. Weber,[177] S. A. Weber,[31] J. S. Webster,[6] A. R. Weidberg,[122] B. Weinert,[64] J. Weingarten,[57] M. Weirich,[86] C. Weiser,[51] H. Weits,[109] P. S. Wells,[32] T. Wenaus,[27] T. Wengler,[32] S. Wenig,[32] N. Wermes,[23] M. D. Werner,[67] P. Werner,[32] M. Wessels,[60a] K. Whalen,[118] N. L. Whallon,[140] A. M. Wharton,[75] A. S. White,[92] A. White,[8] M. J. White,[1] R. White,[34b] D. Whiteson,[166] B. W. Whitmore,[75] F. J. Wickens,[133] W. Wiedenmann,[176] M. Wielers,[133] C. Wiglesworth,[39] L. A. M. Wiik-Fuchs,[51] A. Wildauer,[103] F. Wilk,[87] H. G. Wilkens,[32] H. H. Williams,[124] S. Williams,[109] C. Willis,[93] S. Willocq,[89] J. A. Wilson,[19] I. Wingerter-Seez,[5] E. Winkels,[151] F. Winklmeier,[118] O. J. Winston,[151] B. T. Winter,[23] M. Wittgen,[145] M. Wobisch,[82,v] T. M. H. Wolf,[109] R. Wolff,[88] M. W. Wolter,[42] H. Wolters,[128a,128c] V. W. S. Wong,[171] S. D. Worm,[19] B. K. Wosiek,[42] J. Wotschack,[32] K. W. Wozniak,[42] M. Wu,[33] S. L. Wu,[176] X. Wu,[52] Y. Wu,[92] T. R. Wyatt,[87] B. M. Wynne,[49] S. Xella,[39]

Z. Xi,[92] L. Xia,[35c] D. Xu,[35a] L. Xu,[27] T. Xu,[138] B. Yabsley,[152] S. Yacoob,[147a] D. Yamaguchi,[159] Y. Yamaguchi,[120] A. Yamamoto,[69] S. Yamamoto,[157] T. Yamanaka,[157] M. Yamatani,[157] K. Yamauchi,[105] Y. Yamazaki,[70] Z. Yan,[24] H. Yang,[36c] H. Yang,[16] Y. Yang,[153] Z. Yang,[15] W-M. Yao,[16] Y. C. Yap,[83] Y. Yasu,[69] E. Yatsenko,[5] K. H. Yau Wong,[23] J. Ye,[43] S. Ye,[27] I. Yeletskikh,[68] E. Yigitbasi,[24] E. Yildirim,[86] K. Yorita,[174] K. Yoshihara,[124] C. Young,[145] C. J. S. Young,[32] J. Yu,[8] J. Yu,[67] S. P. Y. Yuen,[23] I. Yusuff,[30,yy] B. Zabinski,[42] G. Zacharis,[10] R. Zaidan,[13] A. M. Zaitsev,[132,mm] N. Zakharchuk,[45] J. Zalieckas,[15] A. Zaman,[150] S. Zambito,[59] D. Zanzi,[91] C. Zeitnitz,[178] G. Zemaityte,[122] A. Zemla,[41a] J. C. Zeng,[169] Q. Zeng,[145] O. Zenin,[132] T. Ženiš,[146a] D. Zerwas,[119] D. Zhang,[92] F. Zhang,[176] G. Zhang,[36a,zz] H. Zhang,[35b] J. Zhang,[6] L. Zhang,[51] L. Zhang,[36a] M. Zhang,[169] P. Zhang,[35b] R. Zhang,[23] R. Zhang,[36a,ww] X. Zhang,[36b] Y. Zhang,[35a] Z. Zhang,[119] X. Zhao,[43] Y. Zhao,[36b,aaa] Z. Zhao,[36a] A. Zhemchugov,[68] B. Zhou,[92] C. Zhou,[176] L. Zhou,[43] M. Zhou,[35a] M. Zhou,[150] N. Zhou,[35c] C. G. Zhu,[36b] H. Zhu,[35a] J. Zhu,[92] Y. Zhu,[36a] X. Zhuang,[35a] K. Zhukov,[98] A. Zibell,[177] D. Zieminska,[64] N. I. Zimine,[68] C. Zimmermann,[86] S. Zimmermann,[51] Z. Zinonos,[103] M. Zinser,[86] M. Ziolkowski,[143] L. Živković,[14] G. Zobernig,[176] A. Zoccoli,[22a,22b] R. Zou,[33] M. zur Nedden,[17] and L. Zwalinski[32]

(ATLAS Collaboration)

[1]*Department of Physics, University of Adelaide, Adelaide, Australia*
[2]*Physics Department, SUNY Albany, Albany, New York, USA*
[3]*Department of Physics, University of Alberta, Edmonton, Alberta, Canada*
[4a]*Department of Physics, Ankara University, Ankara, Turkey*
[4b]*Istanbul Aydin University, Istanbul, Turkey*
[4c]*Division of Physics, TOBB University of Economics and Technology, Ankara, Turkey*
[5]*LAPP, CNRS/IN2P3 and Université Savoie Mont Blanc, Annecy-le-Vieux, France*
[6]*High Energy Physics Division, Argonne National Laboratory, Argonne, Illinois, USA*
[7]*Department of Physics, University of Arizona, Tucson, Arizona, USA*
[8]*Department of Physics, The University of Texas at Arlington, Arlington, Texas, USA*
[9]*Physics Department, National and Kapodistrian University of Athens, Athens, Greece*
[10]*Physics Department, National Technical University of Athens, Zografou, Greece*
[11]*Department of Physics, The University of Texas at Austin, Austin, Texas, USA*
[12]*Institute of Physics, Azerbaijan Academy of Sciences, Baku, Azerbaijan*
[13]*Institut de Física d'Altes Energies (IFAE), The Barcelona Institute of Science and Technology, Barcelona, Spain*
[14]*Institute of Physics, University of Belgrade, Belgrade, Serbia*
[15]*Department for Physics and Technology, University of Bergen, Bergen, Norway*
[16]*Physics Division, Lawrence Berkeley National Laboratory and University of California, Berkeley, California, USA*
[17]*Department of Physics, Humboldt University, Berlin, Germany*
[18]*Albert Einstein Center for Fundamental Physics and Laboratory for High Energy Physics, University of Bern, Bern, Switzerland*
[19]*School of Physics and Astronomy, University of Birmingham, Birmingham, United Kingdom*
[20a]*Department of Physics, Bogazici University, Istanbul, Turkey*
[20b]*Department of Physics Engineering, Gaziantep University, Gaziantep, Turkey*
[20c]*Istanbul Bilgi University, Faculty of Engineering and Natural Sciences, Istanbul, Turkey*
[20d]*Bahcesehir University, Faculty of Engineering and Natural Sciences, Istanbul, Turkey*
[21]*Centro de Investigaciones, Universidad Antonio Narino, Bogota, Colombia*
[22a]*INFN Sezione di Bologna, Italy*
[22b]*Dipartimento di Fisica e Astronomia, Università di Bologna, Bologna, Italy*
[23]*Physikalisches Institut, University of Bonn, Bonn, Germany*
[24]*Department of Physics, Boston University, Boston, Massachusetts, USA*
[25]*Department of Physics, Brandeis University, Waltham, Massachusetts, USA*
[26a]*Universidade Federal do Rio De Janeiro COPPE/EE/IF, Rio de Janeiro, Brazil*
[26b]*Electrical Circuits Department, Federal University of Juiz de Fora (UFJF), Juiz de Fora, Brazil*
[26c]*Federal University of Sao Joao del Rei (UFSJ), Sao Joao del Rei, Brazil*
[26d]*Instituto de Fisica, Universidade de Sao Paulo, Sao Paulo, Brazil*
[27]*Physics Department, Brookhaven National Laboratory, Upton, New York, USA*
[28a]*Transilvania University of Brasov, Brasov, Romania*
[28b]*Horia Hulubei National Institute of Physics and Nuclear Engineering, Bucharest, Romania*
[28c]*Department of Physics, Alexandru Ioan Cuza University of Iasi, Iasi, Romania*

[28d]National Institute for Research and Development of Isotopic and Molecular Technologies, Physics Department, Cluj Napoca, Romania
[28e]University Politehnica Bucharest, Bucharest, Romania
[28f]West University in Timisoara, Timisoara, Romania
[29]Departamento de Física, Universidad de Buenos Aires, Buenos Aires, Argentina
[30]Cavendish Laboratory, University of Cambridge, Cambridge, United Kingdom
[31]Department of Physics, Carleton University, Ottawa, Ontario, Canada
[32]CERN, Geneva, Switzerland
[33]Enrico Fermi Institute, University of Chicago, Chicago, Illinois, USA
[34a]Departamento de Física, Pontificia Universidad Católica de Chile, Santiago, Chile
[34b]Departamento de Física, Universidad Técnica Federico Santa María, Valparaíso, Chile
[35a]Institute of High Energy Physics, Chinese Academy of Sciences, Beijing, China
[35b]Department of Physics, Nanjing University, Jiangsu, China
[35c]Physics Department, Tsinghua University, Beijing 100084, China
[36a]Department of Modern Physics and State Key Laboratory of Particle Detection and Electronics, University of Science and Technology of China, Anhui, China
[36b]School of Physics, Shandong University, Shandong, China
[36c]Department of Physics and Astronomy, Key Laboratory for Particle Physics, Astrophysics and Cosmology, Ministry of Education; Shanghai Key Laboratory for Particle Physics and Cosmology, Shanghai Jiao Tong University, Shanghai(also at PKU-CHEP), China
[37]Université Clermont Auvergne, CNRS/IN2P3, LPC, Clermont-Ferrand, France
[38]Nevis Laboratory, Columbia University, Irvington, New York, USA
[39]Niels Bohr Institute, University of Copenhagen, Kobenhavn, Denmark
[40a]INFN Gruppo Collegato di Cosenza, Laboratori Nazionali di Frascati, Italy
[40b]Dipartimento di Fisica, Università della Calabria, Rende, Italy
[41a]AGH University of Science and Technology, Faculty of Physics and Applied Computer Science, Krakow, Poland
[41b]Marian Smoluchowski Institute of Physics, Jagiellonian University, Krakow, Poland
[42]Institute of Nuclear Physics Polish Academy of Sciences, Krakow, Poland
[43]Physics Department, Southern Methodist University, Dallas, Texas, USA
[44]Physics Department, University of Texas at Dallas, Richardson, Texas, USA
[45]DESY, Hamburg and Zeuthen, Germany
[46]Lehrstuhl für Experimentelle Physik IV, Technische Universität Dortmund, Dortmund, Germany
[47]Institut für Kern- und Teilchenphysik, Technische Universität Dresden, Dresden, Germany
[48]Department of Physics, Duke University, Durham, North Carolina, USA
[49]SUPA - School of Physics and Astronomy, University of Edinburgh, Edinburgh, United Kingdom
[50]INFN e Laboratori Nazionali di Frascati, Frascati, Italy
[51]Fakultät für Mathematik und Physik, Albert-Ludwigs-Universität, Freiburg, Germany
[52]Departement de Physique Nucleaire et Corpusculaire, Université de Genève, Geneva, Switzerland
[53a]INFN Sezione di Genova, Italy
[53b]Dipartimento di Fisica, Università di Genova, Genova, Italy
[54a]E. Andronikashvili Institute of Physics, Iv. Javakhishvili Tbilisi State University, Tbilisi, Georgia
[54b]High Energy Physics Institute, Tbilisi State University, Tbilisi, Georgia
[55]II Physikalisches Institut, Justus-Liebig-Universität Giessen, Giessen, Germany
[56]SUPA - School of Physics and Astronomy, University of Glasgow, Glasgow, United Kingdom
[57]II Physikalisches Institut, Georg-August-Universität, Göttingen, Germany
[58]Laboratoire de Physique Subatomique et de Cosmologie, Université Grenoble-Alpes, CNRS/IN2P3, Grenoble, France
[59]Laboratory for Particle Physics and Cosmology, Harvard University, Cambridge, Massachusetts, USA
[60a]Kirchhoff-Institut für Physik, Ruprecht-Karls-Universität Heidelberg, Heidelberg, Germany
[60b]Physikalisches Institut, Ruprecht-Karls-Universität Heidelberg, Heidelberg, Germany
[61]Faculty of Applied Information Science, Hiroshima Institute of Technology, Hiroshima, Japan
[62a]Department of Physics, The Chinese University of Hong Kong, Shatin, N.T., Hong Kong, China
[62b]Department of Physics, The University of Hong Kong, Hong Kong, China
[62c]Department of Physics and Institute for Advanced Study, The Hong Kong University of Science and Technology, Clear Water Bay, Kowloon, Hong Kong, China
[63]Department of Physics, National Tsing Hua University, Taiwan, Taiwan
[64]Department of Physics, Indiana University, Bloomington, Indiana, USA
[65]Institut für Astro- und Teilchenphysik, Leopold-Franzens-Universität, Innsbruck, Austria
[66]University of Iowa, Iowa City, Iowa, USA

[67]*Department of Physics and Astronomy, Iowa State University, Ames, Iowa, USA*
[68]*Joint Institute for Nuclear Research, JINR Dubna, Dubna, Russia*
[69]*KEK, High Energy Accelerator Research Organization, Tsukuba, Japan*
[70]*Graduate School of Science, Kobe University, Kobe, Japan*
[71]*Faculty of Science, Kyoto University, Kyoto, Japan*
[72]*Kyoto University of Education, Kyoto, Japan*
[73]*Research Center for Advanced Particle Physics and Department of Physics, Kyushu University, Fukuoka, Japan*
[74]*Instituto de Física La Plata, Universidad Nacional de La Plata and CONICET, La Plata, Argentina*
[75]*Physics Department, Lancaster University, Lancaster, United Kingdom*
[76a]*INFN Sezione di Lecce, Italy*
[76b]*Dipartimento di Matematica e Fisica, Università del Salento, Lecce, Italy*
[77]*Oliver Lodge Laboratory, University of Liverpool, Liverpool, United Kingdom*
[78]*Department of Experimental Particle Physics, Jožef Stefan Institute and Department of Physics, University of Ljubljana, Ljubljana, Slovenia*
[79]*School of Physics and Astronomy, Queen Mary University of London, London, United Kingdom*
[80]*Department of Physics, Royal Holloway University of London, Surrey, United Kingdom*
[81]*Department of Physics and Astronomy, University College London, London, United Kingdom*
[82]*Louisiana Tech University, Ruston, Louisiana, USA*
[83]*Laboratoire de Physique Nucléaire et de Hautes Energies, UPMC and Université Paris-Diderot and CNRS/IN2P3, Paris, France*
[84]*Fysiska institutionen, Lunds universitet, Lund, Sweden*
[85]*Departamento de Fisica Teorica C-15, Universidad Autonoma de Madrid, Madrid, Spain*
[86]*Institut für Physik, Universität Mainz, Mainz, Germany*
[87]*School of Physics and Astronomy, University of Manchester, Manchester, United Kingdom*
[88]*CPPM, Aix-Marseille Université and CNRS/IN2P3, Marseille, France*
[89]*Department of Physics, University of Massachusetts, Amherst, Massachusetts, USA*
[90]*Department of Physics, McGill University, Montreal, Québec, Canada*
[91]*School of Physics, University of Melbourne, Victoria, Australia*
[92]*Department of Physics, The University of Michigan, Ann Arbor, Michigan, USA*
[93]*Department of Physics and Astronomy, Michigan State University, East Lansing, Michigan, USA*
[94a]*INFN Sezione di Milano, Italy*
[94b]*Dipartimento di Fisica, Università di Milano, Milano, Italy*
[95]*B.I. Stepanov Institute of Physics, National Academy of Sciences of Belarus, Minsk, Republic of Belarus*
[96]*Research Institute for Nuclear Problems of Byelorussian State University, Minsk, Republic of Belarus*
[97]*Group of Particle Physics, University of Montreal, Montreal, Québec, Canada*
[98]*P.N. Lebedev Physical Institute of the Russian Academy of Sciences, Moscow, Russia*
[99]*Institute for Theoretical and Experimental Physics (ITEP), Moscow, Russia*
[100]*National Research Nuclear University MEPhI, Moscow, Russia*
[101]*D.V. Skobeltsyn Institute of Nuclear Physics, M.V. Lomonosov Moscow State University, Moscow, Russia*
[102]*Fakultät für Physik, Ludwig-Maximilians-Universität München, München, Germany*
[103]*Max-Planck-Institut für Physik (Werner-Heisenberg-Institut), München, Germany*
[104]*Nagasaki Institute of Applied Science, Nagasaki, Japan*
[105]*Graduate School of Science and Kobayashi-Maskawa Institute, Nagoya University, Nagoya, Japan*
[106a]*INFN Sezione di Napoli, Italy*
[106b]*Dipartimento di Fisica, Università di Napoli, Napoli, Italy*
[107]*Department of Physics and Astronomy, University of New Mexico, Albuquerque, New Mexico, USA*
[108]*Institute for Mathematics, Astrophysics and Particle Physics, Radboud University Nijmegen, Nijmegen, Nikhef, Netherlands*
[109]*Nikhef National Institute for Subatomic Physics and University of Amsterdam, Amsterdam, Netherlands*
[110]*Department of Physics, Northern Illinois University, DeKalb, Illinois, USA*
[111]*Budker Institute of Nuclear Physics, SB RAS, Novosibirsk, Russia*
[112]*Department of Physics, New York University, New York, New York, USA*
[113]*Ohio State University, Columbus, Ohio, USA*
[114]*Faculty of Science, Okayama University, Okayama, Japan*
[115]*Homer L. Dodge Department of Physics and Astronomy, University of Oklahoma, Norman, Oklahoma, USA*
[116]*Department of Physics, Oklahoma State University, Stillwater, Oklahoma, USA*
[117]*Palacký University, RCPTM, Olomouc, Czech Republic*

[118]Center for High Energy Physics, University of Oregon, Eugene, Oregon, USA
[119]LAL, Univ. Paris-Sud, CNRS/IN2P3, Université Paris-Saclay, Orsay, France
[120]Graduate School of Science, Osaka University, Osaka, Japan
[121]Department of Physics, University of Oslo, Oslo, Norway
[122]Department of Physics, Oxford University, Oxford, United Kingdom
[123a]INFN Sezione di Pavia, Italy
[123b]Dipartimento di Fisica, Università di Pavia, Pavia, Italy
[124]Department of Physics, University of Pennsylvania, Philadelphia, Pennsylvania, USA
[125]National Research Centre "Kurchatov Institute"
B.P.Konstantinov Petersburg Nuclear Physics Institute, St. Petersburg, Russia
[126a]INFN Sezione di Pisa, Italy
[126b]Dipartimento di Fisica E. Fermi, Università di Pisa, Pisa, Italy
[127]Department of Physics and Astronomy, University of Pittsburgh, Pittsburgh, Pennsylvania, USA
[128a]Laboratório de Instrumentação e Física Experimental de Partículas - LIP, Lisboa, Portugal
[128b]Faculdade de Ciências, Universidade de Lisboa, Lisboa, Portugal
[128c]Department of Physics, University of Coimbra, Coimbra, Portugal
[128d]Centro de Física Nuclear da Universidade de Lisboa, Lisboa, Portugal
[128e]Departamento de Fisica, Universidade do Minho, Braga, Portugal
[128f]Departamento de Fisica Teorica y del Cosmos, Universidad de Granada, Granada, Portugal
[128g]Dep Fisica and CEFITEC of Faculdade de Ciencias e Tecnologia, Universidade Nova de Lisboa, Caparica, Portugal
[129]Institute of Physics, Academy of Sciences of the Czech Republic, Praha, Czech Republic
[130]Czech Technical University in Prague, Praha, Czech Republic
[131]Charles University, Faculty of Mathematics and Physics, Prague, Czech Republic
[132]State Research Center Institute for High Energy Physics (Protvino), NRC KI, Russia
[133]Particle Physics Department, Rutherford Appleton Laboratory, Didcot, United Kingdom
[134a]INFN Sezione di Roma, Italy
[134b]Dipartimento di Fisica, Sapienza Università di Roma, Roma, Italy
[135a]INFN Sezione di Roma Tor Vergata, Italy
[135b]Dipartimento di Fisica, Università di Roma Tor Vergata, Roma, Italy
[136a]INFN Sezione di Roma Tre, Italy
[136b]Dipartimento di Matematica e Fisica, Università Roma Tre, Roma, Italy
[137a]Faculté des Sciences Ain Chock, Réseau Universitaire de Physique des Hautes Energies - Université Hassan II, Casablanca, Morocco
[137b]Centre National de l'Energie des Sciences Techniques Nucleaires, Rabat, Morocco
[137c]Faculté des Sciences Semlalia, Université Cadi Ayyad, LPHEA-Marrakech, Morocco
[137d]Faculté des Sciences, Université Mohamed Premier and LPTPM, Oujda, Morocco
[137e]Faculté des sciences, Université Mohammed V, Rabat, Morocco
[138]DSM/IRFU (Institut de Recherches sur les Lois Fondamentales de l'Univers), CEA Saclay (Commissariat à l'Energie Atomique et aux Energies Alternatives), Gif-sur-Yvette, France
[139]Santa Cruz Institute for Particle Physics, University of California Santa Cruz, Santa Cruz, California, USA
[140]Department of Physics, University of Washington, Seattle, Washington, USA
[141]Department of Physics and Astronomy, University of Sheffield, Sheffield, United Kingdom
[142]Department of Physics, Shinshu University, Nagano, Japan
[143]Department Physik, Universität Siegen, Siegen, Germany
[144]Department of Physics, Simon Fraser University, Burnaby, British Columbia, Canada
[145]SLAC National Accelerator Laboratory, Stanford, California, USA
[146a]Faculty of Mathematics, Physics & Informatics, Comenius University, Bratislava, Slovak Republic
[146b]Department of Subnuclear Physics, Institute of Experimental Physics of the Slovak Academy of Sciences, Kosice, Slovak Republic
[147a]Department of Physics, University of Cape Town, Cape Town, South Africa
[147b]Department of Physics, University of Johannesburg, Johannesburg, South Africa
[147c]School of Physics, University of the Witwatersrand, Johannesburg, South Africa
[148a]Department of Physics, Stockholm University, Sweden
[148b]The Oskar Klein Centre, Stockholm, Sweden
[149]Physics Department, Royal Institute of Technology, Stockholm, Sweden
[150]Departments of Physics & Astronomy and Chemistry, Stony Brook University, Stony Brook, New York, USA
[151]Department of Physics and Astronomy, University of Sussex, Brighton, United Kingdom

[152]*School of Physics, University of Sydney, Sydney, Australia*
[153]*Institute of Physics, Academia Sinica, Taipei, Taiwan*
[154]*Department of Physics, Technion: Israel Institute of Technology, Haifa, Israel*
[155]*Raymond and Beverly Sackler School of Physics and Astronomy, Tel Aviv University, Tel Aviv, Israel*
[156]*Department of Physics, Aristotle University of Thessaloniki, Thessaloniki, Greece*
[157]*International Center for Elementary Particle Physics and Department of Physics, The University of Tokyo, Tokyo, Japan*
[158]*Graduate School of Science and Technology, Tokyo Metropolitan University, Tokyo, Japan*
[159]*Department of Physics, Tokyo Institute of Technology, Tokyo, Japan*
[160]*Tomsk State University, Tomsk, Russia*
[161]*Department of Physics, University of Toronto, Toronto, Ontario, Canada*
[162a]*INFN-TIFPA, Italy*
[162b]*University of Trento, Trento, Italy*
[163a]*TRIUMF, Vancouver, British Columbia, Canada*
[163b]*Department of Physics and Astronomy, York University, Toronto, Ontario, Canada*
[164]*Faculty of Pure and Applied Sciences, and Center for Integrated Research in Fundamental Science and Engineering, University of Tsukuba, Tsukuba, Japan*
[165]*Department of Physics and Astronomy, Tufts University, Medford, Massachusetts, USA*
[166]*Department of Physics and Astronomy, University of California Irvine, Irvine, California, USA*
[167a]*INFN Gruppo Collegato di Udine, Sezione di Trieste, Udine, Italy*
[167b]*ICTP, Trieste, Italy*
[167c]*Dipartimento di Chimica, Fisica e Ambiente, Università di Udine, Udine, Italy*
[168]*Department of Physics and Astronomy, University of Uppsala, Uppsala, Sweden*
[169]*Department of Physics, University of Illinois, Urbana, Illinois, USA*
[170]*Instituto de Fisica Corpuscular (IFIC), Centro Mixto Universidad de Valencia - CSIC, Spain*
[171]*Department of Physics, University of British Columbia, Vancouver, British Columbia, Canada*
[172]*Department of Physics and Astronomy, University of Victoria, Victoria, British Columbia, Canada*
[173]*Department of Physics, University of Warwick, Coventry, United Kingdom*
[174]*Waseda University, Tokyo, Japan*
[175]*Department of Particle Physics, The Weizmann Institute of Science, Rehovot, Israel*
[176]*Department of Physics, University of Wisconsin, Madison, Wisconsin, USA*
[177]*Fakultät für Physik und Astronomie, Julius-Maximilians-Universität, Würzburg, Germany*
[178]*Fakultät für Mathematik und Naturwissenschaften, Fachgruppe Physik, Bergische Universität Wuppertal, Wuppertal, Germany*
[179]*Department of Physics, Yale University, New Haven, Connecticut, USA*
[180]*Yerevan Physics Institute, Yerevan, Armenia*
[181]*Centre de Calcul de l'Institut National de Physique Nucléaire et de Physique des Particules (IN2P3), Villeurbanne, France*
[182]*Academia Sinica Grid Computing, Institute of Physics, Academia Sinica, Taipei, Taiwan*

[a]Deceased.
[b]Also at Department of Physics, King's College London, London, United Kingdom.
[c]Also at Institute of Physics, Azerbaijan Academy of Sciences, Baku, Azerbaijan.
[d]Also at Novosibirsk State University, Novosibirsk, Russia.
[e]Also at TRIUMF, Vancouver, British Columbia, Canada.
[f]Also at Department of Physics & Astronomy, University of Louisville, Louisville, Kentucky, USA.
[g]Also at Physics Department, An-Najah National University, Nablus, Palestine.
[h]Also at Department of Physics, California State University, Fresno, California, USA.
[i]Also at Department of Physics, University of Fribourg, Fribourg, Switzerland.
[j]Also at II Physikalisches Institut, Georg-August-Universität, Göttingen, Germany.
[k]Also at Departament de Fisica de la Universitat Autonoma de Barcelona, Barcelona, Spain.
[l]Also at Departamento de Fisica e Astronomia, Faculdade de Ciencias, Universidade do Porto, Portugal.
[m]Also at Tomsk State University, Tomsk, and Moscow Institute of Physics and Technology State University, Dolgoprudny, Russia.
[n]Also at The Collaborative Innovation Center of Quantum Matter (CICQM), Beijing, China.
[o]Also at Universita di Napoli Parthenope, Napoli, Italy.
[p]Also at Institute of Particle Physics (IPP), Canada.
[q]Also at Horia Hulubei National Institute of Physics and Nuclear Engineering, Bucharest, Romania
[r]Also at Department of Physics, St. Petersburg State Polytechnical University, St. Petersburg, Russia.
[s]Also at Borough of Manhattan Community College, City University of New York, New York City, USA.
[t]Also at Department of Financial and Management Engineering, University of the Aegean, Chios, Greece.

[u]Also at Centre for High Performance Computing, CSIR Campus, Rosebank, Cape Town, South Africa.
[v]Also at Louisiana Tech University, Ruston, Louisiana, USA.
[w]Also at Institucio Catalana de Recerca i Estudis Avancats, ICREA, Barcelona, Spain.
[x]Also at Graduate School of Science, Osaka University, Osaka, Japan.
[y]Also at Fakultät für Mathematik und Physik, Albert-Ludwigs-Universität, Freiburg, Germany.
[z]Also at Institute for Mathematics, Astrophysics and Particle Physics, Radboud University Nijmegen/Nikhef, Nijmegen, Netherlands.
[aa]Also at Department of Physics, The University of Texas at Austin, Austin, Texas, USA.
[bb]Also at Institute of Theoretical Physics, Ilia State University, Tbilisi, Georgia.
[cc]Also at CERN, Geneva, Switzerland.
[dd]Also at Georgian Technical University (GTU),Tbilisi, Georgia.
[ee]Also at Ochadai Academic Production, Ochanomizu University, Tokyo, Japan.
[ff]Also at Manhattan College, New York, New York, USA.
[gg]Also at Departamento de Física, Pontificia Universidad Católica de Chile, Santiago, Chile.
[hh]Also at Department of Physics, The University of Michigan, Ann Arbor, Michigan, USA.
[ii]Also at The City College of New York, New York, New York, USA.
[jj]Also at School of Physics, Shandong University, Shandong, China.
[kk]Also at Departamento de Fisica Teorica y del Cosmos, Universidad de Granada, Granada, Portugal.
[ll]Also at Department of Physics, California State University, Sacramento, California, USA.
[mm]Also at Moscow Institute of Physics and Technology State University, Dolgoprudny, Russia.
[nn]Also at Departement de Physique Nucleaire et Corpusculaire, Université de Genève, Geneva, Switzerland.
[oo]Also at Institut de Física d'Altes Energies (IFAE), The Barcelona Institute of Science and Technology, Barcelona, Spain.
[pp]Also at School of Physics, Sun Yat-sen University, Guangzhou, China.
[qq]Also at Institute for Nuclear Research and Nuclear Energy (INRNE) of the Bulgarian Academy of Sciences, Sofia, Bulgaria.
[rr]Also at Faculty of Physics, M.V.Lomonosov Moscow State University, Moscow, Russia.
[ss]Also at National Research Nuclear University MEPhI, Moscow, Russia.
[tt]Also at Department of Physics, Stanford University, Stanford, California, USA.
[uu]Also at Institute for Particle and Nuclear Physics, Wigner Research Centre for Physics, Budapest, Hungary.
[vv]Also at Giresun University, Faculty of Engineering, Turkey.
[ww]Also at CPPM, Aix-Marseille Université and CNRS/IN2P3, Marseille, France.
[xx]Also at Department of Physics, Nanjing University, Jiangsu, China.
[yy]Also at University of Malaya, Department of Physics, Kuala Lumpur, Malaysia.
[zz]Also at Institute of Physics, Academia Sinica, Taipei, Taiwan.
[aaa]Also at LAL, Univ. Paris-Sud, CNRS/IN2P3, Université Paris-Saclay, Orsay, France.